Universität für Bodenkultur Wien
University of Natural Resources
and Life Sciences, Vienna

Master Thesis

Studying The Influence of Hypoxia on Breast Cancer Cell Mechanics with Atomic Force Microscopy

Submitted by

Barbara ZBIRAL, BSc

in the framework of the Master programme

Biotechnology

in partial fulfilment of the requirements for the academic degree

Diplom-Ingenieurin

Vienna, 03.04.2023

Supervisor:

Univ.-Prof. Dipl. Phys. Dr. rer. nat. José Luis Toca-Herrera
Institute of Biophysics, Department of BionanosciencesCo-Supervisor: Dr. Andreas Weber

Institute of Biophysics, Department of Bionanosciences

Eidesstattliche Erklärung

Ich, Barbara Zbiral, erkläre eidesstattlich, dass ich die Arbeit selbständig angefertigt habe. Es wurden keine anderen als die angegebenen Hilfsmittel benutzt. Die aus fremden Quellen direkt oder indirekt übernommenen Formulierungen und Gedanken sind als solche kenntlich gemacht. Diese schriftliche Arbeit wurde noch an keiner Stelle vorgelegt.

Affidavit

I, Barbara Zbiral, hereby confirm that the work presented in this thesis is my own. No means were used other than permitted and declared means during the process of this work and thesis. All sources and statements not of my own are declared as such and listed. No part of this work has been published elsewhere yet.0,32165498654321,0

Table of Contents

Abstract

Cells experience and respond to a variety of mechanical forces from their microenvironment. Healthy tissue is in mechanical homeostasis, while mechanical dysregulation is associated with disease. Within the cell, the cytoskeletal components are the main modulators of measurable cell mechanical properties. Breast cancer is a common malignancy among women. Solid tumors develop a hypoxic core, which is implicated in processes associated with malignant progression, such as neovascularization and cancer cell migration. Cancer cell aggressiveness and migratory potential are strongly associated with cytoskeletal rearrangements and cell softening. In this work, the effect of hypoxia on the mechanical properties and structural features of three different subtypes of MCF-7 breast cancer cells have been studied via atomic force microscopy (AFM)-based force spectroscopy and optical microscopy, respectively. The subtypes used were a standard MCF-7 cells, a tamoxifen-resistant MCF-7 variant, and a Sox2-overexpressing MCF-7 variant. Elastic and viscoelastic parameters of the cells were calculated from continuum mechanical models. For all three cell lines, hypoxia significantly altered the viscoelastic properties of the cells and lead to cell softening. Morphologically, the cells show reduced cell-to-cell contacts and formation of tether-like membrane structures between cells in response to hypoxia exposure. These results suggest a link between tumor hypoxia, cytoskeletal rearrangement, and cancer cell aggressiveness.

Zusammenfassung

Zellen spüren und reagieren auf eine Vielzahl mechanischer Reize aus ihrer unmittelbaren Umgebung. Gesundes Gewebe befindet sich in einem mechanischen Gleichgewicht, während Entgleisungen dieses Gleichgewichts mit Gewebspathologien assoziiert sind. Innerhalb der Zelle ist das Zytoskelett der wichtigste Modulator der messbaren Zellmechanik. Brustkrebs ist die häufigste bösartige Erkrankung unter Frauen. Feste Tumore entwickeln einen hypoxischen Kern, der an Prozessen beteiligt ist, welche mit Krankheitsprogression in Zusammenhang stehen, beispielsweise Angiogenese und Krebszellmigration. Die Aggressivität und das Migrationspotenzial von Krebszellen stehen zudem in engem Zusammenhang mit Umstrukturierungen des Zytoskeletts, welches zu einem weicheren mechanischen Phänotyp führt. In der daliegenden Arbeit wurde die Auswirkung von Hypoxie auf die mechanischen Eigenschaften drei verschiedener MCF-7 Brustkrebszellsubtypen mittels Rasterkraftmikroskopie (AFM) untersucht. Eine reguläre MCF-7-Zelllinie, eine Tamoxifen-resistente MCF-7 Variante und eine Sox2-überexprimierende MCF-7 Variante wurden untersucht. Die elastischen und viskoelastischen Eigenschaften der Zellen wurden mittels mechanischer Modelle berechnet. Hypoxische Kulturbedingungen führten bei allen drei Zelllinien zu veränderten viskoelastischen Eigenschaften, sowie zu einem signifikant weicheren Phänotyp. Morphologisch betrachtet zeigen hypoxisch kultivierte Zellen reduzierte Zell-Zell-Kontakte. Zudem bilden sich lange, spindelartige Membranstrukturen zwischen den Zellen aus. Diese Ergebnisse deuten auf einen Zusammenhang zwischen Tumorhypoxie, Zytoskelett-Umstrukturierung und Krebszellaggressivität hin.

List of Abbreviations and Symbols

Abbreviation	Meaning
ABP	Actin-binding protein
AFM	Atomic force microscope/microscopy
ANOVA	Analysis of variance
BRCA	Breast cancer gene
CLSM	Confocal laser scanning microscopy
CMR	Cell microrheology
CP	Contact point
CTRL	Control
DIC	Differential interference contrast
DMEM	Dulbecco's Modified Eagle Medium
DMOG	Dimethyloxallyl glycine
DP	Detachment point
ECM	Extracellular matrix
EMT	Epithelial-to-mesenchymal
EPO	Erythropoietin
ER	Estrogen receptor
ER(+)	Estrogen receptor positive
ER(-)	Estrogen receptor negative
FA	Focal adhesion
FACS	Fluorescence-activated cell sorting
FBS	Fetal bovine serum
HER2	Human epidermal growth factor 2
HIF	Hypoxia-inducible factor
IF	Intermediate filament
MCF-7	Michigan Cancer Foundation-**7** (cells)
MTC	Magnetic twisting cytometry
N	Number
n. s.	Not significant
OS	Optical stretcher
P/S	Penicillin/Streptomycin
PBS	Phosphate-buffered saline
PHD	Prolyl hydroxylase
PR	Progesterone receptor
PR(+)	Progesterone receptor positive
PR(-)	Progesterone receptor negative
ROS	Reactive oxygen species
SD	Standard deviation
SEM	Standard error of the mean
SERM	Selective estrogen receptor modulator
Sox2	Sex determining region Y box 2
Sox2-OE	Sex determining region Y box 2 overexpressing

SR	Stress relaxation
Tam	Tamoxifen
TamR	Tamoxifen resistant
TNF-β	Tumor necrosis factor β
VE	Viscoelastic
VEGF	Vascular endothelial growth factor
WHO	World health organization
YM	Young's modulus

Symbol	**Meaning**	**Unit**
d	Distance	µm
E	Elasticity, apparent elasticity	Pa
E_1	Compressive modulus 1 (short-scale)	Pa
E_2	Compressive modulus 2 (long-scale)	Pa
E_{inf}	Infinity modulus	Pa
E_{inst}	Instantaneous modulus	Pa
ε	Strain	
F	Force	nN
G	Shear modulus	Pa
k_b	Boltzmann constant	
k_c	Cantilever spring constant	nN/nm
k_m	Measured spring constant	nN/nm
k_s	Sample spring constant	nN/nm
R_c	Radius of contact	µm
t	Time	s
δ	Indentation, deformation	µm
δ_0	Initial indentation/deformation	µm
η_1	Short-scale viscosity	Pa s
η_2	Long-scale viscosity	Pa s
ν	Poisson ratio	
σ	Stress	nN/µm^2
τ_1	Short-scale relaxation time	s
τ_2	Long-scale relaxation time	s

Motivation

Breast cancer continues to be a front-runner in cancer diagnoses and cause of cancer death worldwide. Continuing the efforts in not only applied, but also in basic research maintains relevant. Basic research aims to uncover the fundamental cell biological, molecular, and physical alterations which happen during cancer progression and should contribute to a broader understanding of the processes involved. Mechanobiology is a field which continues to gain relevance as the roles of physical forces for the fate of cells and tissues are being elucidated, put into context of existing knowledge, and inspiring more and new questions to ask.

Cell mechanics by now is a decently established field and many methods exist to explore the material response of biological samples, be it single proteins, single cells, or whole tissues. Thus, the differences in cell mechanics between a healthy cell and a cancerous cell have been studies for many cell types in various ways and for different aspects. However, to my knowledge, which changes breast cancer cells undergo mechanically in response to hypoxia – a condition which cells inside a solid tumor experience – has not been examined. Thus, I focused my research on studying this condition to hopefully contribute a small piece of understanding to a much bigger picture.

1. Introduction

1.1. Breast Cancer

Breast cancer is the most frequently diagnosed form of cancer – as well as the leading cause of cancer-related death – among women worldwide [1,2]. As of December 2020, out of a WHO report conducted via the IARC Global Cancer Observatory, breast cancer has overtaken lung cancer as the most diagnosed cancer worldwide. Out of a global estimate of 19.3 million total new cancer cases in 2020, female breast cancer accounted for 11.7% (2.3 million) of cases [3,4]. Albeit less common, men can develop breast cancer as well. However, male breast cancer (MBC) accounts for less than 1% of all breast cancers and less than 0.5% of all male cancer deaths. Globally, the female-to-male ratio for breast cancer is 122:1, however, differences in ratio between different ethnicities have been observed. Risk factors for MBC are similarly to female breast cancer genetic and environmental factors, however, Klinefelter syndrome (XXY chromosome genotype) presents the greatest risk [5,6]. In terms of prognosis, which is defined as the probability of a certain outcome (such as effect on the quality of life, disease-related complications, pain, or death) occurring within a given time, predictions vary. Overall, the 5-year relapse-free survival chances range from 65–80% and the 10-year overall survival chance from 55–96% [2]. Due to medical advances such as early diagnoses and progress in treatment capabilities, survival rates have improved annually over the past decades for all subtypes and stages of breast cancer to a certain extent. However, in case of several late-stage subtypes of breast cancer, 5-year survival rates can be as low as 20%. Specifically, subtypes which are both estrogen receptor negative and progesterone receptor negative (ER-/PR-) , thus increasingly dissimilar to normal breast tissue, maintain poor prognosis [7]. Nevertheless, around 80% of all diagnosed breast cancer cases are estrogen-receptor positive.

Cancer progresses gradually and is accompanied by a range of alterations in biological processes on several orders of (biological) organization. The molecular, biochemical, and cellular traits shared by most – possibly all – cancer types are summarized as the “hallmarks of cancer” This reflects the fact that tumorigenesis is a multistep process in which each step reflects certain genetic alterations which drive the progression from normal to malignant. Originally, six hallmarks were considered by Hanahan and Weinberg (2000) who coined the term. Those are, as described in their original publication in from the year 2000 self-sufficiency in growth signals, as tumor cells can produce their own growth signals, whereas healthy cells require exogenous growth signaling to proliferate. A second hallmark is the insensitivity to anti-

growth signals, as well as acquiring the ability to evade apoptosis by expression of telomerase. Subsequently, cancer cells acquire limitless replicative potential. Upon rapid increase in nutrient and oxygen requirements, cancer cells start sending out their own angiogenic signals, which induce neo-vascularization into the tumor mass. Lastly, primary tumors ultimately intravasate into the blood stream and extravasate at distant sites where they may form new colonies, so-called metastases [8]. A decade after the original publication, Hanahan and Weinberg (2011) extended their concept by two additional hallmarks. One of those is the reprogramming of the cellular energy metabolism [9]. Normally, cells process glucose to pyruvate first via glycolysis, an anaerobic process, then oxidate it further in the TCA cycle aerobically to CO_2 to convert energy. Only in conditions of low oxygen availability are anaerobic glucose oxidation pathways favored. Cancer cells seemingly favor anaerobic pathways over aerobic oxidation in the mitochondria even in environments of ample oxygen availability. This effect was first observed by German physician Otto Warburg and thus dubbed the Warburg effect [10]. Why cancer cells favor this option is unclear, however, it is hypothesized that Warburg-metabolism effects serve a role in cellular biosynthesis of various intermediates and macromolecules for tissue generation [11]. Additionally, the hypoxic microenvironment leads to upregulation of glycolysis and production of metabolite intermediates which are readily used in biosynthesis [9]. When faced with hypoxia, several cellular responses are triggered, among those pathways mediated by hypoxia-inducible factor (HIF) transcriptional regulators as well as 2-oxoglutarate dependent dioxygenases, which interact with HIFs (*note: the hypoxia-mimetic DMOG used in the experiments for this thesis is a 2-oxoglutarate analogue which stabilizes HIF-1α*). HIFs contribute significantly to the Warburg effect by upregulating glycolytic enzymes and glucose transporters and between substrate, enzymes and products and HIFs, feedback loops enable reciprocal modulation of one another [12,13].

As an enabling characteristic rather than a hallmark of cancer, genome instability and mutation were defined. Normal, non-cancerous human cells replicate DNA with high accuracy and a low error rate. In contrast, cancer cells are gnomically instable and mutate far more readily. The high mutation incidence in both clonal and random mutations of cancer cells has been described as the mutator phenotype [9,14]. The idea of the mutator phenotype was first proposed in 2001 [15]. The most common mutation in tumor cells is of the p53 tumor suppressor gene. Up to 50%-60% of cancers are affected, and in the process mutant p53 not only loses its original function of cell cycle control, but may gain additional oncogenic functions [16,17]. At this time, the hypothesis of cancer-specific mutations was merely speculative [15]. However, with progress made in diagnostic techniques and genome sequencing, more cancer-type specific mutator phenotypes have been identified. For example, mutations in the Ras protein family were often

compounded as found in 30% of malignancies, however which Ras isoform exhibits a mutation was found to be cancer type correlated [18]. In both male and female hereditary breast cancer, mutations in the BRCA gene family are a major player. About 0.25% of the population carry mutations in either BRCA 1 or BRCA2 by family heritage, out of which an estimated 55-65% of women carrying a BRCA1 mutation and 45% of women with a BRCA2 mutation will develop breast cancer by the age of 70 [19–22]. For reference, an estimated 12-13% of women will be diagnosed with breast cancer in their life irrespective of mutations [23]. Another common mutation in breast cancer with an incidence of around 15-30% is that of the erbB-2 gene, which encodes for HER-2 [24]. The relevance of the mutator phenotype and the genetic fingerprints of different cancers lies not only in its diagnostic value, but is also promising with respect to developing targeted therapies [24,25].

The other amendment to the hallmarks is the ability of cancer cells to actively evade immune response. Cancer cells may secrete TNF-β or other immunosuppressant factors to quench the host immune response of natural killer cells or cytotoxic T-cells. Immune evasion can go as far as to cancer cells actively recruiting macrophages and regulatory T-cells [26,27].

1.2. The MCF-7 Cell Line

In 1973, a breakthrough in breast cancer research was accomplished by isolating and establishing the MCF-7 cell line. The cells originate form a pleural effusion of a breast cancer sufferer with metastatic disease and were the first known ER+ and PR+ breast cancer cell line, making it possible to demonstrate and investigate hormone-receptiveness in tumors [28]. Not much later it was shown that the anti-estrogen tamoxifen could inhibit growth of MCF-7 cells, which could later be reversed via the addition of estrogen [29,30]. At the time, the ability to demonstrate that estrogen directly influences tumor growth was a remarkable jump in knowledge. Intrinsically, the MCF-7 cell line is heterogenous in population, due to the cells remaining individual in phenotype (in the form of sub-populations rather than identical clones) even after weeks of continuous subculturing, with populations differing in gene expression, receptor expression and signaling pathways [31]. Yet, a balance of those multiple phenotypes is somehow naturally maintained during progressive culturing, despite differences in proliferation rates of subpopulations, suggesting perhaps some type of signaling cooperation being involved [32]. Nowadays, the MCF-7 cell line is commercially available as a standardized cell line and used worldwide as a model system for ER+/PR+ breast cancer. In fact, the MCF-7 line has been used in breast cancer research more abundantly than any other breast cancer cell line [31].

Tamoxifen is a selective estrogen-receptor modulator (SERM) used as a chemotherapeutic agent and among the first line in treatment for ER+ breast cancer. The most common cause of relapse in breast cancer patients is due to tumors acquiring tamoxifen resistance after initially responding to the drug [33]. Drug resistance generally accompanies malignant cancer progression; however, it happens gradually with a series of biochemical events involved. Particularly for tamoxifen resistance, cellular stemness marker Sox2 overexpression was found to be relevant [34]. Sox2 is a stem/progenitor cell marker and is associated with aggressive ER- tumor and overall increased tumor aggressiveness [35]. Its role in tamoxifen resistance seems to be connected to other signaling pathways such as the Wnt signaling pathway, which, among other things, influences cytoskeletal arrangement and is associated with EMT once signaling becomes abnormal [34,36]. Additionally, tamoxifen resistant cultures contain a higher proportion of stem/progenitor cells and therefore are thought to be more invasive than parental cells [37]. Findings like these suggest pathways such as the Wnt pathway to be attractive future therapeutical targets in cancer treatment and Sox2 levels as a prognostic factor [34].

1.3. Tumor Hypoxia

The solid tumor generally is a heterogenous mass, influenced by many different factors within its microenvironment and containing cells of different properties and derangement level. As indicated before, one of the most influential factors to the solid tumor microenvironment is local tissue hypoxia, typically accumulating within the tumor core [38]. Especially regarding to the cell metabolism, tissue invasiveness and metastatic potential the role of the hypoxic tumor microenvironment is significant. Generally, tumor hypoxia is associated with poor prognosis and worse disease outcome, increased aggressiveness and it co-occurs with metastasis-associated processes like epithelial-to-mesenchymal transition (EMT) [39]. In general, tissue hypoxia occurs when the normal oxygen concentration in a tissue falls below a certain threshold and cells residing within that tissue are supplied with less than the required oxygen to uphold regular pathways. As a result, several metabolic reactions are suppressed, such as those of the respiratory chain (mitochondrial electron transport chain and oxidative phosphorylation) and generally those relying on ATP hydrolyzation [40]. Hypoxia itself induces its own gene expression pattern by promoting the stabilization of hypoxia-inducible factors (HIFs) which act as key players in oxygen-sensitive feedback loops. As such, HIFs modulate the transcriptional up- or downregulation of certain metabolic enzymes and tissue signaling molecules (*see* **figure 1**) [12].

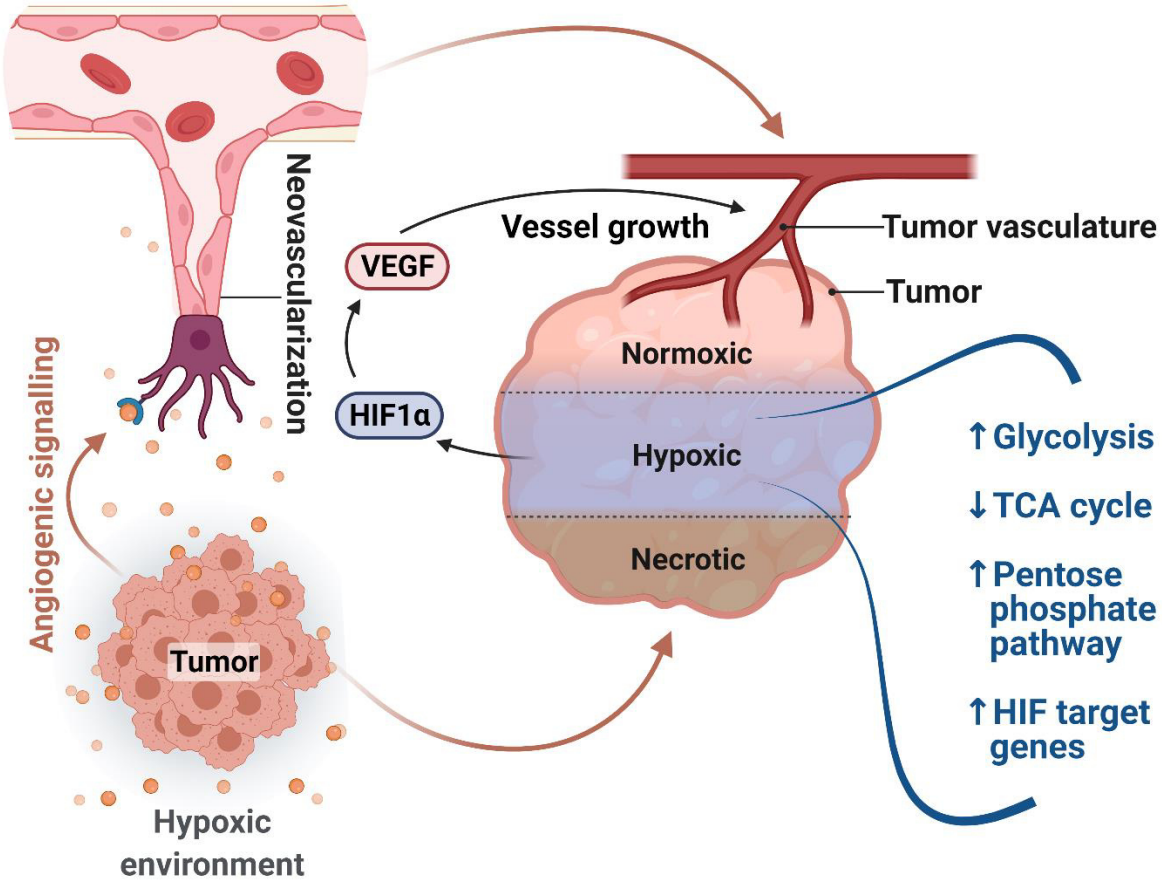

Figure 1: *Schematic tumor with hypoxic microenvironment and hypoxia-associated signalling. Tumor cells send out angiogenic signalling molecules to initiate neovascularization and metabolic pathways are altered Created with biorender.com*

Oxygen tension (pO_2) in normal tissues is typically between 10–80 mmHg, while tumors contain regions of intermediate (0.5– 20 mmHg) and severe hypoxia (<0.5 mmHg) [41]. Within those given ranges, normal and sub-normal oxygen concentrations vary by tissue and organ [42]. What constitutes as hypoxia is not uniformly defined and the idea of a 20% oxygen atmosphere as the definition for normoxia is debated. Rather, levels of "physioxia" are defined per tissue, ranging from 3% to 7.4%, whereas the median oxygenation of untreated tumors has been reported to fall between 0.3% and 4.2% [43] Aside from the actual tissue oxygen concentration, duration of exposure to hypoxic conditions matters. Short term or acute hypoxia is any exposure duration ranging from a few minutes up to 72 h. Conditions like these occur when supply from the blood stream is cut off for at least several minutes. Acute hypoxia is reversible and often leads to cycles of poor oxygenation and normoxia, which is called cycling hypoxia. Both short- and long-term hypoxia are associated with increased radio-resistance in cancer cells, as well as changes in oxidative metabolism, reactive oxygen species (ROS) levels and more aggressive tumor phenotype [43]. Long-term hypoxia is associated with significant increase in DNA damage

and genomic instability, due to disrupted DNA repair machinery. Nevertheless, short-term and cycling hypoxia are thought to represent tumor hypoxia conditions [44,45].

1.3.1. Hypoxia on the Molecular Scale

Hypoxia is toxic to normal cells, however, tumor cells can still grow in hypoxic conditions [39,46]. Solid tumors, although they grow by clonal propagation, are a heterogenous population due to cells at the core of the tumor being in later stages of tumor progression than those at the borders of the mass. The core tends to get crowded over time, leading to local nutrient deficiencies, increased tissue pressure, and poor blood supply [47]. Tumor cells in general tend to have an increased oxygen demand due to higher metabolic rate and proliferation than healthy cells and when competing for supply from the blood stream, cells at the periphery tend to retain an advantage over core tumor cells [48]. Hypoxic signaling induced by hypoxia-stabilized transcription factors is regarded as a main driver of angiogenesis, the process of neovascularization of blood vessels into undersupplied core tumor tissue [43]. The hypoxia-inducible factors (HIFs) are considered the major downstream transcription factor activated in hypoxic conditions and in non-hypoxic conditions by stimuli such as nitric oxide (NO), reactive oxygen species (ROS) cytokines and some G-protein coupled receptors [45]. Out of the HIF subunits, HIF-1α is the one best characterized. Under normoxic conditions, HIF-1α is hydroxylated by HIF-1α prolyl hydroxylases (PHDs) and inhibited by inhibitory proteins containing oxygen-dependent domains [49]. HIF-1α upregulation is the predominant response to short term hypoxic intervals at very low oxygen levels, whereas HIF-2α upregulation is associated with moderate hypoxia at longer time spans [41]. For a long time, HIFs were seen as a master regulator at the top of a metabolic hierarchical pyramid, which gets triggered into activation exclusively by a lack of oxygen [12]. More recently, however, scenarios have been described wherein in tumor models HIFs get stabilized by factors unrelated to tissue oxygenation. For example, metabolite accumulation of TCA cycle intermediates has been found to inhibit prolyl hydroxyl domains (PHDs) and thus stabilize HIFs [50]. Under normoxic conditions, HIF-1α resides in the cytoplasm. Hypoxia induces translocation of HIF-1α from the cytoplasm to the nucleus, where it acts as a transcription factor [45]. HIF-1α target genes are associated with 20 distinct pathways [51], among those genes encoding for glucose metabolism enzymes such as Glut-1, and regulators of vascularization and erythrocyte stimulation like VEGF and EPO, respectively [52]. Further, HIF-1α has been found to be stimulatory for WNT11 expression, which acts as a stimulus for proliferation, migration, and invasion in cancer cells, and upregulates the activity of matrix metalloproteases [53].

In culture, hypoxia can be achieved in several different ways. Specialized incubators exist which regulate the chamber pO_2 and create true hypoxic conditions, however, such chambers can be costly, and during cell handling in routine passage and experiments, hypoxia cannot be maintained. Some chemical mimetics for hypoxia are known and accepted in hypoxia research, such as $CoCl_2$ and DMOG (dimethyloxalylglycine), which stabilize HIF-1α and thus induce hypoxic downstream signaling [45,49,54]. Chemical hypoxia mimetics which act on HIF-1α stabilization are in practice easy to include in cell culture assays and any experiments, which require the cells to spend a significant time outside of an atmosphere-controlled culturing chamber. Chemical mimetics also work well to experiments demanding high repeatability, as their ability to stabilize HIF-1α at a certain concentration has been proven in western blots both directly as well as for upregulation of HIF-1α-related elements [55].

1.3.2. Hypoxia on the Cellular Scale

There seems to be a generally held consensus that hypoxia mediates EMT, enhancement of proliferation and invasion in cancer cells, all of which are strongly linked to tumor metastasis [39,45,56]. Tumor neo-vascularization is a disorganized and imperfect process. Neo-vascularization outside of the context of tumors is a tightly gate-kept process requiring a very certain and defined signaling milieu [57]. In contrast, tumor angiogenesis creates poorly organized and leaky vessels. The rationale is that hypoxic cells at the tumor core signal to the vascularized tumor periphery in response to accumulated acidic anaerobically produced metabolites and vice versa, utilizing lactate as substrate for their oxidative cycle [45,58,59]. However, this hypothesis is not without faults or inconsistencies. Hypoxic cells reside in the interior core of the tumor and would have to migrate through a dense network of vascularized, more normal-like tissue to directly contact blood vessels. Additionally, due to the hostile conditions created by hypoxic environments and metabolite accumulation, hypoxic core cancer cells proliferation rate initially decreases [60], while oxygenated cells at the tumor periphery actively proliferate and are generally under more favorable conditions to metastasize outwards [45]. The proliferative response of cells to hypoxic simulation is not uniform. MCF-7 and other breast cancer cell lines have been described to increase proliferation as a response to hypoxia simulation under certain conditions, whereas other cancer cell types seem to decrease their proliferative rate in simulated hypoxia [61]. At extremely aggressive conditions, some cells may even become apoptotic [45]. MCF-7 cells were also reported to show increased motility in response to hypoxic treatment, strengthening the suggestion that hypoxia increases metastatic potential. Similarly, hypoxia both in culture

and in xenograft mice models promotes EMT in breast cancer cells due to upregulation of proteins modulating the actin cytoskeleton [56,62,63]. For instance, actin invadopodium bundling protein CSRP2, which localizes at actin protrusions and remodels the cytoskeleton, has been found upregulated in several breast cancer cell lines in response to hypoxia, providing strong evidence that hypoxic cells themselves contain migratory potential [64]. Regarding the controversy of cellular escape from the hostile, hypoxic tumor core, in cell culture assays and miRNA-based molecular biology studies it was demonstrated repeatedly that hypoxic cancer cells do in fact have altered or increased proliferative behaviour and increased invasive potential compared to cells growing under physiological oxygen concentration [45,61,65,66].

1.4. Mechanical Forces in Cell and Tissue Biology

Mechanical forces are ubiquitous in biology. They occur on every size scale and on several timescales. For example, for a joint to move, a muscle must contract. For a muscle to contract, muscle fibers – sarcomeres – must spend energy to activate a machinery of proteins to change in conformation. Resulting from the conformational change, these proteins pull against one another and change the shape of the fiber, basically at an instance. The arterial walls sense the shear force resulting from the blood flow through the vessels, and volume changes are registered as circumferential stretch [67]. The laminar shear stress registered by the endothelial machinery triggers a feedback loop for regulating vascular function, shape, and level of vessel inflammation, as the drag force is translated into a biochemical signal [68,69]. In the biology of higher organisms specialized tissues evolved to carry out specialized biological functions. The structural and mechanical properties of the tissue in question depend on its function. Bone, for instance, serves as a rigid support structure for tendons and muscle and thus bones are very stiff (in the GPa range). On the other hand, brain tissue is extremely plastic and constantly reshapes and remodels in learning processes. Thus, it is the softest tissue in the human body, in the range of only tens of Pascals [70,71]. Regarding size, the scale on which mechanotransduction, cellular mechanobiology and protein mechanics act ranges from a few micrometers (µm) to nanometers (nm).

The idea that mechanical forces play an essential role in tissue formation has first been proposed over a century ago [72]. Still, the diverse mechanisms and interplay of cell and tissue structures involved in the ability of individual cells to modulate mechanical forces is quite a way from being comprehensively understood. Yet, there is ample evidence demonstrating mechanical forces, such as stress, traction, shear and pressure as ubiquitous and direct determinants regarding cell and tissue function *in vivo*. Additionally, physical forces play a role in molecular

signaling, cell differentiation, and proliferation, and remain relevant up to complex multi-level processes, such as inflammatory cascades, tissue development and tissue mass homeostasis [73]. Regarding the latter, the role of mechanical forces may reach as far as to play an integral part in human energy metabolism by comprising its inherent and own feedback system dubbed the Gravitostat. Previously, the hormone leptin has been the only known regulator of fat mass, but Gravitostat theory postulates weight loading on the body is being felt by an osteocyte-dependent mechanosensor and contributes to homeostatic body mass and energy regulation [74–76]. On the other hand, the cell is not limited to passively feeling and responding to (micro)environmental mechanical cues but is capable of actively exerting forces on surrounding tissue to shape, modulate and as a means of intercellular communication [77,78]. Regarding the *in vivo* microenvironment of cells, it has been demonstrated repeatedly that cells remodel the extracellular matrix (ECM) via exertion of traction forces, combined with pushing forces of actin protrusions [79,80].

1.5. Role of the Cytoskeleton in Cell Mechanics

Within the cell, the main structure associated with modulating cell mechanics is the cytoskeleton, which is a dynamic intracellular network with the ability to rapidly rearrange [81]. The cytoskeleton consists of the three polymers: actin filaments, intermediate filaments, and microtubules. The cytoskeleton spatially organizes the contents of a cell and confers structure to it, connects a cell to its surroundings, and generates contractile forces. In addition, it reassembles itself to move a cell and change its shape [81]. Actin is the main cytoskeletal protein in the eukaryotic cell. It polymerizes to actin filaments, which are semi-flexible fibers approximately 7 nm in diameter and up to several micrometers in length. Actin filaments form structures of higher order within the cell, such as actin stress fibers or the actomyosin cortex [81,82]. The former are thick, long, parallel bundles of actin which can spread across the whole cell and serve as anchorage points between cells and cells or cells and the extracellular matrix. The latter is a gel-like meshwork made of actin together with myosin and actin crosslinkers, situated below the cell membrane serving roles in cell shape, cell migration mechanical support, signal transduction and anchorage of some membrane-bound proteins [82]. The different actin supramolecular structures are facilitated by a diverse set of actin-binding proteins, leading to different cross-linking geometries, interaction with adhesion molecules such as integrin, and connection to other cell compartments. Intermediate filaments (IFs) are cytoskeletal structures formed by several different IF proteins encoded on at least 65 different genes. Some examples include vimentin, desmin, nestin and to some extent, keratins [81]. They are diverse in structure

variety in their primary structure and often carry cell type-specific roles. Cytoplasmic intermediate filaments play a vital role in regulating cell shape and mechanical integrity. Their ability to associate with adhesion receptors such as cadherins and integrins exposes them directly to the forces a cell is exposed to in its microenvironment. Consequentially, post-translational modifications and remodeling of the cytoskeleton impacts signal transduction and cell behavior [81]. Microtubules are the third major structure of the cytoskeleton. They form dynamic polymers of tubulin-proteins and serve functions in intracellular organization, organelle trafficking and chromosome segregation. They grow and shrink via rapid tubulin polymerization and depolymerization and actively engage in cell mechanics by pushing or pulling against loads. Several conformations of tubulin subunits exist which dictate their role in mechanics, cytoskeleton dynamics and forge generation [83]. Different microtubule-associated proteins associate specifically with different tubulin conformations, adding a level of detail and organization within cell compartmentalization and dynamics [83,84]. Tubulins have also been found to influence each other in their conformation, giving rise to an intracellular structural system capable of long-range force interactions [83]. Aside from provision of directionality for intracellular transport and long-range force transmission, microtubules modulate chromosome segregation in cell division, by generating forces on the piconewton (pN) scale to align the chromosomes and pull them apart [85]. To facilitate this, "molecular motors" – motor proteins capable of switching in conformation to move along a tubulin filament by dynamic binding and unbinding – slide tubulin filaments against one another to generate contraction or extension of the machinery. Unsurprisingly, errors in this process can have detrimental consequences for the genetic integrity of the daughter cells. Consequences like genomic instability, mutations, birth defects and cancer may arise lest the cells are rendered inviable [86].

In terms of measurable cell mechanics, the key role often gets ascribed to actin filaments and the actomyosin cortex, for which many models to describe their structure and response exist [87]. Aside from the cytoskeleton, cellular adhesion plays a role in cell mechanics. Cytoskeletal structures at and around the borders of a cell facilitate attachment to substrate, neighboring cells, or ECM. Namely, actin filaments link to focal adhesions at cell–substrate contact sites and to adherens junctions at cell–cell contact sites, where they exert contractile forces by complexing with the motor protein myosin II and push the plasma membrane forward by polymerizing towards a certain direction [88]. Further, they act as cellular mechanosensors for tensile forces, which induce and reinforce stress fiber formation in adherent cells, leading to changing affinities for some associated molecules, like integrins [89].

1.5.1. Actomyosin Cortex

Out of all the structures of the cytoskeleton, the actomyosin cell cortex has been identified as a main contributor to the elastic response of the cell [87,90]. The cell cortex is a thin (literature values vary, but ranging from as little as 20 nm to as much as 1000 nm [91,92], with a mean thickness often reported between 100-300 nm [92,93]) layer of actin fibers, cross-linked by different actin-binding proteins (ABPs) into a gel-like meshwork. The cortex is attached to the cell membrane, thus conferring shape and structure to the cell [92]. Within the mesh, myosin motors exert contractile forces. The cytoskeletal components undergo rapid turnover, permitting dynamic remodeling and network rearrangements on the timescale of seconds [94]. This allows the actomyosin cortex to be both mechanically rigid as well as highly plastic.

As one of its major functions, the cell cortex resists external mechanical stresses while opposing intracellular osmotic pressure [95]. Interestingly, the actin filament is incredibly well conserved across different species and even across kingdoms. It has essentially remained unchanged over a billion years [96]. As for the arrangement of the network itself, one study has found the mesh size of the actomyosin cortex to be classifiable as polygonal on two area scales, a coarse- and a fine-grained mesh [97]. Other research deems the structure to be more akin to a fractal-like self-similar network [98]. When a cell changes its shape in instances of e. g., mitotic cell rounding or cell body retraction during migration, the actin cortex drives those cell deformations via precisely controlled localized changes in tension [99,100]. Cell deformation typically requires changes in cell surface area into either direction. These changes require interplay between cortex contractions and membrane mechanics. The Membrane- and actin-filament tension is facilitated by different myosins, which generate stress via ATP hydrolysis [101,102]. Different models for myosin-mediated actin cortex contractibility have been established. Some predict myosin as a linker of multiple individual actin fibers with the ability of pulling them in towards, and out from each other. Others hypothesize single filaments to be associated with single myosin units, which, as myosin draws the fiber in on itself, eventually buckles in the middle and breaks and compacts [103]. Additionally, theoretical models provide mechanisms for myosin-independent, actin dynamics-mediated active tension. Between cytoplasmic membrane and actomyosin cell cortex, proteins like the ERMs – erzin, radixin and moesin – interlink these two structures on the filamentous actin and transmembrane proteins and lipids [104]. In structures with high membrane curvature, some of these proteins have been reported to occur clustered and enriched, suggesting they play a crucial role in upholding cell morphology [103,104]. Other research attributes an additional fence-like function to the cell cortex, in which actin filaments partition the cell membrane into a three-tiered domain system with distinct functions, such as raft

domains, signal-transduction domains or domains involved in transmembrane trafficking [105]. Considering the importance of cytoskeleton dynamics for the fate of a normal cell, errors and deregulation in these processes caused by improper arrangement of actin filaments or mutations in cytoskeletal proteins can lead to severe consequences, such as immunodeficiencies, neural disorders, fibrosis and arthritis [106–108].

1.6. Cell Motility, Cytoskeleton, and Cancer

Cell migration is a vital process in tissue biology. Migration occurs in embryonic development, when stem cells differentiate and relocate to their target sites to form tissue and organs, in wound healing, and as part of immune responses. Further, cells can migrate individually – epithelial-like via actin-driven protrusions or mesenchymal-like through integrin-mediated focal adhesions (FA) mediated [109] – or collectively as groups, sheets or chains [110]. Once a tumor cell becomes malignant, successful metastasis strongly depends on invasive potential, angiogenesis and cell migration [111]. Metastasis is the process by which cancer cells migrate from their primary tumor site to distant organs and form colonies as novel lesions. It is a complex, multistep progress, influenced by changes in tissue biochemistry and by biophysical signaling within the tumor microenvironment. It is a complex cascade of active and passive processes, like cells crawling towards blood vessels and being engulfed by leaky vessels respectively, and significantly worsens disease outcome for the patient once it manifests [62]. Why cancer metastasizes is unclear. However, several key signaling pathways mediating collective or individual cancer cell migration have been identified, among those both Wnt and HIF-1α signaling [62,112,113].

Mechanical forces within the tumor microenvironment influence pathophysiology and tumor progression and are critical modulators in disease outcome [114]. At the primary tumor site, abnormal growth of cells in the tissue causes accumulation of cellular- and ECM material, causing the pressure inside the solid tumor to rise. Different stresses in the solid tumor microenvironment (compression, shear, tensile, substrate rigidity) promote mechanotransduction cascades, which directly influence gene expression [115,116]. As a result, intracellular architecture is altered drastically, mediated by actin filament- and microtubule arrangement [117]. Along the way, malignant transformation is accompanied by a progressive loss of tissue integrity. Such perturbations in tissue architecture and loss of structure allow cancer cells to migrate away from their original site and invade surrounding tissue. Further, they have been found to be accompanied by a measurable mechanical phenotype, both on the scale of whole tissue, as well as on a single-cell level [118,119]. For example, malignant progression of

breast cancer cells is generally associated with cell softening [120]. Additionally, malignant breast cancer cells have been found significantly more pliable than their benign counterparts, which is also generally attributed to a loss of organized actin filaments [121]. It is hypothesized that this observed increase in deformability and decrease in stiffness help the cell escape its native environment and move to distant tissue implying importance of cell mechanics alterations for metastatic progression and cancer malignancy [120–123]. Considering these factors, the surge in popularity and recognition the field of cell mechanics has enjoyed in the more recent decades is hardly surprising.

Experimental Approaches to Measuring Cell Mechanics

Today it is widely understood that mechanical forces in cancer progression are more than a by-product of malignancy but play a much more integrated role when it comes to tumor fate. As cell physics research gained traction, many elegant and potent methods of quantifying cellular forces and the mechanical properties of biological materials on different scales have been developed and successfully employed. Among these methods, each retains its own set of inherent strength and drawbacks.

Parallel plate rheology experiments allow studying cell mechanics on a whole-cell deformation level. Parallel plate rheometry allows for deformability (compliance), Young's modulus, stress relaxation and creep functions of individual cells to be measured, however, it requires the cell to be kept in suspension while it is placed between a flexible and a rigid plate [124,125]. The optical stretcher (OS) consists of a dual-beam optical trap which confers a defined mechanical stress on a suspended cell and allows creep compliance (deformation under constant strain) to be measured. The applied forces arise from the differences in refractive index between the cell and the medium, allowing for transfer of momentum from the light onto the cell. As the method is typically integrated in a microfluidics system for ease of cell trapping, a relatively high throughput (upwards of 100 cells/h) can be achieved. However, optical stretching required – additionally to suspended cells – a laser wavelength in the infrared range, which causes heating, thus damage, to the cells [125,126].

Several techniques have been developed for multicellular measurements. For example, cell monolayer rheology (CMR) allows for determination of elastic and shear modulus, as well as creep compliance, of a sparse cell monolayer by trapping the monolayer sheet between a rotational rheometer and rotating the upper plate, which is of glass so deformation can be observed optically. However, as monolayers require some sparsity and depending on the

inherent shape or directionality of the cell, the relevance for confluent monolayers and the reproducibility of force application between cells may be limited [125,127].

Bead-based measurements embed the probe into the cell to monitor some kind of mechanical response. In magnetic twisting cytometry (MTC), a ferromagnetic bead is bound to the surface of a cell and by application of a magnetic field the bead twists and rotates. From the contact geometry and the recorded bead displacement, the cell stiffness can be quantified [128]. Similarly, particle-tracking rheology embeds sub-micrometer sized fluorescent beads into the cytoplasm and nucleus of cells and they are then tracked for their spontaneous movement within the cell. Bead trajectories can be computed and used as the basis of mechanical calculations. Compared to other (non-AFM) methods, bead-based methods allow for adherent cells to be measured and rather than studying mechanics on a whole-cell basis, the sum and average of subcellular structures is measured [129]. However, bead localization within the cell cannot be controlled, so depending on the mechanics of the measured compartments, the result obtained for a single cell may vary strongly [125].

Other methods to address specific questions regarding cell mechanics have been developed, yet some of them require very specific operator expertise as they may rely on in-house builds instead of commercially available, conventional equipment [130–132].

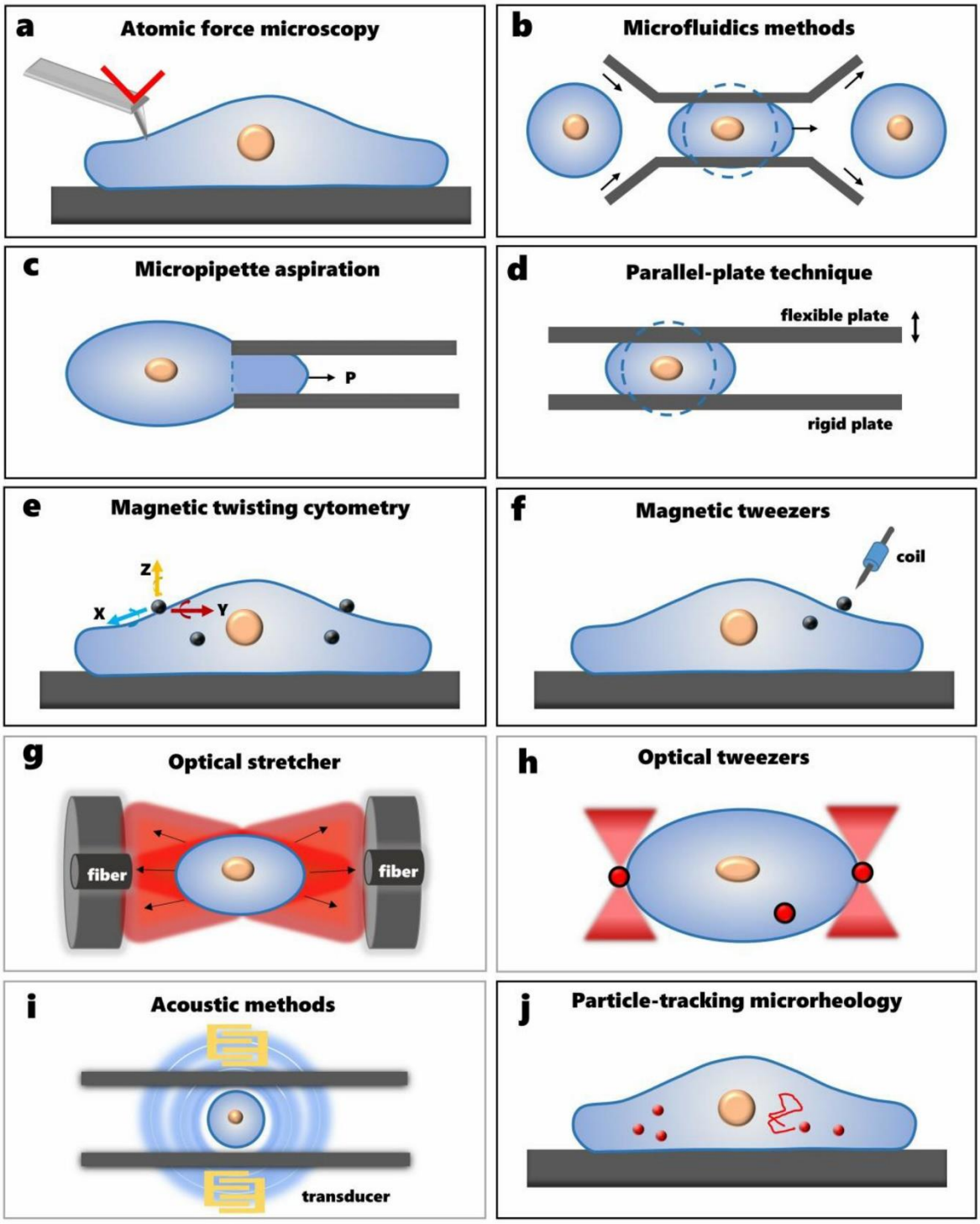

Figure 2: *Comparison of different methods for evaluating cell mechanics, by Hao et al,* [133].

The method applied in this work is AFM-based force spectroscopy. It combines several advantages of the methods discussed. Namely, adherent cells can be measured in a native-like environment. A single cell can be probed on a whole-cell basis, as well as more localized depending on indenter geometry (e.g., sharp tip with a nanometer-sized tip radius versus micrometer-sized spherical particle). The position of the indenter can be precisely controlled with sub-micrometer accuracy, conferring control over which area of each cell is probed.

1.7. Atomic Force Microscopy (AFM)

Atomic force microscopy (AFM), invented in 1986, is a scanning probe microscopy technique with very high spatial and force resolutions, down to sub-nanometer and piconewtons, respectively [134]. Since then, the AFM has secured a place for itself among the methods most used in mechanobiology and cell mechanics measurements, mainly for the possibility to acquire mechanical data in native-like milieus. The AFM is a versatile tool allowing a wide range of data to be acquired from a sample. High-resolution imaging modes optimized for different biological samples have been developed, as well as methods to force-map samples. Additionally, it allows acquisition of different types of force-spectroscopy data.

The AFM is a scanning probe microscope capable of imaging and profiling all kinds of surfaces – including biological surfaces like cells – with nanometer resolution, both in air as well as in liquid. Several modes for imaging are available, like contact mode scanning or tapping mode, in which the scanning probe interacts in different ways with the sample surface to optimize image quality. The imaging process relies on the probe scanning along the surface of the sample in lines, wherein sample-tip interactions arise which are measured and converted into a high-resolution surface profile. The AFM is also a force-spectroscope capable of recording force as a function of z-position or and time. The force resolution spans from piconewton (pN) range to the micronewton (µN) range. Force mapping provides an intersection between imaging and force-spectroscopy, whereby a grid is defined along which the probe moves and acquires a force spectroscopy curve for every point in the grid, yielding a stiffness profile of the whole imaged surface. Within force spectroscopy, simplicity and complexity of measurements can be adapted from simple force cycles consisting only of indentation and retract segments, up to curves with several segments. For instance, pause segments can be set to constant height or constant force holds, replicating stress relaxation and creep experiments, respectively. Experiments can be conducted in temperature-controlled liquid sample, on live cells. The technical flexibility of the AFM permits approximating physiological conditions closely using clever add-ons which have been commercialized by industry leaders.

The AFM itself consists of a voltage-sensitive piezoelectric element, a cantilever in the hundred-micrometer length scale, with an indenter (probe) of specified geometry and size, a laser, and a photodiode. The cantilever backside is coated with a reflective material e.g., gold, which deflects the laser onto a four-quadrant photodiode. When the probe interacts with a sample via attractive and repulsive forces, it bends, and the photodiode reports the resulting vertical and lateral deflection. The cantilever is calibrated at the beginning of an experiment.

Through calibration, all properties of the cantilever are known and from its interaction with the sample, the sample's mechanical properties can be deduced. The force of the interaction can be quantified by applying Hooke's law. As the probe extends towards or retracts from the sample, the cantilever deflection is monitored as a function of the piezo position and the vertical deflection is converted into units of force [135]. By acquiring force spectroscopy data of living, adherent cells, the material response of the cell is recorded as a force-distance (*F-d*) and a force-time (*F-t*) curve.

Parameters such as maximal load, loading- and unloading rate, and pause segment duration can be chosen by the operator and optimized for the experiment and sample. Cantilever choice and design adds an extra layer of flexibility. Cantilevers of different stiffness exist – typically the cantilever stiffness is to be chosen in the range of the sample stiffness – of different shape to optimize signal-to-noise ratio, and with different indenter geometries. The latter include pyramidal, conical, or flat punch tips, as well as spherical or paraboloid indenters. Tipless cantilevers are also available. Those can be used to attach an indenter oneself among others. Further, the cantilever or indenter can be chemically modified to explore different probe-sample interactions [136]. Each segment of a force curve contains discrete information about the sample mechanics. The indentation segment of the approach curve can be fitted with a Hertzian contact mechanics model to determine an apparent Young's modulus (YM, *E*, elasticity). Constant height and constant force pause segments allow derivation of time-dependent mechanical parameters. This is relevant as cells behave like viscoelastic materials due to their complexity. The retract segment contain information about adhesive properties. For example, membrane tethering behavior can be studied, cell-to-cell or cell-to-ECM binding strength can be quantified, and the total work of adhesion can be determined by integrating the force response over the z-distance. Further, the probe can be oscillated in contact with the cell as another way to study microrheology [137–141].

This work focuses on parameters derived from indentation segments and pause segments. A Hertz model modified for a spherical contact geometry was used to derive apparent Young's modulus values from the indentation segments. Stress relaxation experiments were conducted and evaluated via a viscoelastic model. to study indentation segments were used to derive an apparent Young's modulus for the sampled cells. Stress relaxation segments were acquired to study cell viscoelasticity and time-dependent force relaxation. Parameters were calculated using ca contact mechanics model and a viscoelastic model. Normal MCF-7 cells, tamoxifen resistant MCF-7 (TamR) cells and Sox2-overexpressing MCF-7 (Sox2) cells were compared to each

other in this way. Then, each cell line was exposed to a hypoxia mimetic and measured via AFM to study the mechanical changes breast cancer cells undergo in response tumor hypoxia.

2. Materials and Methods

2.1. Cell Culture

MCF-7 and tamoxifen-resistant MCF-7 (TamR) cells were grown in T25 cell culture flasks and cultivated in high-glucose Gibco® DMEM (+ L-glutamine, - Pyruvate) supplemented with 10% FBS and 1% penicillin/streptomycin. Sox2-overexpressing MCF-7 cells (Sox2) were grown in T25 flasks and cultivated in Gibco® DMEM supplemented with 10% FBS and 0.5 mg/mL Puromycin as a selection marker. Cells were cultivated at 37 °C in a 5% CO2 atmosphere and 95% relative humidity to 80% confluence before passaging. Routine passaging was done 2-3 times per week, with TrypLE™ Express as a detachment reagent and a centrifugation step after detachment reagent inactivation. Sub-cultivation ratios ranged from 1:3-1:6 depending on cell type. Cells were kept in culture for no longer than 12 weeks on provider recommendations to avoid phenotype changes. All cells were kindly gifted by Dr. Maria dM Vivanco of CIC Cancer Heterogeneity bioGUNE laboratory in Bilbao, Spain.

2.2. Sample Preparation and Hypoxic Treatment

For AFM measurements, cells were grown on 24 mm borosilicate glass coverslips. Before seeding, coverslips were cleaned with 70% ethanol, dried with N_2, and oxygen-plasma cleaned for 60 seconds. After plasma cleaning, coverslips were immediately transferred into a sterile F-bottom cell culture 6-well plate and submerged in 1x PBS to promote retention of surface functionalization. Cells were harvested and seeded in their respective cultivation medium to a density of 1×10^5 cells per well. Floating glass coverslips were gently pressed to the bottom using a sterile pipette tip. Samples were incubated at 37 °C, 5% CO_2 and 95% humidity for 24 h before conducting measurements.

For hypoxia-mimetic treatment, cells were cultivated with 1 mM dimethyloxalylglycine (DMOG, Sigma-Aldrich; dissolved in MilliQ ultrapure water) for 24 h prior to measurements. For MCF-7, additional treatment times of 48 h and 72 h were conducted. DMOG is a prolyl 4-hydroxylase (P4H) inhibiting chemical which stabilizes HIF-1α, thus mimicking the cell

physiological response to hypoxia. Sample incubation conditions were analogous to those of untreated samples. DMOG concentration was chosen according to literature suggestions [49] and pre-testing concentrations in a 6-well plate.

2.3. Phase Contrast Microscopy

Cells were seeded at a density of 100.000 cells/mL in culture medium (DMEM (Gibco®), 10% FBS, 1% P/S for MCF-7, TamR, 0.5 mg/mL puromycin for Sox2) in 6-well culture plates. For each cell line, untreated controls, and a hypoxia-treated samples (1 mM DMOG) were prepared and incubated for 24 h. For MCF-7, additional timepoints of 48 h and 72 h were prepared. Phase contrast images were acquired with a Nikon Eclipse TE2000-S Phase Contrast Polarization Fluorescence Inverted Microscope coupled to a camera. For MCF-7 control versus hypoxia images, a Plan Fluor 10x/.30 Ph1 DL objective was used, for all other images, a Plan Fluor ELWD 20x/0.45 DIC L objective was used. Images were adjusted for brightness and scale bars were added with FIJI (ImageJ) software.

2.4. AFM Measurements

2.4.1. Experimental Set-Up

Atomic force microscopy measurements were conducted with a JPK Nanowizard® III (JPK BioAFM by Bruker, Germany) containing a long-range piezo CellHesion® module (JPK, Bruker) mounted on an inverse optical microscope (Axio Observer Z1, Zeiss). To reduce noise in the curves, an anti-vibration table was used. To approximate culturing conditions, samples were washed and then mounted into a temperature-controlled liquid-sample chamber in Leibovitz's L15 serum-free, CO_2-independent microscopy medium and measured at 37 °C.

Silica nitride tipless NP-O cantilevers (cantilever B, Bruker) with a nominal spring constant of 0.12 N/m, a resonance frequency of 23 kHz in air and functionalized with a 10 µm-diameter spherical silica particle were used in experiments (*see* **figure 3**) [142]. Prior to each experiment, cantilevers were treated with UV/ozone for 30 minutes to remove organic residue.

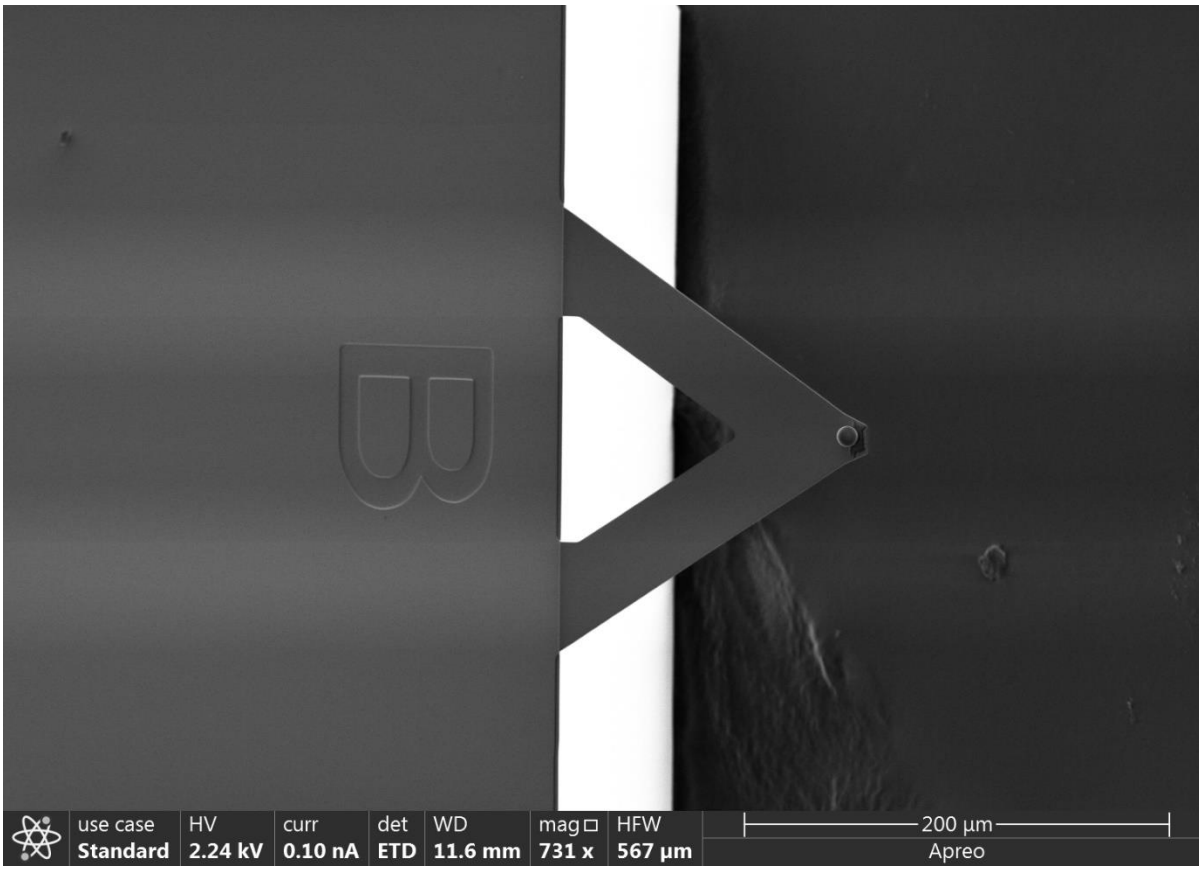

Figure 3: *SEM micrograph of a 10 µm silica particle glued to an AFM cantilever. Image acquired by Jacqueline Friedmann and Andreas Weber.*

2.4.2. Calibration

Before every cell experiment, the used cantilever was calibrated. To determine the spring constant via application of the equipartition theorem, thermal tuning was performed [143]. To determine sensitivity, a force-distance curve was acquired on a standard microscopy glass slide and a linear function was fit onto the contact segment of the curve. The interaction of the sample with the cantilever is measured as the bending of the cantilever in response to attractive/repulsive forces. The cantilever is considered an ideal linear elastic spring of constant (k_c), therefore the bending z is proportional to the applied force F

$$F = k_c \times z. \qquad \textbf{Equation 1}$$

The bending is recorded as a change of the position of the deflected laser point on the photodiode (*see* **figure 4**). As glass can be approximated as infinitely stiff relative to the cantilever and is not indented, only the bending of the cantilever is seen in the curve, thus

allowing derivation of its own mechanical properties. The sensitivity readout is given in nm/V, meaning a certain deflection of the laser on the photodiode is recorded by each nanometer Z-position. For this value to be converted to a force, the spring constant of the cantilever must be determined. To do that, the cantilever is vibrated freely away from the surface under the thermal noise of the system. The spring constant is determined subsequently by applying the equipartition theorem

$$\frac{1}{2}k_c\langle \Delta z_c{}^2\rangle = \frac{1}{2}k_bT. \qquad \textbf{Equation 2}$$

In **equation 2**, k_b is the Boltzmann constant, T the temperature of the system system and z_c the vertical oscillation of the cantilever. The calibration step allows defining the cantilever's mechanical properties precisely. Thus, the mechanical properties and force response of the samples can be derived by monitoring its interaction with it, by

$$\frac{1}{k_m} = \frac{1}{k_s} + \frac{1}{k_c}, \qquad \textbf{Equation 3}$$

where k_m is the measured stiffness and k_s the sample stiffness.

Each calibration was performed according to these steps in air, and then in liquid on a cell-free area of the sample surface. **Figure 4** and **figure 5** show schematic force-distance curves acquired on glass in air and in liquid respectively with the linear fit for sensitivity calibration. **Figure 6** shows a thermal noise spectrum fitted with a Lorentzian function to determine the cantilever's spring constant.

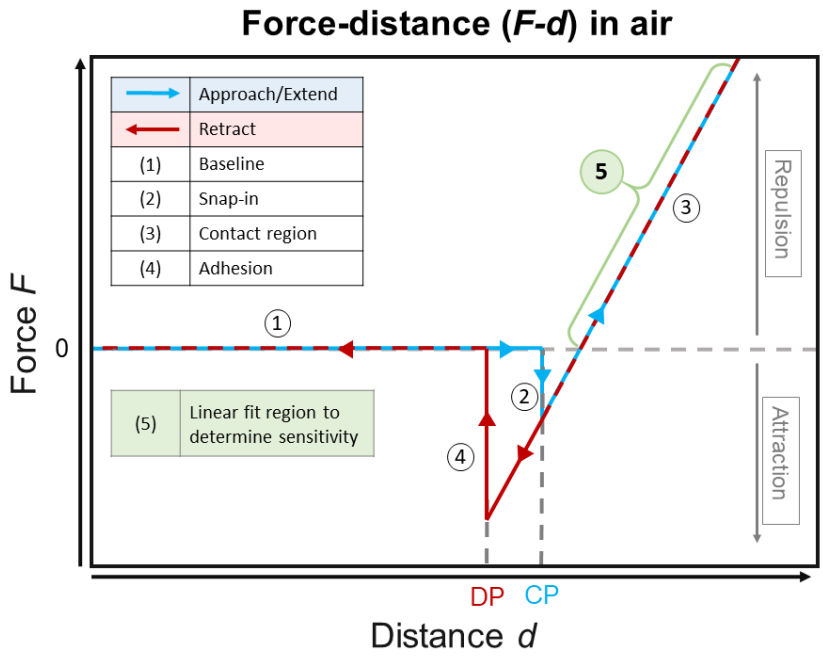

***Figure 4**: Schematic force-distance curve for cantilever sensitivity calibration. Illustration of a force-distance curve acquired on glass in air. Segments marked by the green bracket indicate fit region for sensitivity. CP = contact point, DP = detachment point.*

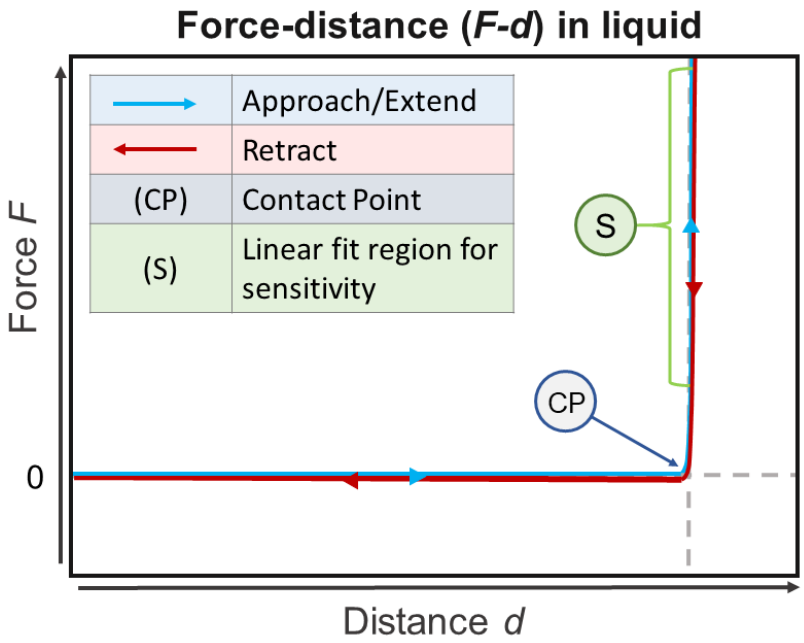

***Figure 5:** Schematic force-distance curve for cantilever sensitivity calibration. Illustrated force-distance curve taken on glass in liquid. Segments marked by the green bracket indicate fit region for sensitivity. CP = contact point, DP = detachment point.*

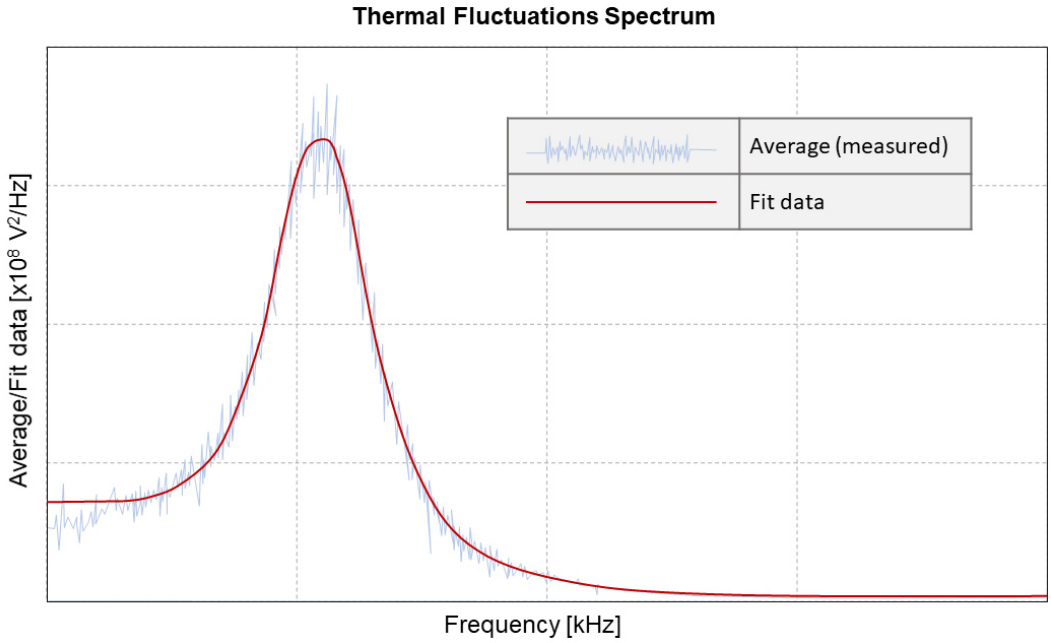

Figure 6: *Illustration of a thermal noise spectrum. The red line represents the fitted Lorentz function and the greyed-out line in the background illustrates the sample data set.*

2.4.3. Force Spectroscopy Measurements

After sample mounting, the system was left for 30 minutes to equilibrate and reduce thermal drift before starting measurements. For cell data acquisition, each individual cell was indented 10 times at a spot above the nuclear region (5 times stress relaxation and 5 times creep, note that creep measurements were not regarded further in this work) and between every cell measurement series, the cantilever was checked for contaminations by pressing on glass. Cells were indented to a nominal force of 1 nN, with 5 µm/s approach speed, a constant-height pause segment (i.e., a stress relaxation segment) of 10 s and 5 µm/s retract speed, to a total curve z-range of 50 µm. A schematic drawing of a stress relaxation force curve is shown in **figure 7**.

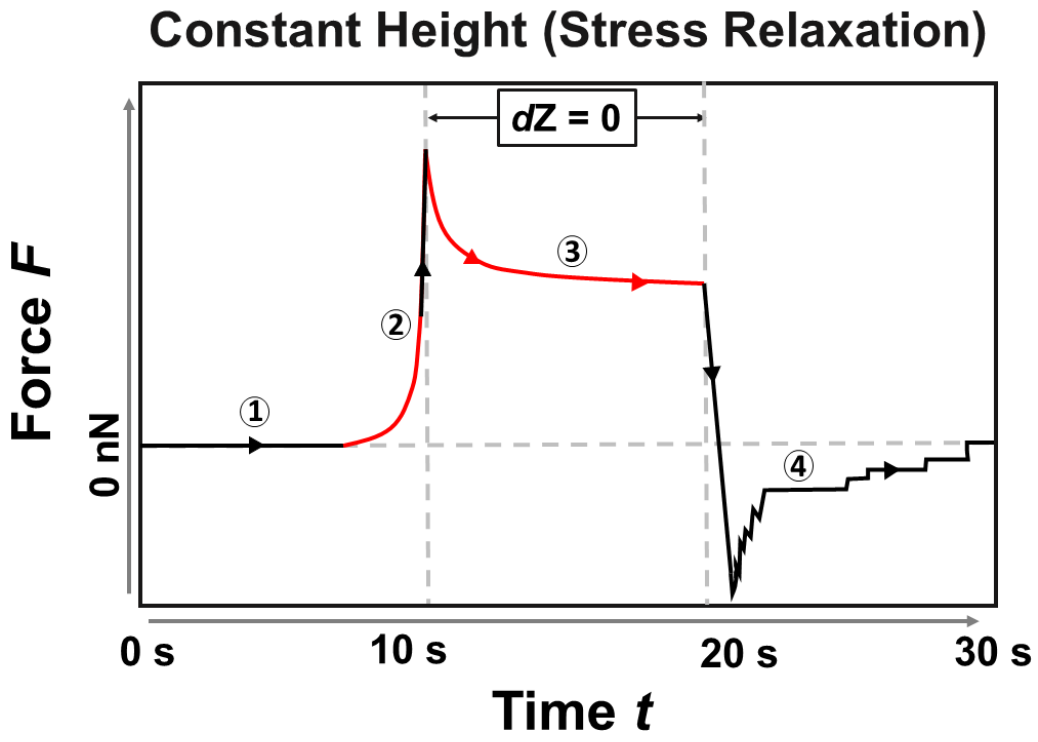

Figure 7: *Schematic representation of a force-time curve with constant height (stress relaxation) segment on a living cell. The baseline of the approach segment is denoted by (1), the contact region up to the nominal set force is (2), with the red part of the indentation segment showing the region of the Hertzian fitting. On the pause segment (3), the red line shows the bi-exponential decay fitting and (4) represents the retract segment with stepwise membrane tether rupture events.*

A sampling rate of 1024 Hz was used for approach and retract segments and one of 512 Hz for pause segments. A single sample was measured for a maximum of 4 h, as experience from previous studies shows that cells remain stable and unchanged within that time frame [144], and a minimum of two samples were measured for each condition, yielding 30-50 cells per condition.

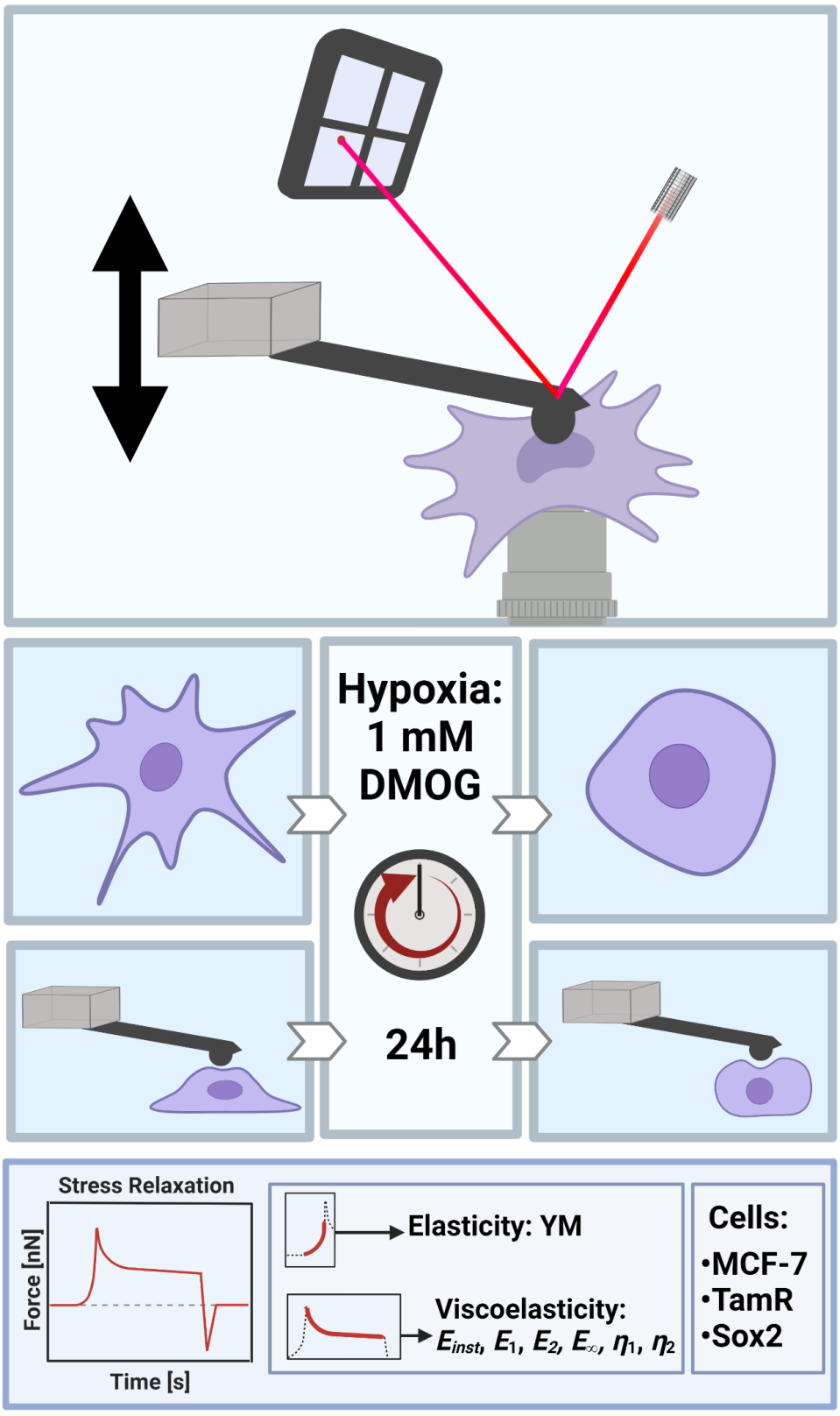

***Figure 8**:Schematic overview of the hypoxia AFM experiments. The top panel shows a typical AFM setup for cell mechanics, the middle some of the morphological changes a cell might undergo upon treatment and the bottom panel indicates which parameters may be derived from a force spectroscopy readout.*

2.5. Data Evaluation

2.5.1. Elastic Properties

The elastic properties of a sample are found in the approach segment of the recorded curve, more precisely in the region of the approach segment in which the probe indents the sample. Thus, the approach segment is the one on which operations are performed to derive elastic data, such as the apparent Young's modulus. Here, the term *apparent* Young's modulus is used as cells as a whole are viscoelastic bodies and the Young's modulus is an elastic property. Additionally, factors such as the substrate stiffness influence the measured elastic modulus. However, for apparent Young's moduli determination, evaluation criteria and boundaries are chosen as such that the conditions for elasticity are largely met. For example, assumptions of linear elasticity, infinite isotropic half space samples, a parabolic contact profile, and small strains below 10% of sample height are made [142]. In continuum mechanics, stress is a quantity arising from the internal forces the particles in a material exert on each other. For uniaxial normal compression – e.g., a cantilever pressing onto a cell – the resulting stress σ is the force over the area,

$$\sigma = \frac{F}{A}. \qquad \textbf{Equation 4}$$

Strain describes the material deformation when force is applied to an object. The strain ε can be expressed simply as a change in length l in respect to the starting length l_0,

$$\varepsilon = \frac{\Delta l}{l_0}. \qquad \textbf{Equation 5}$$

The Young's modulus E expresses the ratio of uniaxial stress to proportional change in length,

$$E = \frac{\sigma}{\varepsilon}. \qquad \textbf{Equation 6}$$

Force-spectroscopy curves were extracted as text files using JPKSPM Data Processing software (Bruker) and imported into R. There, the data was evaluated employing the "homebuilt" R software *afmToolkit* by Benitez et al. 2017 [145]. Contact and detachment points are determined mathematically by the software and the baseline is subtracted [146]. Subsequently, the indentation is calculated by correcting for the cantilever bending, and a contact-mechanics model is fitted

onto the indentation segment of the curve. Only the first 500 nm of indentation are taken into consideration for fitting to minimize artificial increase of the apparent Young's modulus by substrate effects and to remain within the approximate range of the actin cortex, the main contributor to cell elasticity. For shallow indentations <10% of the sample height, the basic assumptions required for validity of the model of linear elasticity, isotropy and approximating the cell as an infinite half-space are also met [147]. To approximate the mechanical properties of the samples, the Sneddon extension of the Hertz model for ideal linear elasticity is used. Due to the contact profile between the indenter and the cell, the equation for a paraboloid indenter is used,

$$F = \frac{4}{3}\sqrt{R_c}\,\frac{E_{\text{app}}}{1-\nu^2}\delta^{\frac{3}{2}}. \qquad \textbf{Equation 7}$$

Equation 5 yields the apparent Young's modulus E_{app} of the cells. R_c is the radius of the spherical particle, δ the indentation and ν the Poisson ratio, which is assumed to be $\nu = 0.5$, thus considering the cells to be fully incompressible. To note, while a spherical particle was used as an indenter probe, apparent Young's moduli are calculated with a formula for a paraboloid contact profile rather than with one for a spherical one, as given the very shallow indentation range of the fitting (only 5% of the particle diameter) the contact profile is more readily approximated as a paraboloid profile.

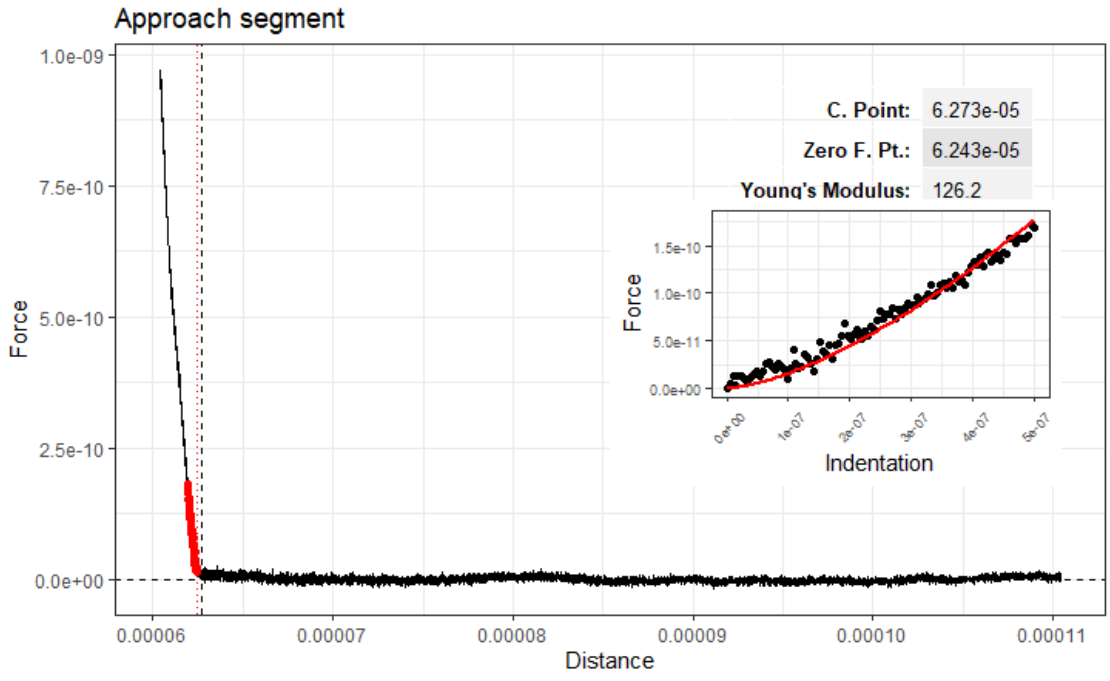

***Figure 9**: Young's modulus fitting performed by the R afmToolkit over the first 500 nm indentation. Data taken from MCF-7 72h DMOG-treated cell.*

Figure 9 shows a Hertzian fit of the data over the first 500 nm of indentation of a force-distance curve acquired on a cell. Out of every data set, at least 10 curves were selected at random and checked for quality of fit. If needed, parameters for contact point detection were adjusted. For subsequent data analysis and graphical representation, Young's moduli fittings with $R^2 > 0.85$ were chosen. Outliers were determined via Grubb's testing and visually via QQ-plots and removed.

2.5.2. Viscoelastic Properties

Cells are complex in structure and behave as viscoelastic bodies [142]. That means, under a given stress or strain, cells will react in a time-dependent way. Classically, stress relaxation- and creep-experiments are performed in material science to determine the time-dependent response of viscoelastic materials. In stress relaxation experiments, the height of the indenter and therefore the strain is kept constant while the force response of the material is recorded as a function of time. In creep experiments, the stress, so the applied force is kept constant, while the Z-axis-deformation of the sample over a given time is recorded. According to the behavior of the material, a mechanical model which best fits the experimental data is chosen to derive further parameters. Different models exist which describe materials with certain properties as serial and parallel arrangement of elastic spring and viscous dashpot elements.

Alternatively, models such as the 'spring-pot' model are used by applying power-law rheology models, for which a single empirical power coefficient is determined. This allows for conclusions about the fluidity of the material are drawn based on the range the power coefficient falls into. While compared to some classical continuum models power law models tend to fit especially cell mechanics data well, the power coefficient as an empirically derived number gives rise to physically unintuitive units.

Here, stress relaxation experiments were conducted by loading the cell to a nominal force of 1 nN and keeping the applied load constant for 10 s. Due to the good quality of fit to the data across the full relaxation spectrum as well as the relative simplicity of the model, the force response of the cells was evaluated by use of a 5-element Maxwell model (Zener's model). That is, a generalized Maxwell model with a spring in parallel with two spring-dashpot (Maxwell) elements was used (*see* **figure 10**) [144].

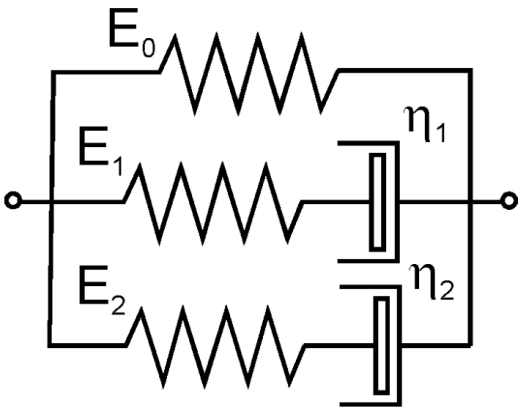

Figure 10: *Two-element Maxwell model (Zener's model) with a spring in parallel with two Maxwell elements.*

The ratio of stress σ to strain ε can be expressed in the Laplace domain as the shear modulus $\tilde{G}$

$$\frac{\tilde{\sigma}}{\tilde{\varepsilon}} = 2\tilde{G}(s),$$

Equation 8

which is connected to the Young's modulus in the Laplace domain $\tilde{E}(s)$ via

$$\tilde{G}(s) = \frac{\tilde{E}(s)}{2(1+\nu)}.$$

Equation 9

Under stress relaxation conditions, **equation 9** can be combined with the Hertzian **equation 8** for determining Young's moduli and approximated with a Heaviside step function *H*(t),

$$F(t) = C * \frac{E(t)}{1-\nu^2} H(t),$$

Equation 10

Where *C* is a geometric constant depending on the contact geometry between indenter and sample, as described by **equation 8**. Transforming the combined equation from the time domain into the Laplace domain and substituting $\tilde{G}$(t) for $\tilde{E}$(s) yields **equations 11** and **12**.

$$\tilde{F}(s) = C * \frac{1}{1-\nu^2} * \frac{\tilde{E}(s)}{s},$$

Equation 11

$$\tilde{F}(s) = C * \frac{2}{1-\nu} * \frac{\tilde{G}(s)}{s},$$

Equation 12

A solution for the viscoelastic model is obtained by transforming **equation 12** back into the time domain. The analytical solution for $\tilde{G}$(t) in a generalized Maxwell model is described by an empirical Prony series in the Laplace domain,

$$\tilde{G}(s) = G_{\text{inf}} + \sum_{i=1}^{N} G_i \frac{\tau_i s}{1 + \tau_i s}, \qquad \textbf{Equation 13}$$

with **equation 14** describing the relaxation time τ as a ratio of the viscosity η and the modulus of the spring G.

$$\tau_i = \frac{\eta_i}{G_i}, \qquad \textbf{Equation 14}$$

G_{inf} is the equilibrium shear modulus and an instantaneous modulus, G_{inst}, is given by a sum of the spring moduli and the equilibrium modulus as in **equation 15** and **16**, where Equation 12 is a time transformed version of equation 13.

$$G(t) = G_{\text{inf}} + \sum G_i * e^{-\frac{t}{\tau_i}}, \qquad \textbf{Equation 15}$$

$$G_{inst} = G_{inf} + \sum G_i. \qquad \textbf{Equation 16}$$

Finally, the **equation 15** for a two element Maxwell model can be combined with **equations 9** and **12** (transformed into the time domain) and the constant C as in **equation 22** to yield

$$F(t) = \frac{C}{1-\nu} * \left(E_{inf} + \sum_{i=1}^{2} E_i * e^{-\frac{t}{\tau_i}} \right). \qquad \textbf{Equation 17}$$

Practically, stress relaxation segments are fitted by the R *afmToolkit* with a bi-exponential decay function,

$$F(t) = A_0 + A_1 * e^{-\frac{t}{\tau_1}} * A_2 * e^{-\frac{t}{\tau_2}}, \qquad \textbf{Equation 18}$$

using a Levenberg-Marquardt least-squares algorithm for non-linear fitting (*see* **figure 18**), yielding two distinct relaxation times, τ_1 and τ_2, and compressive parameters A_0, A_1 and A_2.

From the values derived by fitting, compressive moduli can be calculated based on the principles of **equations 19 – 22** as,

$$E_{inf} = \frac{A_0}{2C}, \qquad \textbf{Equation 19}$$

$$E_1 = \frac{A_1}{2C}, \qquad \textbf{Equation 20}$$

$$E_2 = \frac{A_2}{2C}, \qquad \textbf{Equation 21}$$

$$E_{inst} = E_{inf} + E_1 + E_2\,, \qquad \textbf{Equation 22}$$

and viscosities as **equations 23** and **24,**

$$\eta_1 = E_1\tau_1, \qquad \textbf{Equation 23}$$

$$\eta_2 = E_2\tau_2. \qquad \textbf{Equation 24}$$

The geometric constant C needed for calculating the compressive moduli is calculated from the indenter particle radius R_c and the initial cell deformation δ,

$$C = \frac{4}{3}\sqrt{R_c\delta_0^3}\,. \qquad \textbf{Equation 25}$$

In this model, stress relaxation of a cell is considered to be happening on two distinct time scales. A short-scale relaxation time, which is thought to correspond to membrane- and cytoplasmic response, and a long-scale relaxation time, about a factor 10 of the short-fold, which is considered to arise due to cytoskeleton rearrangements. In this fashion, E_1 and η_1 can be considered part of the membrane response, while E_2 and η_2 correspond to actin filament rearrangement, the actomyosin cortex, and active force response [141].

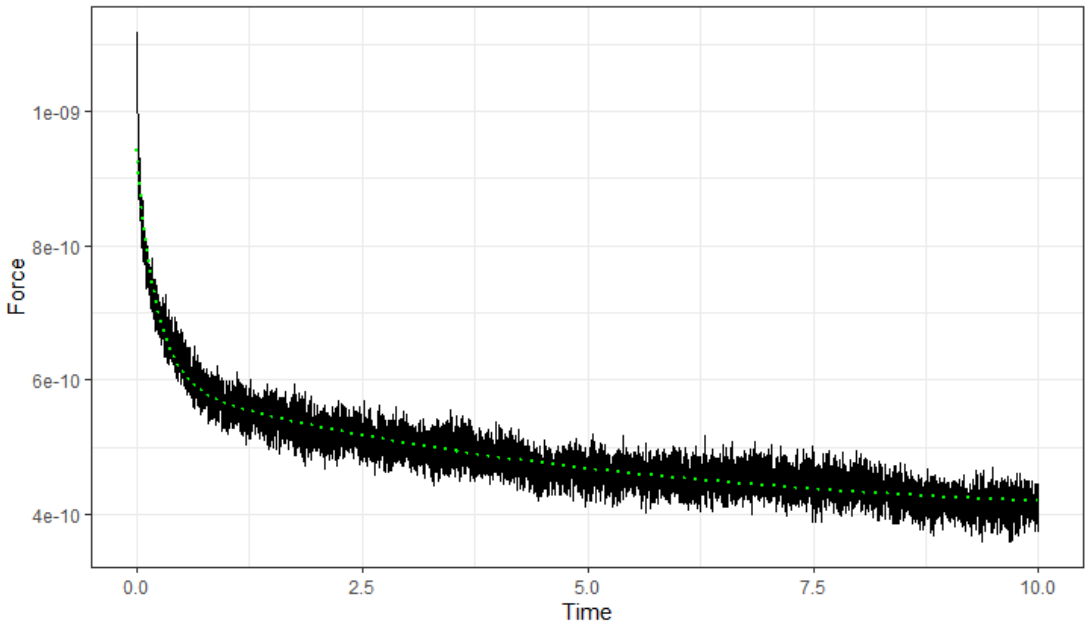

Figure 11: *Biexponential decay fitting performed by the R afmToolkit over the 10-second stress-relaxation segment. Data taken from MCF-7 cell.*

2.5.3. Statistics

For statistical analysis, the software Origin Pro 2018 (OriginLab, USA) was used. Outliers were detected via Grubbs testing and removed. Significances were determined via ANOVA. Levels of significances are indicated as '***' for $p < 0.001$, '**' for $p < 0.01$, '*' for $p < 0.5$ and 'n.s.' for non-significant.

All box plots show boxes ranging from the 25^{th}-75^{th} percentile and whiskers ranging from the 5^{th}-95^{th} percentile. Outliers are not shown in the plots. For histograms, bin size is kept constant per stacked plot and condition. Histograms showing Young's moduli were fitted with a log-normal distribution curve, while histograms showing indentations were fitted with a normal distribution.

3. Results

In this work, the three examined cell lines are mechanically compared directly to each other, and in terms of changes in mechanics under hypoxic culture conditions.

3.1. Comparison of the Cell Lines

3.1.1. Cell Morphology

Morphologically, Sox2 overexpressing cells appear the most distinct of the three cell lines. While MCF-7 and TamR are morphologically and visually hardly distinguishable in culture, Sox2-overexpressing cells appear more elongated and slightly less spread-out. Further, they show alterations in patch formation (*see* **figure 12**), which is especially evident closer to confluency. Patches appear relatively more often in a more "linear" fashion, meaning cells at low densities favoring a patch growth with only two neighbors per cell on either side as opposed to TamR and MCF-7, which favor more classical epithelial-type, clustered, round patches (*see* **figure 12**).

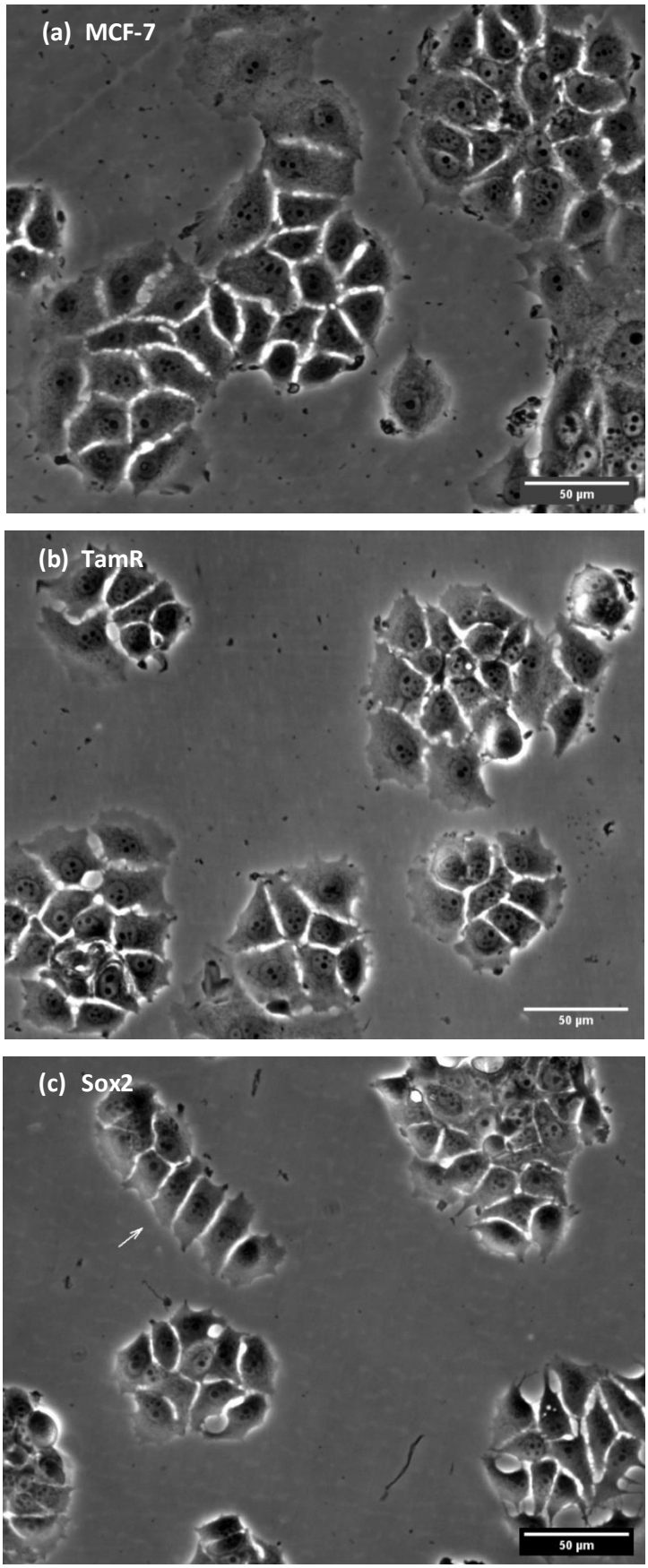

Figure 12: *Phase contrast microscopy images of the three cell: (a) shows MCF-7 cells, (b) shows TamR cells and (c) shows Sox2 overexpressing cells. The arrow in (c) indicates the linear-shaped patches Sox2 cells seem to favor. Note that backdrops have been added to the scale bars in (a) and (c) to increase contrast and enhance visibility.*

3.1.2. Elastic Properties

Tamoxifen-resistant MCF-7 cells (TamR) appear significantly softer than normal MCF-7 cells, while stem-cell marker Sox2-overexpressing MCF-7 cells (Sox2) appear stiffer (*see* **figure 13**). Compared to normal MCF-7 cells, tamoxifen-resistant cells show a mean decrease in apparent Young's modulus by nearly 40%, while Sox2-overexpressing cells seem to be stiffer by just over 20%. The mean maximum indentation at a set force of 1 nN increases by roughly 35% for TamR and decreases by 12.5% for Sox2 in comparison to MCF-7. Sox2-overexpressing cells parameters show the largest spread in all measured and derived values. In contrast, TamR cells and MCF-7 cells show a less spread distribution in values.

Table 1*: Apparent Young's modulus and maximum indentation (at 1 nN load) values for MCF-7, TamR and Sox2.*

E_{app}	***N***	***Mean [Pa]***	***SD [Pa]***	***SEM [Pa]***	***Median [Pa]***
MCF-7	358	242.5	118.5	6.3	213.6
TamR	168	148.1	90.1	7.0	125.9
Sox2	185	297.4	159.7	11.7	253.0
δ	***N***	***Mean [µm]***	***SD [µm]***	***SEM [µm]***	***Median [µm]***
MCF-7	358	1.04	0.36	0.02	0.99
TamR	168	1.40	0.36	0.03	1.38
Sox2	185	0.91	0.31	0.02	0.85

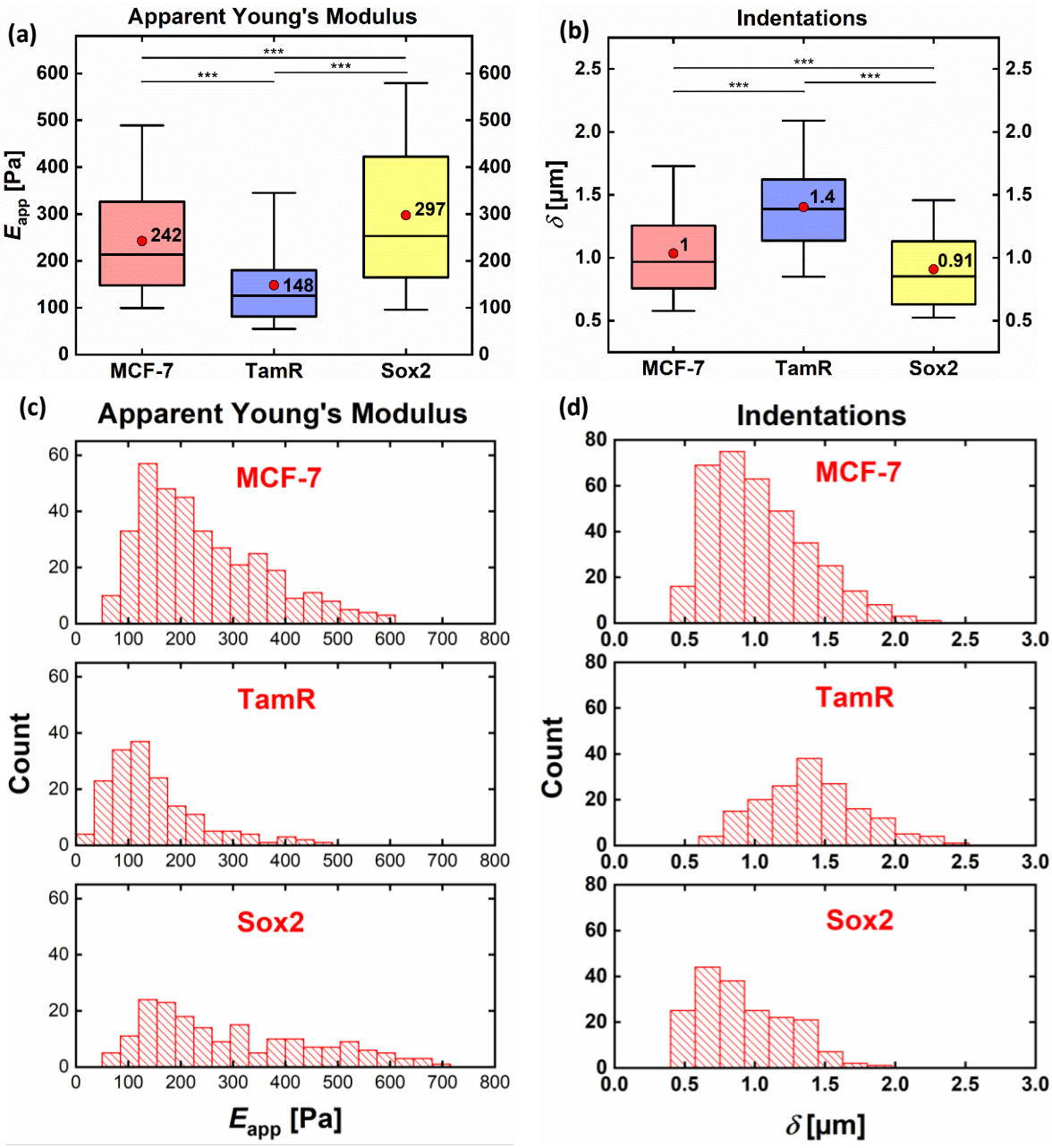

Figure 13: *Comparison of elastic properties of the three cell lines used. Apparent young's moduli are shown in (a), with a 25-75 box and 5-95 whiskers. The mean value is indicated by the red dot and the mean values are shown rounded to 3 significant digits. In (b), apparent young's moduli are shown in respect to their stiffness distribution. Panel (c) shows maximal indentations at 1 nN load, means are indicated by the red dot and rounded, box parameters are analogous to (a). In (d) distributions for indentation profiles are shown. Significance is indicated as '***' for $p < 0.001$, '**' for $p < 0.01$, '*' for $p < 0.5$ and 'n. s.' for non-significant. Plots show no outliers.*

3.1.3. Viscoelastic Properties

Stress relaxation experiments were conducted according to section **2.3. AFM Measurements**. Analogous to the parameters calculated in section **3.1.2. Elastic Properties** from the Hertzian elastic contact model, the compressive moduli calculated from the stress relaxation segments (*see* **figure 14**) indicate a substantial softening of TamR cells compared to MCF-7 cells, and stiffer Sox2-overexpressing cells. The compressive moduli E_{inf}, E_1, E_2 and E_{inst} for TamR are lower by approximately 37%, 36%, 32% and 37% respectively, while those for Sox2 are higher by around 20% for E_{inf}, 40% for E_1, 58% for E_2 and 37% for E_{inst} (*see* **table 3**). The equilibrium modulus E_{inf} indicates the modulus of the cell after the applied force has been relaxed over the system. The instantaneous modulus E_{inst} is the sum of the equilibrium modulus and the moduli E_1 and E_2 and is the immediate response of the cell to the applied load. It corresponds to the elastic (Young's) modulus.

Accordingly, viscosities for TamR cells are the lowest of the three (*see* **table 4**), showing a decrease by around 20% for η_1 and 32% for η_2, making TamR cells the most fluid-like of the compared cell lines. Those for Sox2 cells are higher by roughly 65% and 63%, respectively, indicating a more viscous phenotype.

Table 2: *Relaxation times for MCF-7, TamR and Sox2 derived from the fitting of the results.*

τ_1	***N***	***Mean [s]***	***SD [s]***	***SEM [s]***	***Median [s]***
MCF-7	160	0.15	0.06	0.01	0.15
TamR	72	0.19	0.06	0.01	0.18
Sox2	76	0.18	0.07	0.01	0.16
τ_2	***N***	***Mean [s]***	***SD [s]***	***SEM [s]***	***Median [s]***
MCF-7	160	3.32	1.66	0.13	2.93
TamR	72	3.83	1.68	0.20	3.53
Sox2	76	3.87	2.03	0.23	3.43

Table 3: *Calculated viscoelastic values for MCF-7, TamR and Sox2.*

E_{inf}	***N***	***Mean [Pa]***	***SD [Pa]***	***SEM [Pa]***	***Median [Pa]***
MCF-7	160	66.5	44.6	3.5	49.5
TamR	70	42.1	17.8	2.1	36.7
Sox2	74	79.5	39.2	4.6	79.1
E_1	***N***	***Mean [Pa]***	***SD [Pa]***	***SEM [Pa]***	***Median [Pa]***
MCF-7	160	62.5	29.8	2.4	57.5
TamR	70	40.3	13.1	1.6	36.5
Sox2	72	87.8	41.2	4.9	83.7

E_2	N	Mean [Pa]	SD [Pa]	SEM [Pa]	Median [Pa]
MCF-7	160	45.7	21.7	1.7	43.3
TamR	72	31.2	13.0	1.5	28.6
Sox2	75	72.4	32.6	3.8	72.7
E_{inst}	N	Mean [Pa]	SD [Pa]	SEM [Pa]	Median [Pa]
MCF-7	160	174.6	87.6	7.0	156.0
TamR	68	109.9	34.5	4.2	102.5
Sox2	73	239.6	104.7	12.3	250.4

Table 4: *Cell viscosity values for MCF-7, TamR and Sox2, rounded to one decimal.*

η_1	N	Mean [Pa s]	SD [Pa s]	SEM [Pa s]	Median [Pa s]
MCF-7	160	8.8	4.6	0.4	8.0
TamR	67	7.0	2.5	0.3	6.9
Sox2	70	13.7	7.3	0.9	12.5
η_2	N	Mean [Pa s]	SD [Pa s]	SEM [Pa s]	Median [Pa s]
MCF-7	160	147.7	101.9	8.1	124.4
TamR	65	101.1	46.9	5.8	97.4
Sox2	71	240.4	143.0	17.0	212.3

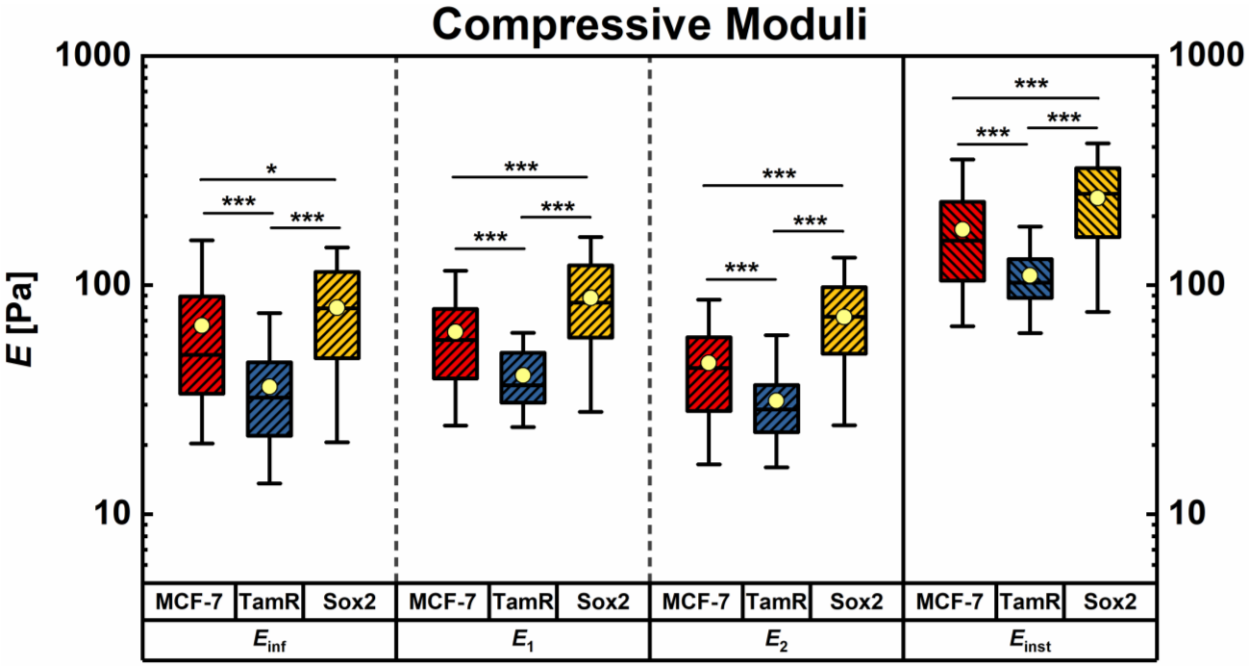

Figure 13: *Compressive moduli for the compared cell lines, calculated from a five-element Maxwell model. The boxes range from the 25th to 75th percentile and the whiskers from 5th to 95th. The yellow dot indicates the mean value. Significance is indicated as '***' for p < 0.001, '**' for p < 0.01, '*' for p < 0.5 and 'n. s.' for non-significant. Plots show no outliers.*

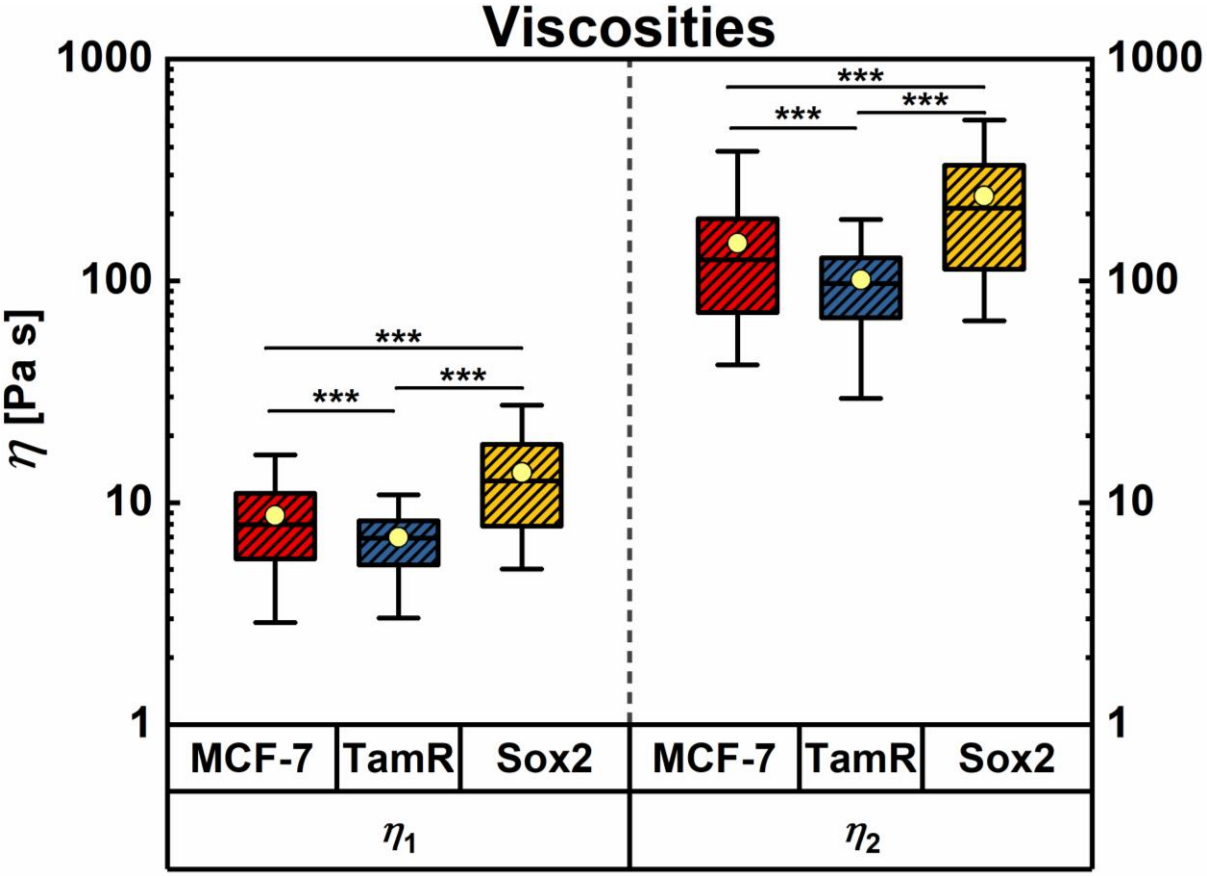

Figure 14: *Viscosities of the compared cell lines, calculated from a five-element Maxwell model. The boxes range from the 25th to 75th percentile and the whiskers from 5th to 95th. The yellow dot indicates the mean value. Significance is indicated as '***' for p < 0.001, '**' for p < 0.01, '*' for p < 0.5 and 'n. s.' for non-significant. Plots show no outliers.*

3.2. MCF-7 and Hypoxia

3.2.1. Cell Morphology

MCF-7 cells were treated with 1 mM hypoxia mimetic DMOG for 24 h, 48 h and 72 h and measured for their elastic and viscoelastic properties via AFM. **Figure 16** shows phase contrast microscopy images of the treated and untreated cells and the morphological changes which they undergo. For treatment timepoints beyond 24 h a medium change containing fresh DMOG was conducted every subsequent 24 h, as cells tend to metabolize DMOG and recover from their hypoxic condition, which was observed as a recovery of a more normal-like phenotype. Cell proliferation continues upon treatment, albeit at a decreased rate, and cell-to-cell contacts are drastically altered even after only a day of treatment. The longer cells are exposed to these conditions, the rounder they get and the higher the loss of tight cell-cell contacts. Manual height evaluation by comparing the contact points of several randomly sampled curves on cells to curves on glass which were acquired before and after every cell measurement show normoxic MCF-7 control cells to be about 5-6 µm in height, while 24 h samples were 5-7 µm, 48 h samples 7-8 µm and 72 h samples up to 9 µm high. The phase contrast images also seem to show increased membrane tethering between cells.

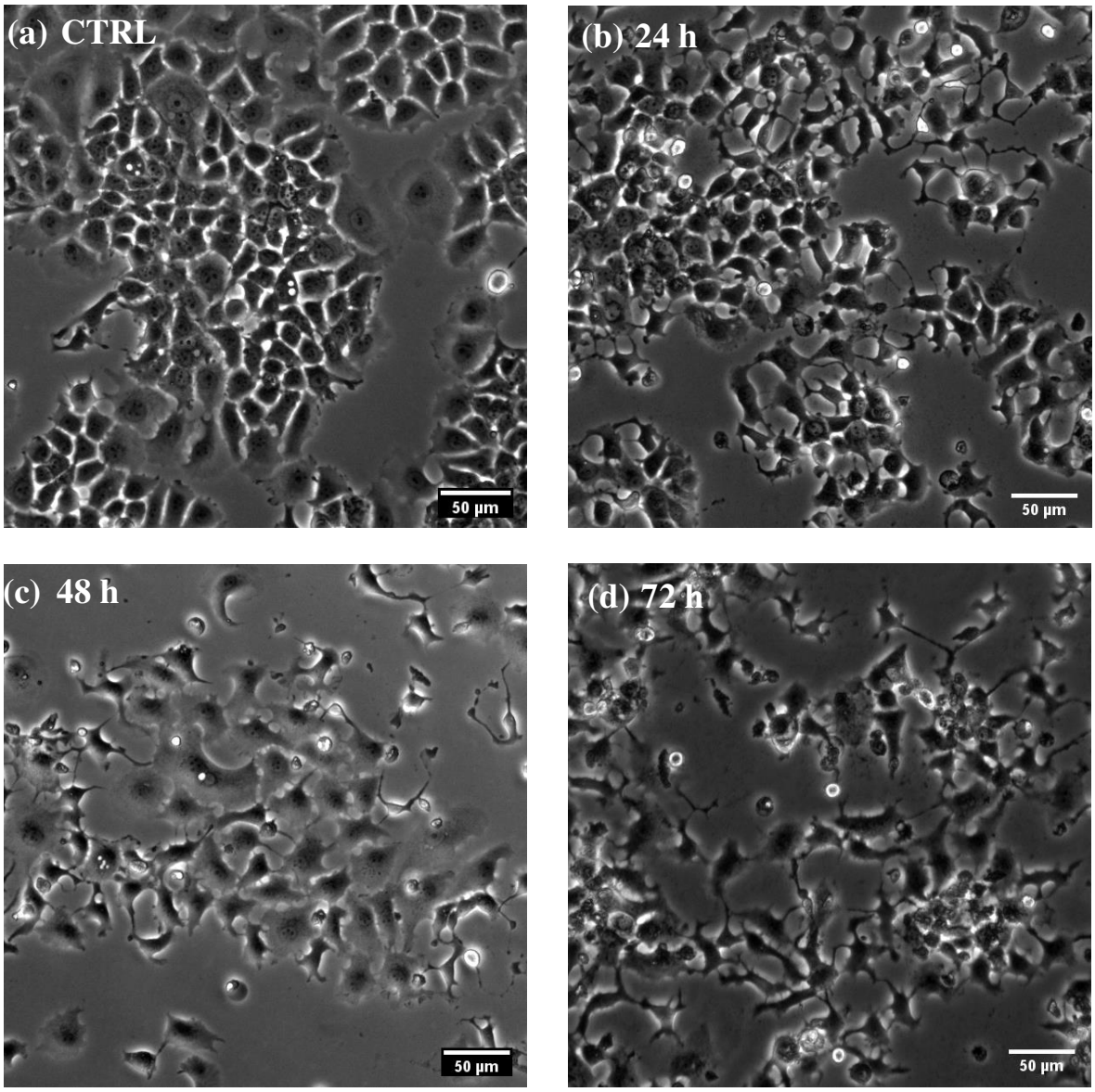

Figure 15: *Brightfield microscopy images taken of MCF-7 breast cancer cells showing (a) the untreated control 24 h after seeding, (b) cells exposed to 1 mM DMOG for 24 h, (c) cells exposed to 48 h of 1 mM DMOG and (d) cells exposed to 1 mM DMOG for 72 h. Note that backdrops have been added to the scale bars in (a) and (c) to increase contrast and enhance visibility.*

3.2.2. Elastic Properties

For AFM experiments, MCF-7 cells were treated analogously to the microscopy samples described in **3.2.1. Cell Morphology**. **Figure 17** (right) and **table 5** (upper) show apparent Young's moduli for treated versus untreated cells, while **figure 17** (left) and **table 5** (lower) indicate indentation values at a force of 1 nN. Mean cell stiffness decreases by around 43% after only 24 h of cultivation under hypoxic conditions and continues to decrease moderately in a time-dependent fashion. Concretely, cells treated for 48 h already show a mean decrease of apparent Young's modulus by 50%, and cells treated for 72 h show a decrease of 60% compared to the normoxic control, respectively. Consequently, indentations at 1 nN nominal force rise with the duration of hypoxia exposure. Cells treated for 24 h show a mean increase of 35.5% in indentation depth, while 48 h and 72 h hypoxia-exposed cells show increases by roughly 72% and 77% respectively when compared to the untreated control.

Table 5: *Apparent Young's modulus and maximum indentation (at 1 nN load) values for control and hypoxia-treated MCF-7 cells.*

E_{app}	***N***	***Mean [Pa]***	***SD [Pa]***	***SEM [Pa]***	***Median [Pa]***
Control	358	242.5	118.5	6.3	213.6
24 h DMOG	235	137.8	82.0	5.4	117.6
48 h DMOG	117	119.7	68.8	6.4	107.5
72 h DMOG	153	95.1	38.5	3.1	85.8
δ	***N***	***Mean [µm]***	***SD [µm]***	***SEM [µm]***	***Median [µm]***
Control	358	1.04	0.36	0.01	0.97
24 h DMOG	235	1.41	0.41	0.02	1.34
48 h DMOG	117	1.79	0.62	0.06	1.64
72 h DMOG	153	1.84	0.36	0.03	1.85

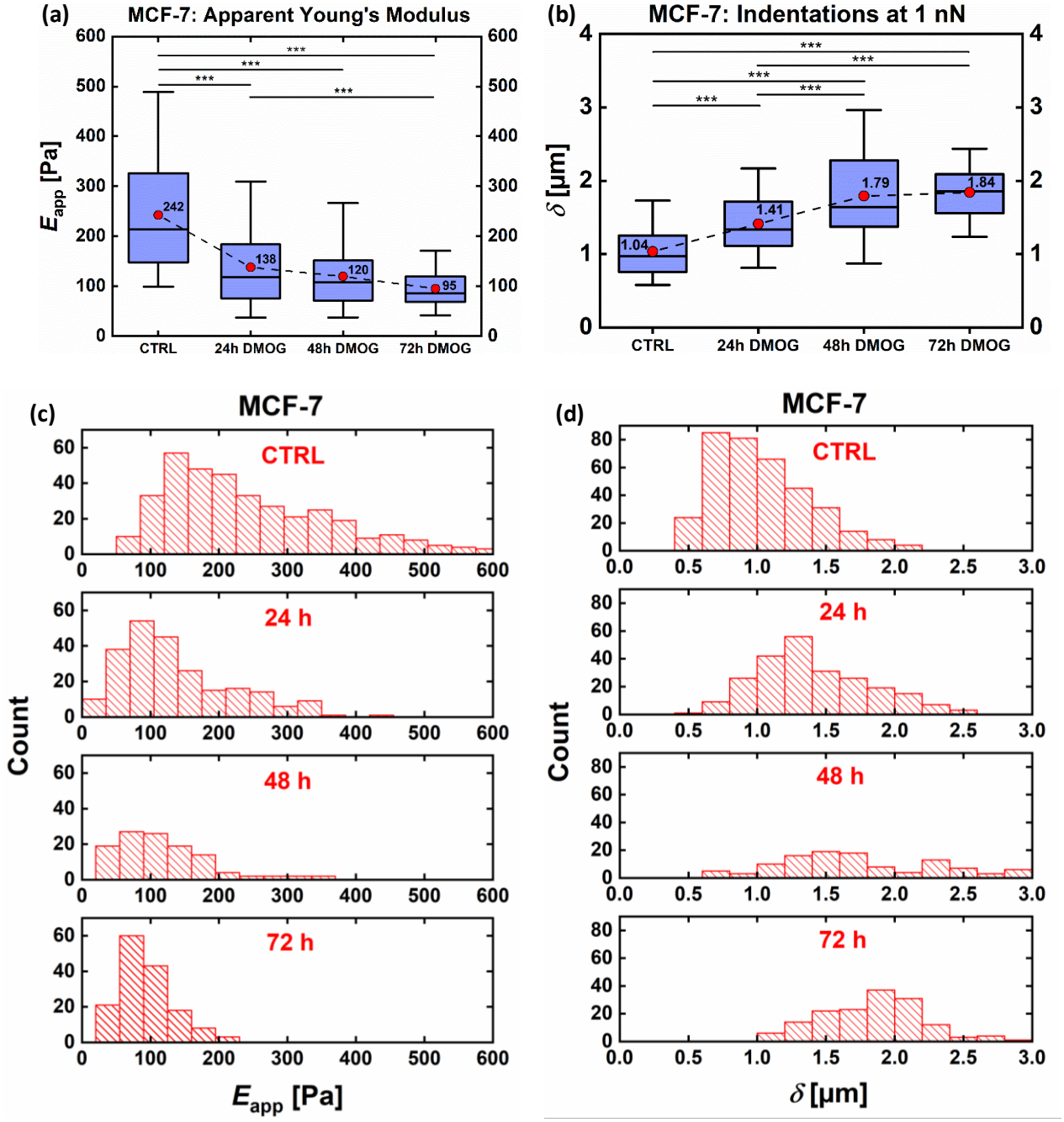

Figure 16: *Elastic properties of MCF-7 cells exposed to hypoxic conditions: (a) and (b) show apparent Young's moduli and maximum indentations at a load of 1 nN respectively, with boxes indicating the 25th-75th percentile and whiskers indicting data ranging from the 5th-95th percentile. The red dot and the number indicate the mean. Outliers are omitted in the graphic. Panels (c) and (d) show the shift in distribution in elasticity and indentation depth, respectively, in regard to treatment time. For each stacked histogram, bin size was conserved. Significance is indicated as '***' for p < 0.001, '**' for p < 0.01, '*' for p < 0.5 and 'n. s.' for non-significant. Plots show no outliers.*

3.2.3. Viscoelastic Properties

Similar to results derived from elasticity analysis, a decrease in compressive moduli correlating with treatment duration can be observed. All hypoxia-exposed cells show increases in relaxation times compared to the control, albeit no significant difference between the exposure times after 24 h. For 24 h hypoxia-exposed cells, the equilibrium modulus E_{inf} decreases by around 34%, for 48 h-exposed cells it decreases by around 61% and by 68% roughly for cells treated for 72 h. E_1 decreases from that of the control cells by approximately 40%, 56% and 64% for 24 h, 48 h and 72 h hypoxia exposure respectively and E_2 by 27% (24 h), 44% (48 h) and 58% (72 h). The instantaneous modulus E_{inst} decreases by 34% after 24 h,0 56% after 48 h and 65% after 72 h treatment time.

Cell viscosities are lower the longer the cells are exposed to hypoxic conditions. For 24 h exposure, η_1 decreases by 19% compared to the control, while 48 h exposure leads to a 39% decrease and 72 h to 53%. The viscosity η_2 falls by 29%, 47% and 45% for 24 h, 48 h and 72 h hypoxic treatment, respectively.

Table 6: *Relaxation times for MCF-7 exposed to hypoxia for 24 h, 48 h and 72 h versus non-exposed control.*

τ_1	***N***	***Mean [s]***	***SD [s]***	***SEM [s]***	***Median [s]***
Control	160	0.15	0.06	0.01	0.15
24 h DMOG	102	0.19	0.06	0.01	0.19
48 h DMOG	52	0.20	0.07	0.01	0.19
72 h DMOG	77	0.19	0.06	0.01	0.19
τ_2	***N***	***Mean [s]***	***SD [s]***	***SEM [s]***	***Median [s]***
Control	160	3.32	1.66	0.13	2.93
24 h DMOG	102	3.83	1.79	0.18	3.58
48 h DMOG	52	4.41	2.25	0.31	3.74
72 h DMOG	77	4.00	1.56	0.18	3.89

Table 7: *Compressive moduli for MCF-7 exposed to hypoxia for 24 h, 48 h and 72 h versus non-exposed control.*

E_{inf}	N	Mean [Pa]	SD [Pa]	SEM [Pa]	Median [Pa]
Control	160	66.5	44.6	3.5	49.5
24 h DMOG	99	44.1	21.3	2.1	42.1
48 h DMOG	47	25.9	13.2	1.9	22.6
72 h DMOG	77	21.1	10.0	1.1	18.0
E_1	N	Mean [Pa]	SD [Pa]	SEM [Pa]	Median [Pa]
Control	160	62.5	29.8	2.4	57.5
24 h DMOG	98	37.7	13.4	1.4	35.0
48 h DMOG	43	27.2	11.4	1.7	26.7
72 h DMOG	74	22.2	5.2	0.6	21.7
E_2	N	Mean [Pa]	SD [Pa]	SEM [Pa]	Median [Pa]
Control	160	45.7	21.7	1.7	43.3
24 h DMOG	101	33.5	16.1	1.7	29.5
48 h DMOG	50	25.4	14.5	2.0	22.5
72 h DMOG	77	19.3	5.2	0.6	18.7
E_{inst}	N	Mean [Pa]	SD [Pa]	SEM [Pa]	Median [Pa]
Control	160	174.6	87.6	6.9	156.0
24 h DMOG	99	115.1	47.0	4.7	111.6
48 h DMOG	46	76.8	34.8	5.1	71.7
72 h DMOG	74	61.4	15.6	1.8	56.9

Table 8: *Viscosities for MCF-7 exposed to hypoxia for 24 h, 48 h and 72 h versus non-exposed control.*

η_1	N	Mean [Pa s]	SD [Pa s]	SEM [Pa s]	Median [Pa s]
Control	160	8.8	4.6	0.4	8.0
24 h DMOG	101	7.1	3.8	0.4	6.1
48 h DMOG	45	5.4	3.0	0.5	4.6
72 h DMOG	75	4.1	1.4	0.2	3.9
η_2	N	Mean [Pa s]	SD [Pa s]	SEM [Pa s]	Median [Pa s]
Control	160	147.7	102.0	8.1	124.4
24 h DMOG	97	115.9	67.5	6.9	109.2
48 h DMOG	39	78.6	46.1	7.4	70.7
72 h DMOG	77	80.3	44.5	5.1	66.7

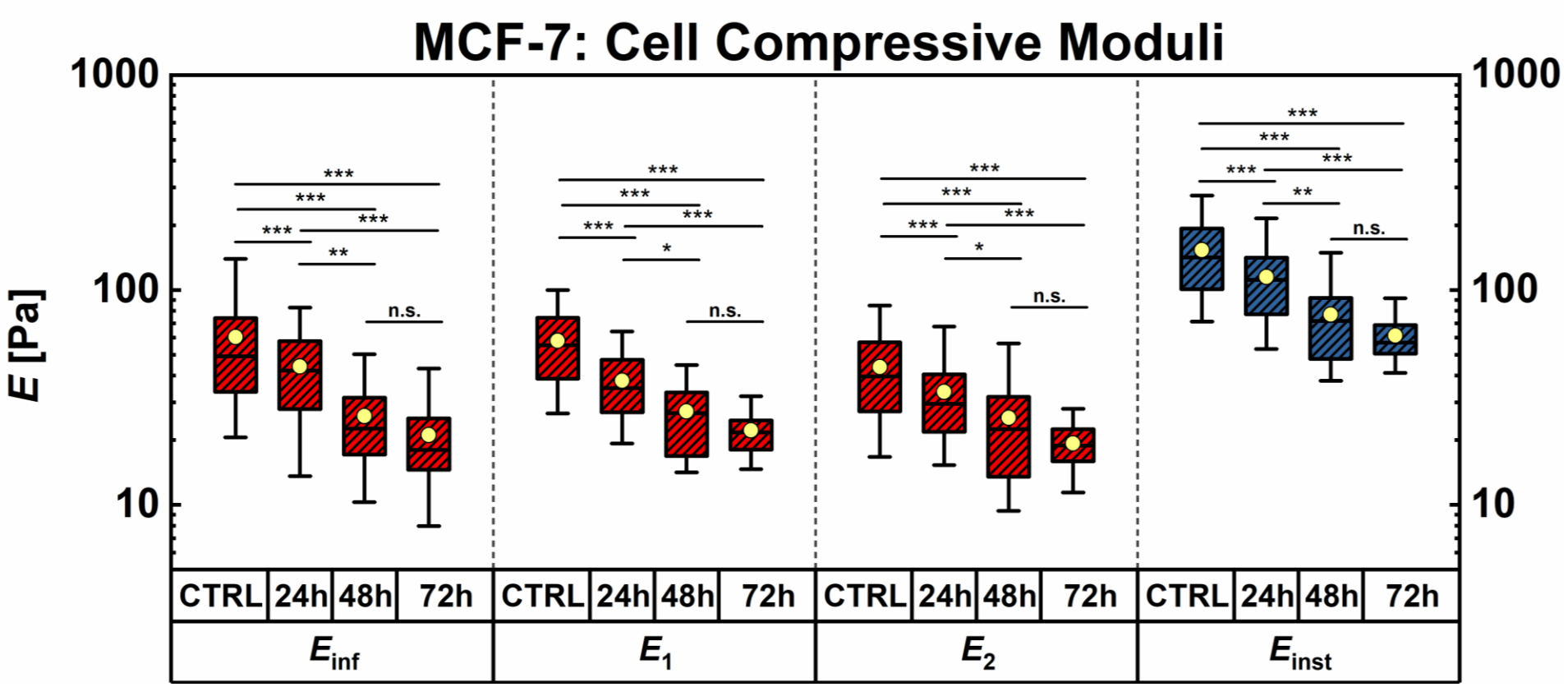

Figure 17: *Compressive moduli for untreated (normoxic) MCF-7 cells versus MCF-7 cells treated with 1 mM DMOG for either 24 h, 48 h or 72 h. Boxes range from 25th-75th percentile and whiskers from 5th-95th. Yellow dots indicate mean values. Significance is indicated as '***' for p < 0.001, '**' for p < 0.01, '*' for p < 0.5 and 'n. s.' for non-significant. Plots show no outliers.*

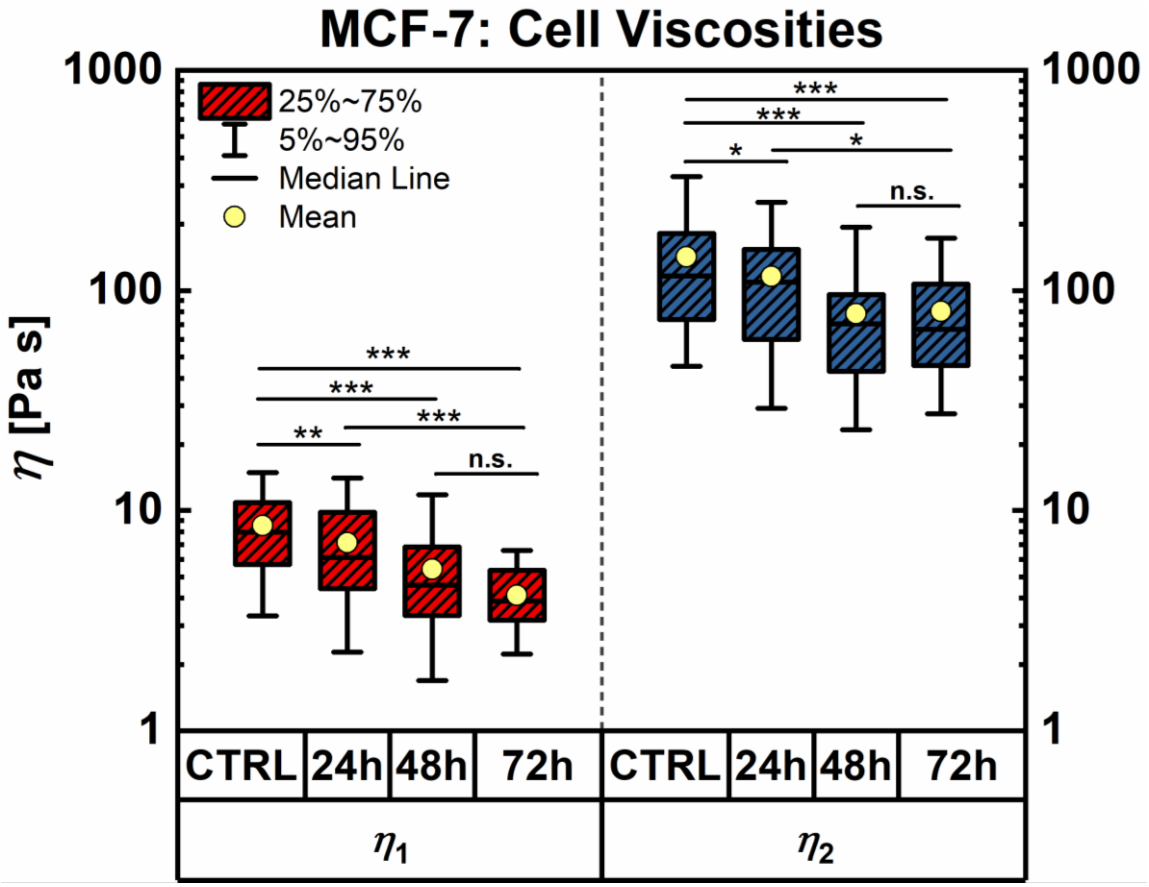

Figure 18: *Viscosities for untreated (normoxic) MCF-7 cells versus MCF-7 cells treated with 1 mM DMOG for either 24 h, 48 h or 72 h. Boxes range from 25th-75th percentile and whiskers from 5th-95th. Yellow dots indicate mean values. Significance is indicated as '***' for p < 0.001, '**' for p < 0.01, '*' for p < 0.5 and 'n. s.' for non-significant. Plots show no outliers.*

3.3. TamR and Hypoxia

3.3.1. Cell Morphology

Like MCF-7 cells, TamR cells were treated with 1 mM hypoxia mimetic DMOG for 24 h and measured for their elastic and viscoelastic properties via AFM force spectroscopy. **Figure 20** shows phase contrast images of the treated cells versus the untreated control. Some morphological changes can be observed, such as increased membrane tethering between the cells and disrupted cell-to-cell contacts. TamR cells show fewer morphology changes upon hypoxia exposure than regular MCF-7 cells. Cell rounding during AFM experiments appears to be less pronounced compared to normal MCF-7. Cell heights increase slightly from approximately 5.5 µm to 6.5 µm, as derived from manual contact point comparison between cell spectroscopy curves and curves acquired on glass (analogous procedure as for MCF-7).

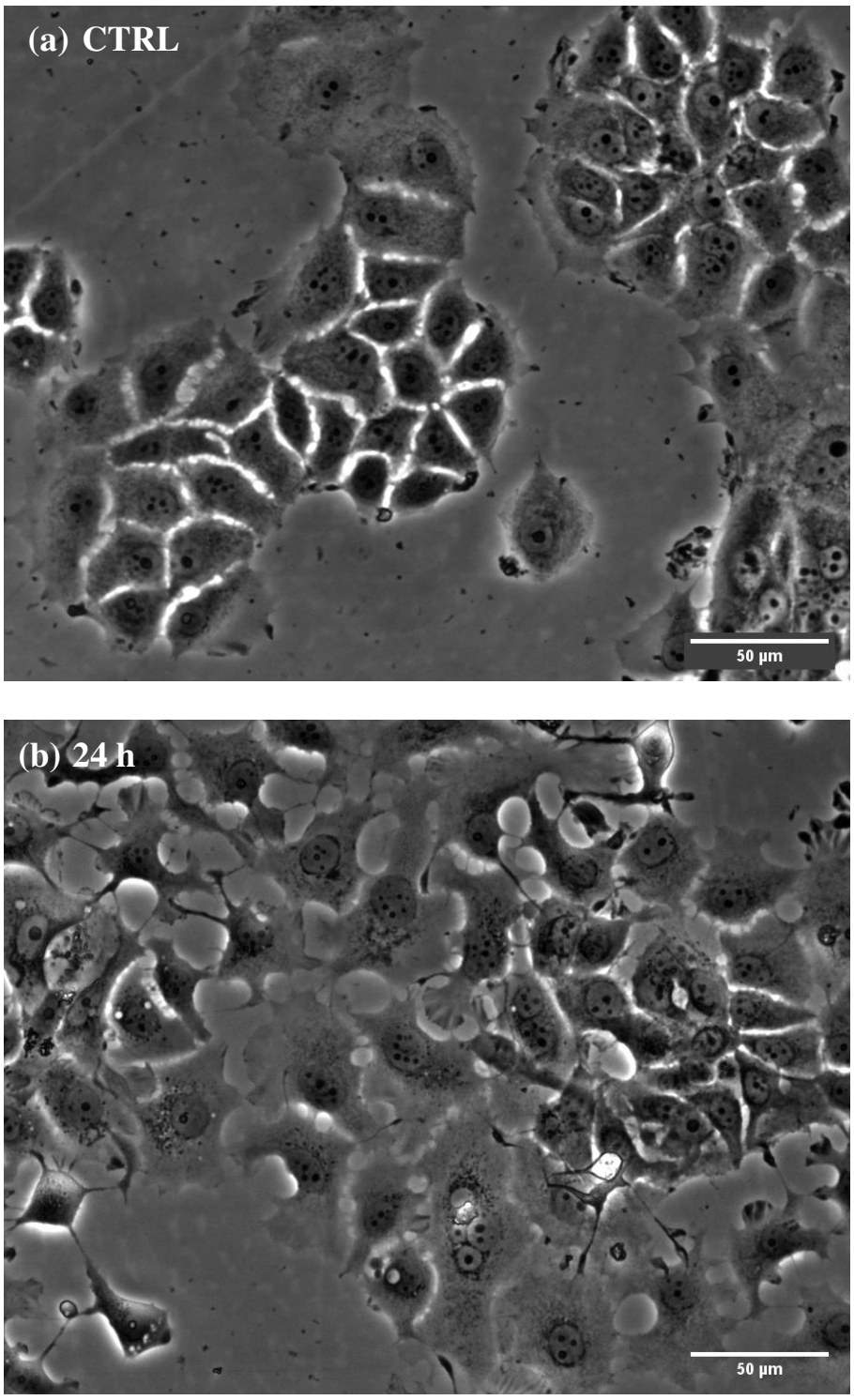

***Figure 19**: Brightfield microscopy images taken of TamR cells showing (a) the untreated control 24 h after seeding and (b) cells exposed to 1 mM DMOG for 24 h. Note that backdrops have been added to the scale bars in (a) and (c) to increase contrast and enhance visibility.*

3.3.2. Elastic Properties

Figure 21 (left) and **table 9** (upper) show apparent Young's moduli for treated versus untreated cells, while **figure 21** (right) and **table 9** (lower) indicate indentation values at a force of 1 nN. Hypoxia-exposed tamoxifen-resistant cells appear softer than non-exposed TamR cells. Mean cell stiffness decreases by around 44% after 24 h exposure, which is approximately the same percentage of decrease as for non-resistant MCF-7 cells treated the same amount of time Indentations at 1 nN nominal force increase by 36% after 24 h of exposure, again roughly the same percentual increase as in non-resistant MCF-7 cells.

Table 9: *Apparent Young's modulus and maximum indentations (at 1 nN) for TamR control vs hypoxia.*

E_{app}	***N***	***Mean [Pa]***	***SD [Pa]***	***SEM [Pa]***	***Median [Pa]***
CTRL	168	148.1	90.1	7.0	125.9
24 h DMOG	256	82.9	53.8	3.4	63.4
δ	***N***	***Mean [µm]***	***SD [µm]***	***SEM [µm]***	***Median [µm]***
CTRL	168	1.4	0.4	0.1	1.4
24 h DMOG	256	1.9	0.5	0.1	1.9

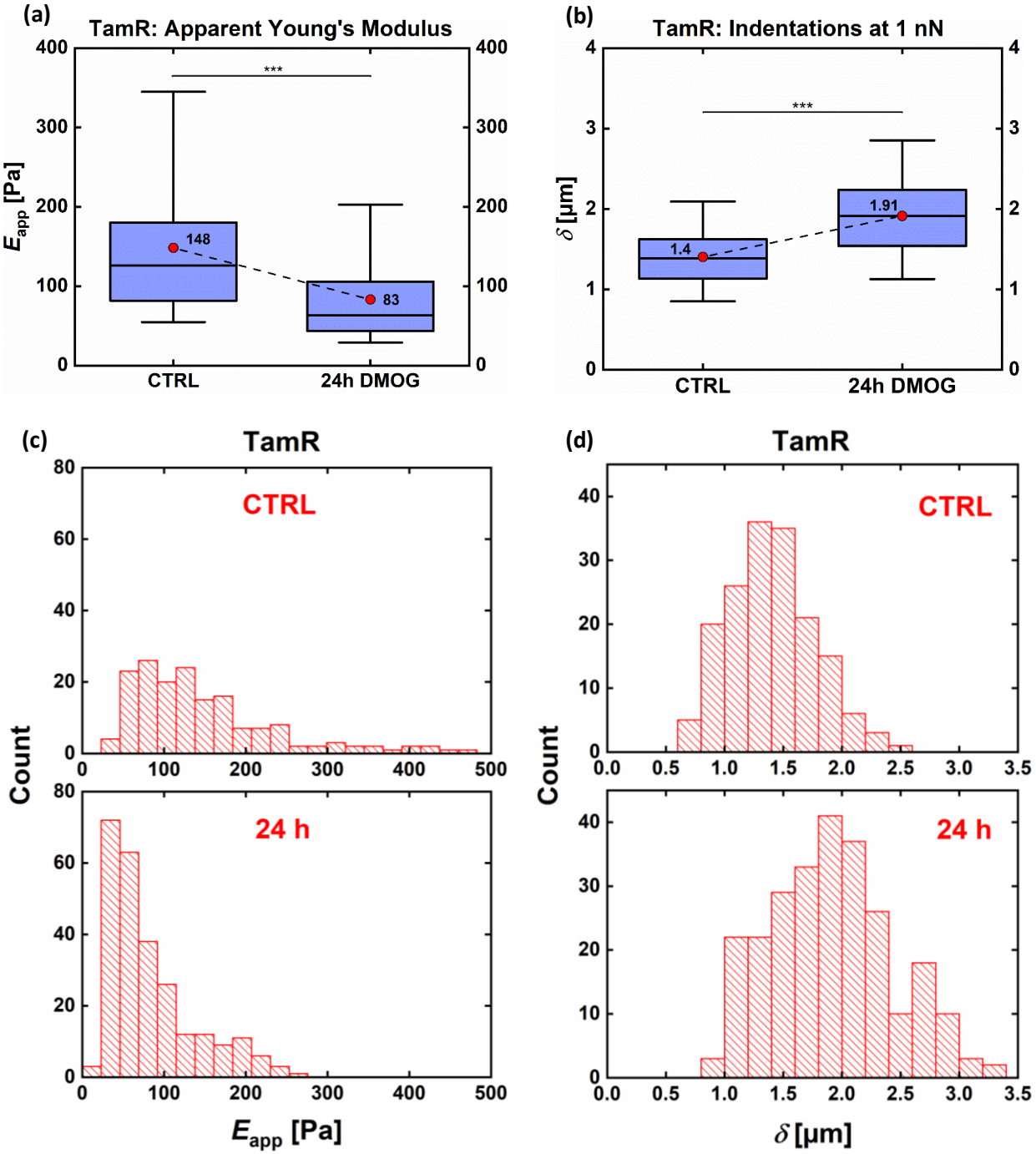

*Figure 20: Elastic properties of MCF-7 cells exposed to hypoxic conditions: (a) and (b) show apparent Young's moduli and maximum indentations at a load of 1 nN respectively, with boxes indicating the 25th-75th percentile and whiskers indicting data ranging from the 5th-95th percentile. The red dot and the number indicate the mean. Outliers are omitted in the graphic. Panels (c) and (d) show the shift in distribution in elasticity and indentation depth, respectively, in regard to treatment time. For each stacked histogram, bin size was conserved. Significance is indicated as '***' for p < 0.001, '**' for p < 0.01, '*' for p < 0.5 and 'n. s.' for non-significant. Plots show no outliers.*

3.3.3. Viscoelastic Properties

Viscoelastic properties for hypoxically cultivated TamR cells are – similar to regular MCF-7 cells – lower than for non-treated TamR cells. In contrast to non-resistant cells, relaxation times for TamR cells decrease upon hypoxia exposure. The mean short-scale relaxation time for DMOG-treated cells falls by roughly 5%, while the long-scale relaxation time records a mean value decrease by around 10% (*see* **table 10**). Compressive moduli record decreases by approximately 40% for E_{inf}, for E_1 by 35%, for E_2 by 33% and for E_{inst} by 55% (*see* **table 11**).

Cell viscosities are lower among the hypoxic cells, as shown in **table 12**. After 24 h exposure, η_1 and η_2 decrease by around 30% compared to the untreated control.

Table 10: *Relaxation times for TamR control vs hypoxia.*

τ_1	***N***	***Mean [s]***	***SD [s]***	***SEM [s]***	***Median [s]***
CTRL	72	0.19	0.06	0.01	0.18
24 h DMOG	131	0.18	0.05	0.01	0.17
τ_2	***N***	***Mean [s]***	***SD [s]***	***SEM [s]***	***Median [s]***
CTRL	72	3.83	1.68	0.20	3.53
24 h DMOG	131	3.44	1.56	0.13	3.31

Table 11: *Compressive moduli for TamR control vs hypoxia.*

E_{inf}	***N***	***Mean [Pa]***	***SD [Pa]***	***SEM [Pa]***	***Median [Pa]***
CTRL	70	42.1	17.8	2.1	36.7
24 h DMOG	130	25.1	13.8	1.2	21.7
E_1	***N***	***Mean [Pa]***	***SD [Pa]***	***SEM [Pa]***	***Median [Pa]***
CTRL	70	40.3	13.2	1.6	36.5
24 h DMOG	128	26.3	10.1	0.9	22.8
E_2	***N***	***Mean [Pa]***	***SD [Pa]***	***SEM [Pa]***	***Median [Pa]***
CTRL	72	31.2	13.0	1.5	28.6
24 h DMOG	131	21.0	10.4	0.9	17.1
E_{inst}	***N***	***Mean [Pa]***	***SD [Pa]***	***SEM [Pa]***	***Median [Pa]***
CTRL	75	72.4	32.6	3.8	72.7
24 h DMOG	103	32.4	19.2	1.9	26.0

Table 12: *Viscosities for TamR control vs hypoxia, rounded to one decimal place.*

η_1	*N*	*Mean [Pa s]*	*SD [Pa s]*	*SEM [Pa s]*	*Median [Pa s]*
CTRL	67	7.0	2.5	0.3	7.0
24 h DMOG	128	4.9	2.5	0.2	4.3
η_2	*N*	*Mean [Pa s]*	*SD [Pa s]*	*SEM [Pa s]*	*Median [Pa s]*
CTRL	65	101.1	46.9	5.8	97.9
24 h DMOG	127	68.6	41.5	3.7	58.0

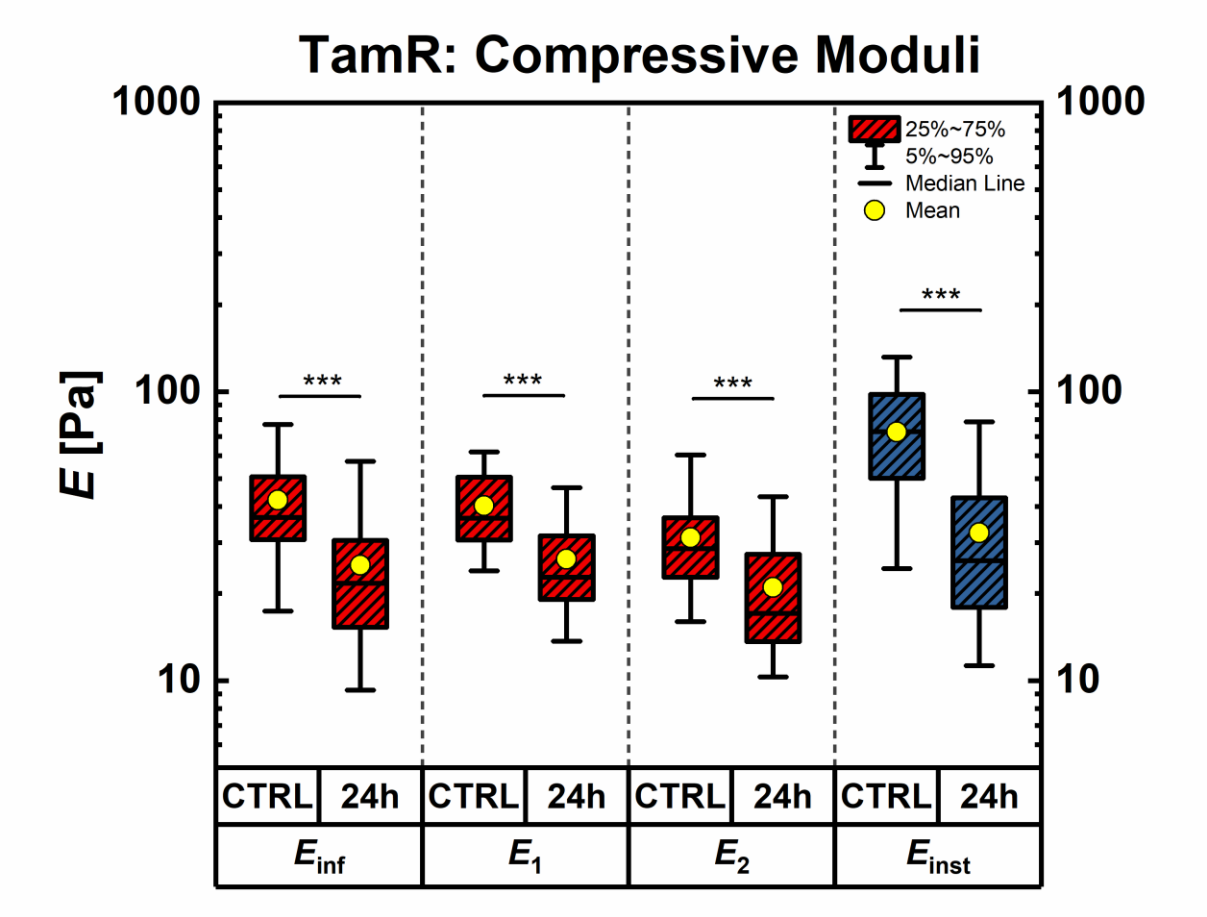

Figure 21*: Compressive moduli for TamR cells treated with 1 mM DMOG for 24 h versus untreated TamR cells. Boxes range from 25th-75th percentile and whiskers from 5th-95th. Yellow dots indicate mean values. Significance is indicated as '***' for p < 0.001, '**' for p < 0.01, '*' for p < 0.5 and 'n. s.' for non-significant. Plots show no outliers.*

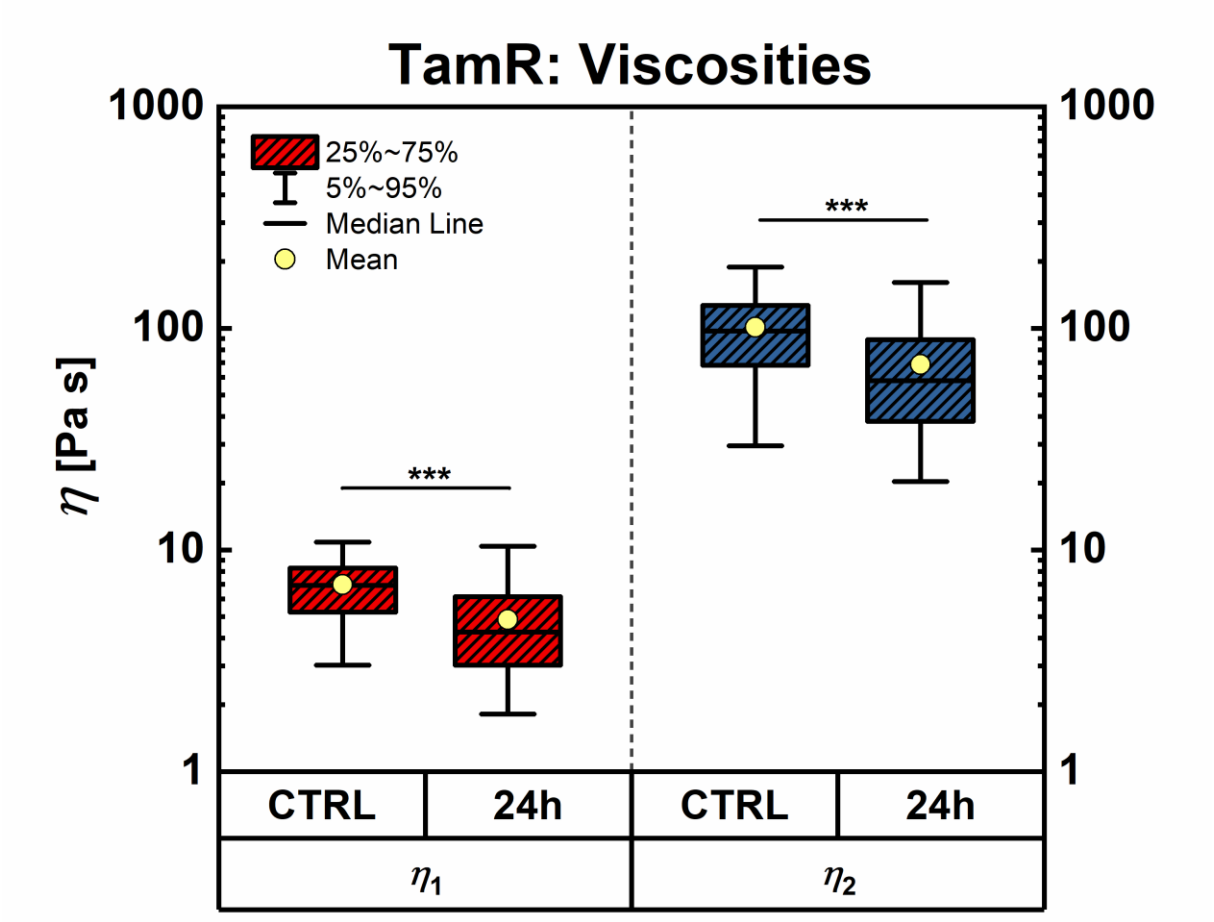

Figure 22**: Viscosities for TamR cells treated with 1 mM DMOG for 24 h versus untreated TamR cells. Boxes range from 25th-75th percentile and whiskers from 5th-95th. Yellow dots indicate mean values. Significance is indicated as '' for p < 0.001, '**' for p < 0.01, '*' for p < 0.5 and 'n. s.' for non-significant. Plots show no outliers.*

3.4. Sox2 and Hypoxia

3.4.1. Cell Morphology

Figure 24 shows phase contrast microscopy images of the treated cells versus the untreated control. Unlike for regular MCF-7 cells and to an extent unlike TamR cells, Sox2 cells maintain their cell-to-cell contacts to a greater extent and continue to grow in small, round, or oblong patches rather than pursuing monolayer sheet formation. In contrast to TamR and regular MCF-7 cells, untreated Sox2 cells appear less spread-out already so visually, there is no dramatic change in cell shape. Cells in the middle of treated patches also alter their morphology minimally while cells on the periphery of the patch develop a more stressed phenotype when exposed to hypoxic conditions. Compared to untreated TamR and MCF-7 cells, untreated Sox2 cells already maintain somewhat looser cell-to-cell contacts in some patches.

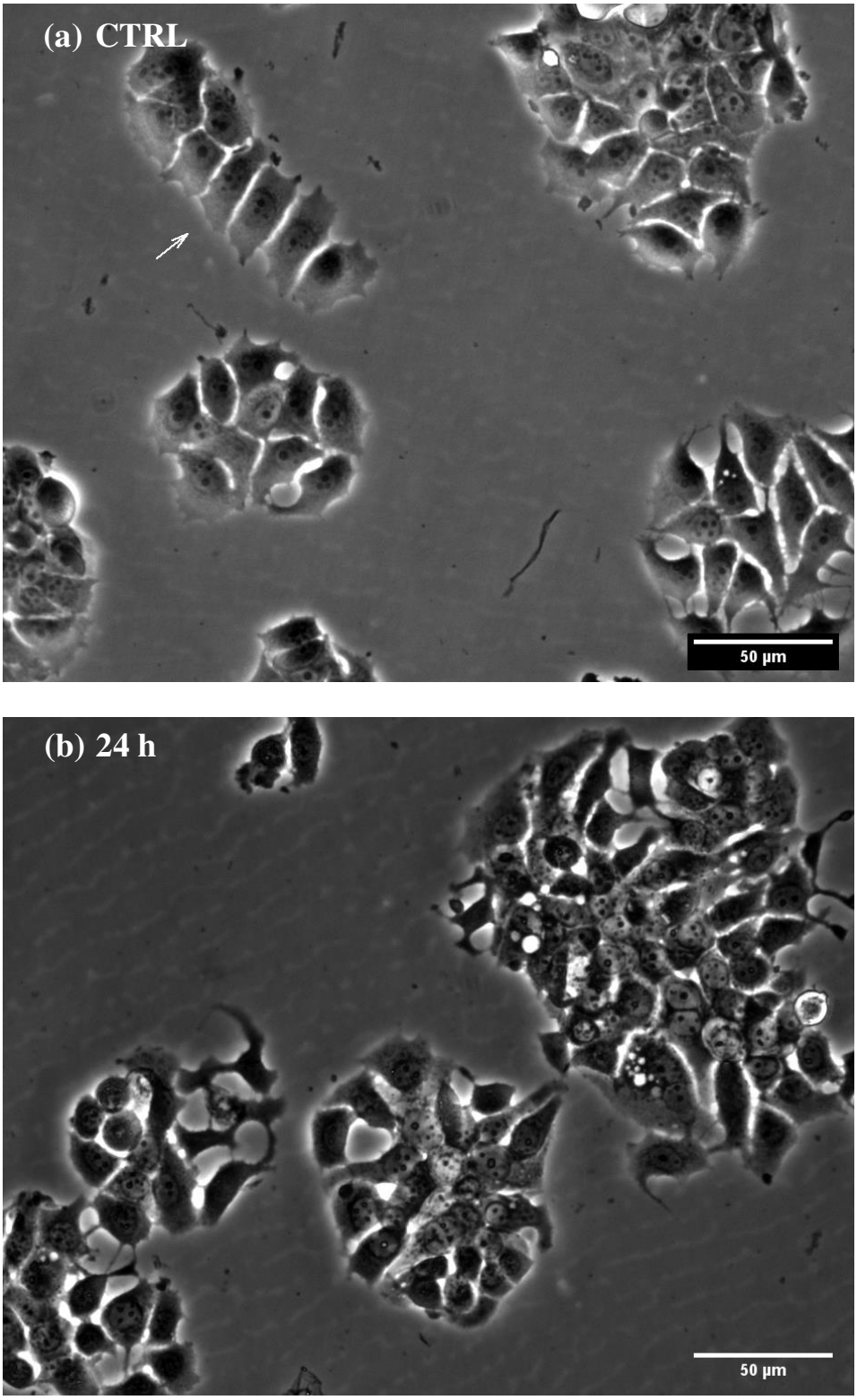

***Figure 23**: Phase contrast microscopy images taken of TamR cells showing (a) the untreated control 24 h after seeding and (b) cells exposed to 1 mM DMOG for 24 h. analogously to AFM samples. Note that backdrops have been added to the scale bars (a) and (c) to increase contrast and enhance visibility.*

3.4.2. Elastic Properties

Like MCF-7 cells, and TamR cells, Sox2-overexpressing cells were treated with 1 mM hypoxia mimetic DMOG for 24 h and measured for their elastic and viscoelastic properties via AFM force spectroscopy. **Figure 25** and **table 13** show and list values for apparent Young's moduli, as well as indentations for untreated Sox2 cells versus hypoxia treated Sox2 cells. After 24 h of treatment, the mean apparent Young's modulus of hypoxic Sox2 cells decrease by about 53%, while the mean maximum indentation at 1 nN force rise roughly by 51%. Of note, while Sox2 cells initially are the stiffest cells among the compared cell lines, upon hypoxic exposure, their apparent Young's modulus decreases by the largest percentage, while their maximum indentation increases most, consequently.

Table 13: *Apparent Young's moduli for Sox2 control vs hypoxia. Maximum indentation values at 1 nN.*

E_{app}	***N***	***Mean [Pa]***	***SD [Pa]***	***SEM [Pa]***	***Median [Pa]***
CTRL	185	297.4	159.6	11.7	253.0
24 h DMOG	141	139.5	88.6	7.5	119.6
δ	***N***	***Mean [µm]***	***SD [µm]***	***SEM [µm]***	***Median [µm]***
CTRL	185	0.91	0.31	0.02	0.85
24 h DMOG	141	1.37	0.34	0.04	1.28

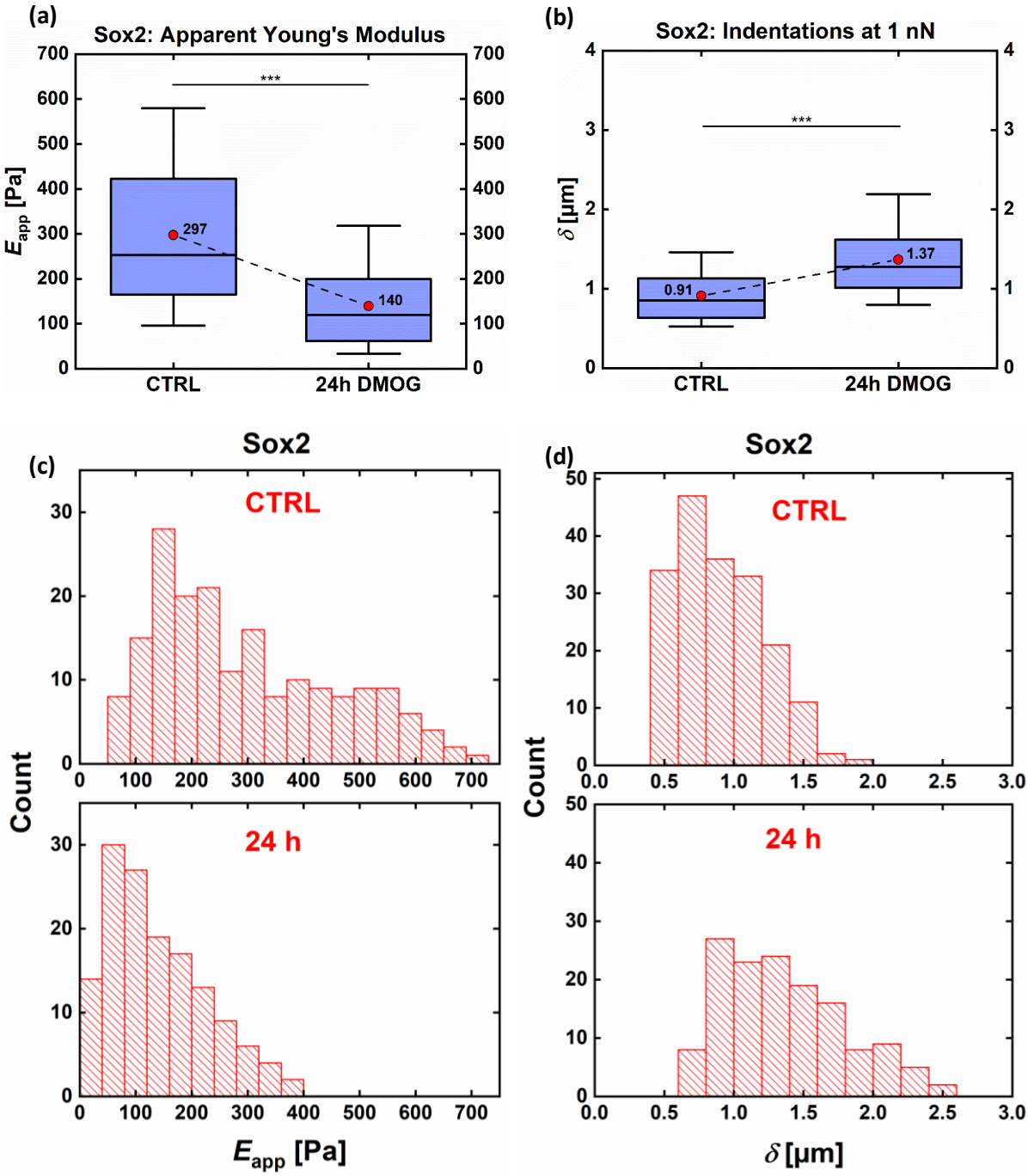

Figure 24: *Elastic properties of MCF-7 cells exposed to hypoxic conditions: (a) and (b) show apparent Young's moduli and maximum indentations at a load of 1 nN respectively, with boxes indicating the 25th-75th percentile and whiskers indicting data ranging from the 5th-95th percentile. The red dot and the number indicate the mean. Outliers are omitted in the graphic. Panels (c) and (d) show the shift in distribution in elasticity and indentation depth, respectively, in regard to treatment time. For each stacked histogram, bin size was conserved. Significance is indicated as '***' for p < 0.001, '**' for p < 0.01, '*' for p < 0.5 and 'n. s.' for non-significant. Plots show no outliers.*

3.4.3. Viscoelastic Properties

Viscoelastic properties for hypoxically cultivated Sox2 cells are likewise as their elastic properties and akin to the other examined cell types lower than those of normoxic Sox2-overespressing cells. Again, Sox2 cells record the steepest decrease in most compressive moduli and in their viscosities. The mean short-scale relaxation time for DMOG-treated cells falls by roughly 6%, while the long-scale relaxation time records a mean value decrease by around 12%. The mean value for the equilibrium modulus E_{inf} falls by around 31%, which is within the range of decrease of regular MCF-7 cells and a smaller decrease than for TamR. The mean compressive moduli E_1, E_2 and E_{inst}, however, decrease by around 58%, 55% and 48%, respectively, while the viscosities η_1 and η_2 both decrease by around 55%. Save for the instantaneous modulus E_{inst}, for which TamR cells record the largest decline, the mean value decreases of compressive moduli and viscosities are largest for Sox2-overexpressing cells.

Table 14: *Relaxation times for Sox2 control vs hypoxia.*

τ_1	***N***	***Mean [s]***	***SD [s]***	***SEM [s]***	***Median [s]***
CTRL	76	0.18	0.07	0.01	0.16
24 h DMOG	103	0.17	0.06	0.01	0.17
τ_2	***N***	***Mean [s]***	***SD [s]***	***SEM [s]***	***Median [s]***
CTRL	76	3.87	2.03	0.23	3.4
24 h DMOG	103	3.42	1.66	0.16	3.0

Table 15: *Compressive moduli for Sox2 control vs hypoxia.*

E_{inf}	***N***	***Mean [Pa]***	***SD [Pa]***	***SEM [Pa]***	***Median [Pa]***
CTRL	74	79.5	39.2	4.6	79.1
24 h DMOG	100	54.6	34.0	3.4	37.7
E_1	***N***	***Mean [Pa]***	***SD [Pa]***	***SEM [Pa]***	***Median [Pa]***
CTRL	72	87.8	41.2	4.9	83.7
24 h DMOG	100	36.5	17.5	1.7	32.5
E_2	***N***	***Mean [Pa]***	***SD [Pa]***	***SEM [Pa]***	***Median [Pa]***
CTRL	75	72.4	32.6	3.8	73.0
24 h DMOG	103	32.4	19.2	2.0	26.0
E_{inst}	***N***	***Mean [Pa]***	***SD [Pa]***	***SEM [Pa]***	***Median [Pa]***
CTRL	73	239.6	104.7	12.3	250.4
24 h DMOG	101	124.7	69.0	6.9	94.5

Table 16: *Viscosities for Sox2 control vs hypoxia.*

η_1	*N*	*Mean [Pa s]*	*SD [Pa s]*	*SEM [Pa s]*	*Median [Pa s]*
CTRL	70	13.7	7.3	0.9	12.5
24 h DMOG	101	6.1	3.3	0.3	5.6
η_2	*N*	*Mean [Pa s]*	*SD [Pa s]*	*SEM [Pa s]*	*Median [Pa s]*
CTRL	71	240.4	143.01827	17.0	212.3
24 h DMOG	102	110.2	85.3	8.4	79.4

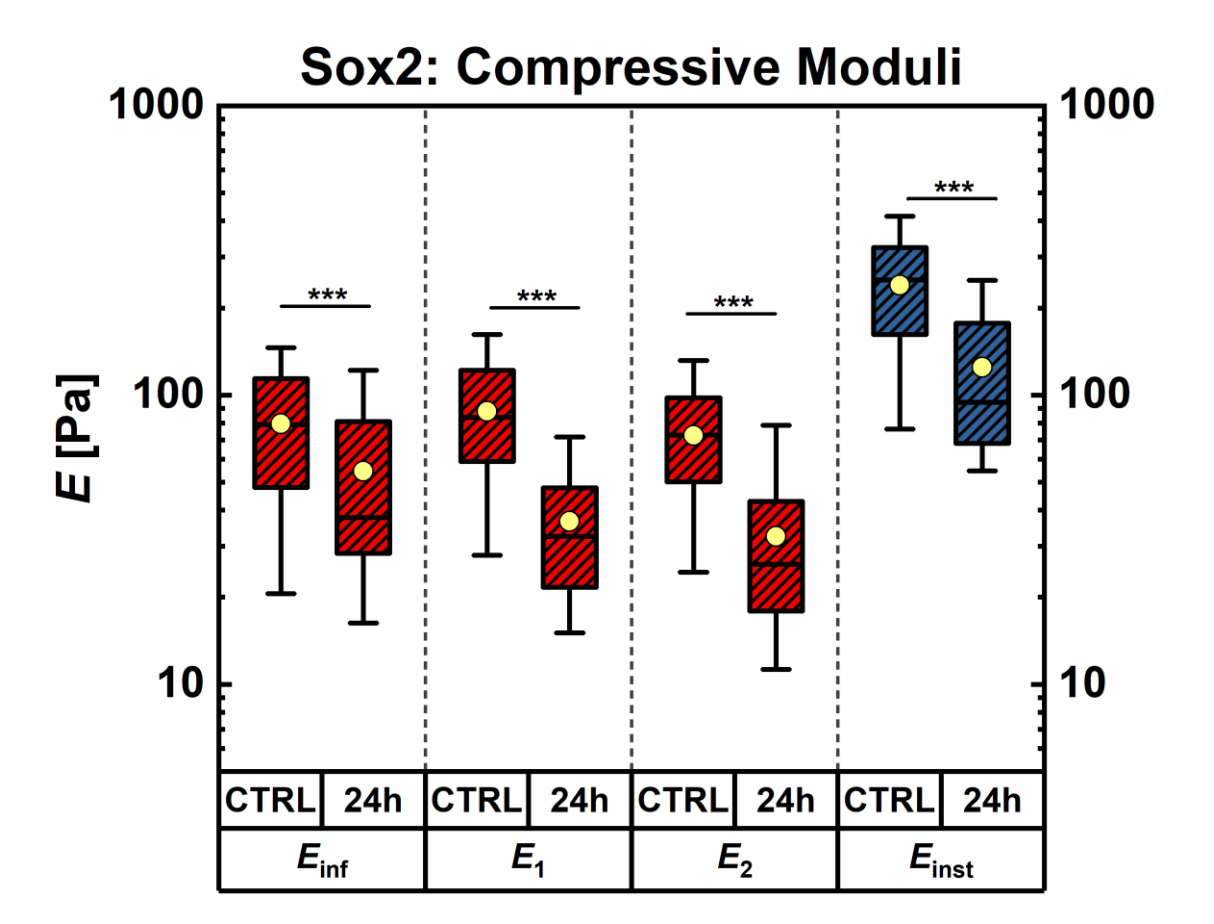

Figure 25: *Compressive moduli for Sox2 cells treated with 1 mM DMOG for 24 h versus untreated Sox2 cells. Boxes range from 25th-75th percentile and whiskers from 5th-95th. Yellow dots indicate mean values. Significance is indicated as '***' for p < 0.001, '**' for p < 0.01, '*' for p < 0.5 and 'n. s.' for non-significant. Plots show no outliers.*

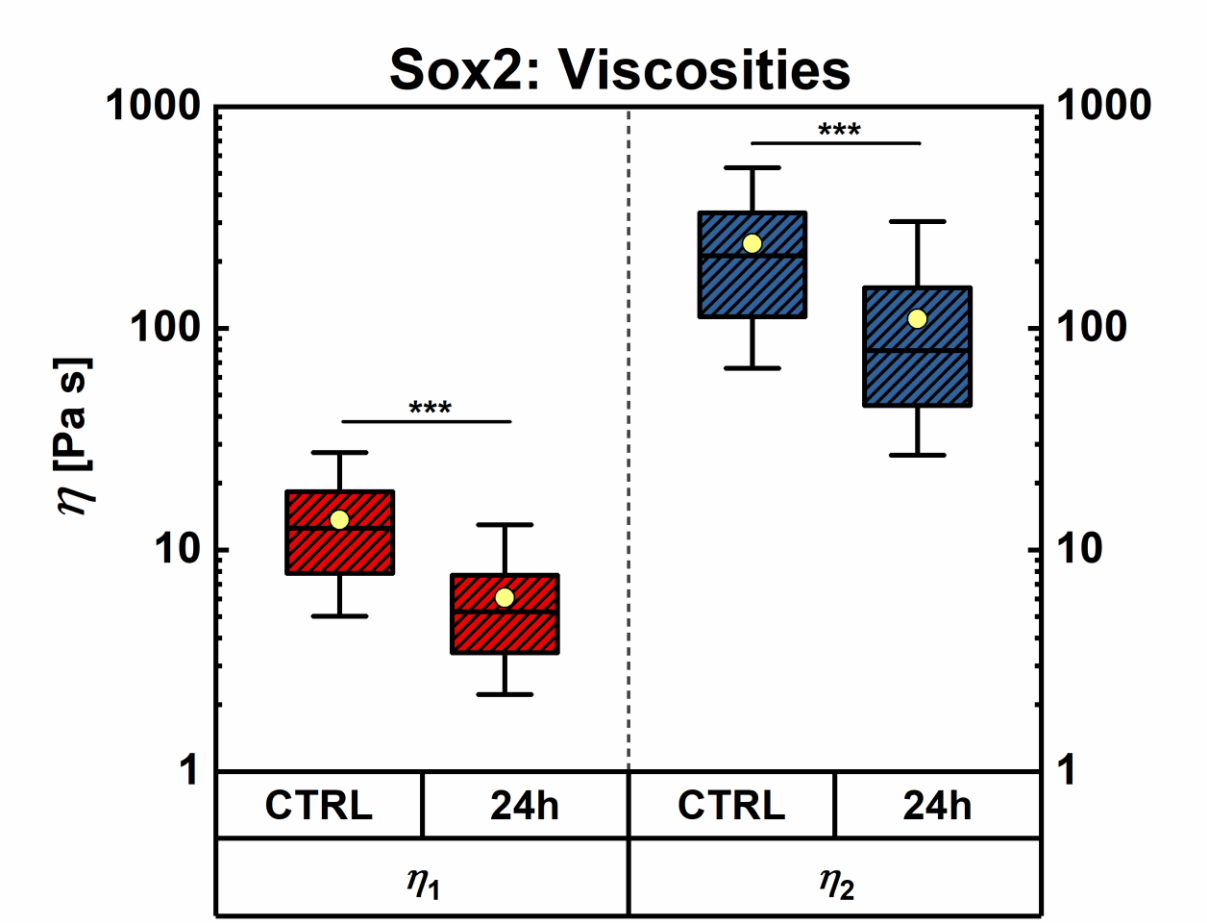

Figure 26: *Viscosities for Sox2 cells treated with 1 mM DMOG for 24 h versus untreated Sox2 cells. Boxes range from 25th-75th percentile and whiskers from 5th-95th. Yellow dots indicate mean values. Significance is indicated as '***' for p < 0.001, '**' for p < 0.01, '*' for p < 0.5 and 'n. s.' for non-significant. Plots show no outliers.*

4. Discussion

4.1. Comparison of the Cell Lines

When compared directly to each other, MCF-7 TamR cells are significantly softer than normal MCF-7 cells, while Sox2 cells appear stiffer. Out of the three cell lines, Sox2-overexpressing cells show the largest spread in all measured and derived values, indicating a gradient in de-differentiation and stem-likeness between individual cells and sub-populations in culture. In contrast, TamR and MCF-7 cells are more similar to each other in terms of value distribution and morphological appearance. Biologically, the overexpression of Sox2 has been shown to promote tamoxifen resistance in breast cancer cells [34]. Therefore, it might be expected for Sox2 cells to fall somewhere between MCF-7 and TamR in terms of their mechanics, if a linear sequence of events in resistance progression is assumed, however, this does not seem to be the case. Morphologically, Sox2 overexpressing MCF-7 cells show a more distinct phenotype and growth pattern than normal MCF-7 and TamR cells. Particularly the difference in patch formation may be relevant to interpret the large spread in mechanical parameters, as cell-to-cell contacts and contact-mediating molecules (e.g., E-cadherin) are playing a role in cell mechanics. In contrast to TamR and MCF-7, Sox2 cells in culture seem to be unable to grow to 100% confluence or form an epithelial monolayer sheet. Rather, at high cell densities they seem to form more densely packed patches of roughly equal sizes.

The linear-like patch formation at low densities may also favor a larger fraction of stiff cells, as in scratch-closing studies bordering cells have been found softer than middle cells [148]. Thus, the fraction of cells at the perimeter of a patch measured compared to those in the middle is relatively larger for Sox2 cells, possibly accounting for some of the data spread. To resolve that question, AFM data could be sorted by cell and correlated with their positions derived from microscopy images acquired during AFM experiments. Alternatively, as MCF-7 cells tend to remain heterogenous in population even after months of passaging [31], cell sorting via FACS for expression levels of Sox2 could be conducted before AFM experiments to relate cell mechanics to stem-likeness. This may be of particular interest as Sox2-overexpressing cells may possibly be more sensitive to their substrate's stiffness than the other studied cells. Sox2 is a self-renewal marker found in stem cells and while cells generally tend to feel and respond to substrate stiffness, for stem cells their mechanical microenvironment is a vital determinant in differentiation fate. As such, mesenchymal stem cells have been found to differentiate either to

osteocytes or to adipocytes solely depending on the stiffness of the substrate they were cultured on [149,150]. For AFM experiments, cells are grown on glass coverslips, which is stiffer by several orders of magnitude compared to their native environment. Therefore, an increased response to substrate mechanical properties may occur. MCF-7 cells have been found to modulate their stiffness in accordance with their substrate [151]. It may also be possible that rather than Sox2 cells being particularly sensitive to their substrate, TamR cells and MCF-7 cells are simply less sensitive in comparison, as cancer ECM has been found stiffer than that of healthy tissue, despite cancer cells being softer [152]. Owing to their aggressiveness, especially for TamR cells this should be considered. However, given the many native-like properties normal MCF-7 cells retain, as well as their limited invasive potential, part of the question would remain unresolved. Considering the implications mechanical cues have for cell- and tissue differentiation, the former seems more likely.

The significant softening of TamR compared to MCF-7 is expected, as tamoxifen resistant breast cancer has been found to be more aggressive and more invasive. This invasiveness of cancer is related to cell softening due to the cytoskeletal remodeling necessary for cell migration to distal tissues [120]. For example, tamoxifen-resistant breast cancer subtypes show increased EMT and have been found to be more resistant to other drug-mediated treatments as well [37], [153]. However, in routine cell culture as well as on the AFM glass coverslips, TamR cells are visually hardly distinguishable from MCF-7 cells.

Indentations are inversely correlated to apparent Young's moduli, meaning softer cells tend to get indented further until the same nominal force setpoint is reached. Interestingly, the mean difference in indentation depth between MCF-7 and Sox2 is relatively minor compared to the difference in their apparent Young's moduli, potentially indicating a larger discrepancy between Sox2 and the other cell lines. For TamR, the increase in indentation is roughly proportional to the decrease in apparent Young's modulus.

4.1.1. Differences in Viscoelastic Properties

Determining the apparent Young's modulus from the contact segment serves as a useful first approximation of the cell's mechanical properties. However, cells are complex, viscoelastic bodies with many functionally and structurally distinct compartments. To get a more comprehensive understanding of cell mechanics, additional analysis conductive to studying

viscoelastic and time-dependent force response of cells is necessary. The compressive moduli from the viscoelastic model indicate a substantial softening of the TamR cells compared to MCF-7 cells, while Sox2 cells are stiffer. The ratios by which softening, or stiffening occurs seem to be conserved roughly for the calculated moduli. This indicates that both short- and long-term relaxation properties are altered for the cell lines. The short-scale relaxation and therefore the parameters E_1 and η_1 have been attributed to membrane arrangements and mechanics in literature, while the longer-scale relaxation time and parameters E_2 and η_2 are linked to F-actin and cytoskeletal rearrangements [141]. Biologically, this is explained by the fluidity of the cell membrane, which is influenced by its lipid composition, and which can flow and arrange nearly immediately. In contrast the cytoskeleton is a structure-conferring, albeit highly dynamic entity, which actively remodels to balance applied loads. Accordingly, viscosities for TamR cells are the lowest of the three, making them the most fluid-like cells, while Sox2 cells appear less fluid-like and more viscous. Overall, these data indicate significant structural differences on a whole-cell basis may arise in MCF-7 cells from either acquiring tamoxifen resistance or Sox2 overexpression. Differences in invasiveness and aggressiveness of breast cancer phenotypes acquiring either of those properties may therefore be expected.

TamR cells appear softer than MCF-7 and Sox2 appear stiffer, irrespective of whether an elastic or a viscoelastic model is used. This indicates that despite their visual similarities in morphology these MCF-7 cell lines differ significantly from each other in regard to mechanically relevant sub-cellular structures. However, to evaluate which structural alterations within the cells occur, further analysis is needed. On the one hand, comparing F-actin arrangement qualitatively via immunofluorescence and CLSM could elucidate the role of cytoskeleton rearrangement within these cells as the actin cortex has the largest influence on cell elasticity. Looking at protein expression for actin and other distinct molecules known to be responsive to mechanotransduction and mechanosignaling, such as cadherins, adhesion molecules, etc., would be an option for more detailed insight.

Chapter header 3: Molecular basis for differences in cell mechanics?

In published research, a total of 629 proteins have been found significantly altered upon acquisition of tamoxifen resistance in MCF-7 cells, including a suppression of estrogen receptor (ER) and ER-regulated genes, an upregulation of survival signaling, and proteins implicated in migratory capacity [154]. Notably, estrogen signaling gets downregulated during resistance

acquisition, but remains functional. As estrogen-dependence decreases, cells upregulate EGFR and HER2, as well as the MAPK and PI3K/Akt pathways to enhance growth signaling. The latter especially has been linked to actin cytoskeleton rearrangements and modulation of cell motility in invasive breast cancer and some other cell types [155–157]. Further, enhanced Rho-ROCK signaling has been connected to increased motility of MCF-7 TamR cells, in addition to increased integrin-mediated actin cytoskeleton regulation [154]. Rho GTPases regulate morphological changes associated with tumor invasiveness and have been classified targets of interest in cancer therapy. Generally, upregulation of ROCK is indicative of invasive tumor subtypes and promotes neovascularization [158]. By treating, for example, the more invasive TamR cells with a ROCK inhibitor before an AFM experiment, the contribution of Rho GTPase signaling to cell softening and cell mechanics could be studied. Upregulation of the actin/MKL1 signaling pathway has been correlated with hormonal escape of ER-positive breast cancer (including for MCF-7 cell line), resulting in subsequent repression of PR and HER2, while estrogen-independent growth factors increase. This would effectively give those cells the expression profile of the highly aggressive, high-invasive triple-negative breast cancer subtype [159]. This is of particular significance as actin/MKL1 signaling has been shown to directly interact with chromatin packing and gene expression by modifying ratios of F(filamentous)-actin to G(globular)-actin, akin to the fashion in which actin rearranges euchromatin and heterochromatin in EMT [160]. To explore possible shifts in protein expression, western blotting could be conducted comparing expression levels for hormone receptors, as well as integrins and molecules associated with migration and cytoskeletal rearrangements.

In this work, the retract segments from the force spectroscopy curves were not analyzed. However, they contain information about membrane adhesive properties, i.e., the work of adhesion and maximum adhesion force, as well as tether formation and membrane rupture events, as well as active (integrin-mediated) binding-unbinding events. In literature, these segments have already been used to derive information about membrane and cell mechanics, as well as to build models for derivation of elastic parameters from retract segments alone [161,162]. As the properties associated with short-scale relaxation time τ_1 are thought to be linked to membrane properties and fluidity, one might expect to find discrepancies between the cell lines here as well.

4.2. MCF-7 and Hypoxia

Hypoxia is a relevant factor in cancer progression. As cells in the tumor's hypoxic core starve for nutrients, the cells able to survive such hostile conditions in turn have been shown to be particularly relevant in terms of invasiveness [45]. DMOG drastically alters the cell phenotype and contact behavior towards neighboring cells, however, it does not induce excessive apoptosis or necrosis, despite the drastic changes in morphology. In fact, results from a resazurin-based viability assay (not included) only show a decrease of viability under 80% of the maximum (which is the untreated control) at concentrations 4-8x above the 1 mM used here, for all exposure times. Cells seem to gain an additional µm in height with every additional day of hypoxia exposure, which suggests cell rounding and cytoskeletal rearrangements. Taken together with the decrease in cell spreading and the thinning of cell-to-cell contacts, it seems that hypoxic conditions promote a decrease in surface-to-volume ratio in MCF-7 cells.

Cell shape alterations have been reported in response to hypoxia for MCF-7 cells. One study looking at hypoxic versus normoxic MCF-7 cells and their EMT progression in response to substrate stiffness found hypoxic MCF-7 cells cultured on stiff (20 kPa) substrates underwent phenotype changes and EMT. However, regardless of substrate stiffness hypoxic cells were found to upregulate among others vimentin, Snail1 and certain matrix metalloproteinases. Simultaneously, epithelial adhesion molecule E-cadherin was found downregulated [151]. Downregulated E-cadherin could account for looser cell-to-cell contacts which are observed for all hypoxically treated cells and is a hallmark of EMT.

The membrane-associated viscosity η_1 seems to be more responsive in a time-dependent manner than the cytoskeleton-associated viscosity η_2, which is evident by the step decrease in between the 48 h and 72 h timepoint in η_1, while η_2 remains roughly constant for these conditions. Interestingly, the relaxation time τ_1 increases markedly between the control and the treated cells but does not increase further in a time-dependent manner with the treatment times, suggesting that the viscous contribution to the short-timescale cell mechanics responds more strongly to hypoxia.

Median time values for τ_2 (the force-relaxation timescale of the membrane) continue to increase with exposure duration. The calculated viscosities are a function of both the compressive moduli as well as the relaxation times and compared to E_2, modulus E_1 is more significantly

affected by hypoxia exposure. Interestingly, when plotted on a logarithmic scale, cell compressive moduli seem to fall roughly in a linear fashion for every day of exposure. This suggests that normal MCF-7 cells respond to hypoxia mechanically in a time-dependent manner. Why this is the case is unclear from these experiments, but several factors may possibly contribute to this.

4.2.1. Hypoxia-induced Molecular Biology of Cell Mechanical Alterations

For example, in a study applying 3D cell culture models to examine hypoxia-driven tumor evolution, the hypoxic niche promotes the selection of aggressive breast cancer cell subtypes, while the less aggressive subpopulations tend to undergo apoptosis [163]. In that same study, MCF-7 cells exhibited high HIF-1α nuclear expression for the full culture time, while other breast cancer cell lines decreased expression after several days. Rho and ROCK are myosin light-chain activators inducing actin-myosin contractions, which is the basis for cell movement. For breast cancer cells, these are downstream targets of HIFs and activators of cancer progression independent of genomic alterations. This is significant as oncogenic mutations in RhoA/ ROCK1 are rare and expression patterns are not fully understood. One study examining the hypoxia-Rho/ROCK axis found evidence that HIF-mediated signaling via RhoA and ROCK1 constitutes a critical signal-transduction pathway in cancer cell motility, invasion and metastasis [164]. As ROCK1 downstream targets mainly acts on actin polymerization, a possible explanation as to why the elastic contribution to MCF-7 cell mechanics seems to change more under hypoxic conditions may be given by this. However, to test whether that is the case, cells would have to be measured mechanically and simultaneously controlled for RhoA/ROCK expression. The AFM setup would allow for this to be done via fluorescence and a live cell staining, if the image resolution is good enough to determine differences in Rho/ROCK expression between hypoxic and normoxic cells. Alternatively, a priori cell sorting via FACS could be performed to separate low- from high-expressing subpopulations in either condition. Indirectly, hypoxia treated cells and normoxic control cells could be quantified for Rho/ROCK expression via Western blotting and confocal fluorescence microscopy.

4.3. TamR and Hypoxia

Like normal MCF-7 cells, tamoxifen-resistant MCF-7 cells, which are already significantly softer than normal MCF-7 cells, soften dramatically with hypoxia exposure. TamR cells seem to undergo fewer phenotype changes under hypoxic conditions, hinting at a potentially better tolerance for hypoxic tumor microenvironment. Interestingly, as opposed to normal MCF-7 cells treated with the hypoxia mimetic, for which the relaxation times tend to increase after hypoxia exposure, for TamR cells, both the short-term, as well as the long-term relaxation times decrease. This implies that the less elastic, more fluid like phenotype TamR cells develop during treatment leads to faster force relaxation over the system.

Biologically, tamoxifen-resistance has been linked with hypoxia in ER(+) tumors. In 1997, it was found that the drug tamoxifen could induce hypoxic milieu in xenografts, after tamoxifen has been found to be antiangiogenic and thrombogenic [165]. Additionally, expression of HIF-1α – the molecule stabilized by physical hypoxic culture conditions as well as the hypoxia-mimetic drug DMOG used in this work – is linked to overall poor cancer prognosis as well as tamoxifen resistance in contralateral breast cancer [166]. In ER(+) breast cancer, acquired tamoxifen resistance generally co-exists with hypoxia [167], therefore it seems plausible that the already tamoxifen-resistant ER(+) MCF-7 breast cancer cells tolerate the treatment conditions better than the non-resistant cells. The estrogen-receptor (ERα) itself seems to play a role in the process intrinsically. A 2015 study found that the ERα directly regulates the HIF-1α pathway in ER(+) breast cancer and that HIF-1α may compensate for ERα function loss in treatment. Thus HIF-1α is shown to confer drug resistance against antiestrogen drugs like tamoxifen [168]. Aside from functional compensation, HIF-1α expression in ER(+) cancer inhibits ERα, which quenches the effectiveness of an estrogen-receptor-binding drug like tamoxifen due to fever available cell surface targets and a higher chance of cancer cell escape [169]. Lack of effective targeting is one of the major challenges in drug-mediated cancer therapy. Notably, the issue of hypoxia-mediated therapy resistance in breast cancers transcends drug therapy, as hypoxic conditions also seem to increase rates of radiation-therapy resistance [170].

To find a morphologically more conserved phenotype, but a mechanically much altered behavior, as well as the inverse relaxation-time response of TamR compared to normal MCF-7 may be expected, however, nevertheless quite interesting for further investigation. To explore further into how far these changes in mechanics are linked to hypoxia for TamR cells, expression analysis for cytoskeleton- and adhesion-molecules, as well as for expression changes of HIF-1α and ERα should be done. Lastly, treating non-resistant MCF-7 cells with low levels of a hypoxia mimetic over an extended period of time and investigating changes in

tamoxifen tolerance as a complimentary experiment could help answer some open questions about the interplay of hypoxia and tamoxifen-resistance in ER(+) breast cancer cells.

Interestingly, E-cadherin has been found to be downregulated by estrogen in breast cancer cells. Antiestrogens have been found to reverse this effect. Thus, tamoxifen-resistant cells, which down-regulate estrogen receptors, could be assumed to express more E-cadherin than non-resistant cells, tightening cell-to-cell junctions [171]. Although hypoxic conditions should have the inverse effect on E-cadherin levels, a disruption of cell-to-cell contacts was observed to a lesser extent in TamR cells as opposed to regular MCF-7 cells. To evaluate this, confocal microscopy for E-cadherin as well as Western blotting should be performed for TamR vs non-resistant MCF-7 cells, both for normoxic and hypoxic conditions.

Particularly with regards to E-cadherin expression, single-cell force spectroscopy (SCFS) AFM-experiments, in which a cell adhering to the downside of a cantilever is used as a probe for sample cells could be of interest. In these experiments the retract segment, which contains information about adhesion, cell-cell binding, and membrane properties is the most relevant one [172,173]. The cell on the cantilever is brought into contact with a cell on the sample surface up to a nominal force and held in contact for a defined amount of time. As the cantilever retracts the work of adhesion is recorded as the integral of the force recorded over the z-position. If TamR cells maintain E-cadherin expression under hypoxic conditions and normal MCF-7 indeed downregulate it, this should be reflected in the work required to separate two cells from a condition from each other. Further, these experiments are, in theory, sensitive enough to record single unbinding events of adhesion receptor-ligand interactions [173]. Particularly by selectively blocking specific adhesion molecules their varying contributions and prevalence could be studied. Comparing with published literature values of SCFS rupture force of adhesion molecules, e.g., 73 pN for E-cadherin (loading rate dependent) [174,175], could possibly contribute significantly to detailing the altered force response of the different cell lines to hypoxic conditions.

4.4. Sox2 and Hypoxia

Sox2 is a transcription factor essential for self-renewal of undifferentiated embryonic stem cells [35]. By expressing Sox2, pluripotency is maintained in the stem cell. Regarding tumorigenicity, Sox2 can take on several roles. While in some tissues, loss of Sox2 is associated with poor disease outcome, in other tissues the overexpression of Sox2 renders it an oncogene [176]. Sox2 interplays with an array of other proteins in cancer progression, some of which are implicated in hypoxic signaling [177–179]. Sox2, together with Nanog and OCT4, forms the "stem cell triad". For various malignancies, expression of these markers is an essential step in disease progression. Further, expression of these proteins has been found to correlate with EMT-associated processes like loss of adhesion molecule E-cadherin in nasopharyngeal carcinoma [180]. In ovarian cancer, the Hypoxia-NOTCH1-Sox2 axis plays a role in maintaining cancer stem cells [177]. In breast cancer, other pluripotency factors which are similar to Sox2 in function or co-occur with it, such as NANOG [47,181], have been found to play a role in maintaining cancer stem cells which are critical in forming both primary tumor tissue as well as distant metastases. As such, Sox2 has been found a downstream transcription target of HIFs [181].

Under the premise that hypoxia-inducible factors and hypoxic conditions promote stemness genes like Sox2 to be expressed in tumors, one study found Sox2 to be an indirect downstream target of HIFs in endometrial cancer stem cells, causing them to maintain their stem-like phenotype [178]. Another study found Sox2 protein levels to be dramatically increased in cancer cells (MDA-MB-231 and MDA-MB-468) as a response to hypoxia in a time-dependent manner and subsequent Sox2 inhibition to inhibit cell migration under hypoxic conditions. Additionally, the study found that HIF-1α expression could be attenuated by silencing Sox2 expression, showing an interplay between Sox2 and the hypoxia pathway, as well as the role of Sox2 in breast cancer cell motility [179]. Considering the vast cytoskeletal and morphological rearrangements a non-invasive cancer cell such as MCF-7 would have to undergo in order to successfully migrate and induce distal metastasis, drastic alterations in mechanical properties could be expected.

In non-stem ER(+) breast cancer cells, Sox2 has been found to have functions unrelated to maintaining a stem like phenotype. As such, Sox2 was found to regulate expression of ERα,

and subsequently found to play a role in anti-estrogen drug resistance, as well as to promote cell growth and be anti-apoptotic [182]. In regard to mechanics and tumor aggressiveness and invasion, more invasive cancer cells have not only been found to be softer as a property or result of their malignancy. However, between soft and stiff cancer cells, the soft cells (among them MCF-7) were found to be highly tumorigenic in SCID mice, while the stiffer cells were unable to form large tumors effectively. These soft MCF-7 cells were additionally found to overexpress stemness markers, such as Sox2, possibly as a direct result of being cultured in a soft environment [122]. While the implications of hypoxia in Sox2 overexpressing breast cancer cells may be less straightforward than for tamoxifen-resistant cells, the functions of Sox2 in cancer cells are manyfold and the effects of hypoxic culture conditions in overexpressing cells may not be singular in nature. After all, Sox2 has been found to promote tamoxifen-resistance in breast cancer and tamoxifen-resistance is strongly linked to hypoxic pathways and invasiveness as a downstream effect [165,166]. Sox2 is known to promote Wnt signaling in breast cancer, which is associated with poor prognosis, increased invasiveness as well as maintenance of cancer stem cells [183]. As discussed before, the Wnt signaling pathway is also activated by hypoxia. Thus, an amplified effect may be achieved by exposing already Sox2-overespressing cells to hypoxia. Considering the role of hypoxia in the tumor microenvironment regarding maintaining tumor stemness together with these factors, a steeper decrease in cell stiffness and overall, more drastically altered cell mechanics when several of these factors are combined seems plausible.

5. Conclusions and Outlook

In this work, the mechanical properties of three different MCF-7 cell lines were examined and compared. Additionally, each cell line was exposed to a hypoxia mimetic for at least 24 h and mechanically compared to the normoxic control. Among the three cell lines, tamoxifen-resistant MCF-7 cells are inherently the softest, while Sox2-overexpressing cells are on average the stiffest cells and show the largest heterogeneity in mechanical properties. Normal MCF-7 cells fall in between these other two. There is a strong association between the invasiveness of cancer cells and their mechanical properties arising from remodeling of subcellular structures like the actin cytoskeleton. Thus, for aggressive antiestrogen-drug-resistant cells to appear softer and more pliable than their non-resistant counterparts would be a plausible outcome. In contrast, the higher stiffness of Sox2-overexpressing cells remains somewhat elusive, considering the link between cancer cell Sox2 expression promotion and soft extracellular matrices which has been described in literature. However, part of the explanation may lie in the wide spread of measured parameters, as Sox2 as a stemness promotor may induce a host of molecular changes within a cell which may influence cell stiffness in several different ways, depending on the concurrent state of the cell at measuring time. In addition, the expression level of Sox2 within the culture may not be homogenous, leading to differently pronounced downstream effects and thus to different observable cell mechanics. Interestingly, the comparatively large spread of values among Sox2-overexpressing cells remains mostly conserved for hypoxia-treated cells, indicating that whatever causes these differences in mechanics within the culture is not attenuated by exposure to hypoxic conditions and thus mechanical heterogeneity may be an intrinsic property of this cell line.

Regardless of which cell line was studied, among exposure to hypoxic culture conditions for 24 h or more, cells significantly decrease in apparent stiffness as well as in viscoelastic properties, while maximal indentations at a given set force increase. Thus, exposure to hypoxia renders MCF-7 breast cancer cells more pliable. Cell pliability is linked to tissue invasion and metastatic potential, as rearrangements in the cytoskeleton and looser cell-cell or cell-substrate contacts allow cells to move away from their original site into distal tissues. This may be necessary for the cell as the hypoxic environment in solid tumors is one of poor nutrient supply and high tissue pressure. Pathways linked to metastatic potential, cancer cell invasiveness and motility have been found directly activated by the hypoxic signaling cascade. An important

open question is whether increased cell pliability is a byproduct of exposure to hostile culture conditions and subsequent phenotype switching, or if cells actively remodel themselves structurally. The latter could be with the goal of decreasing their rigidity for invasive endeavors. This is supported by findings of hypoxic exposure to increase cell invasion in *in vitro* invasion assays and studies showing that from within the same cell line, soft cells have a higher chance of being tumorigenic than stiff cells *in vivo*.

Cell mechanics is not only a mere result of the sum of conditions the cell is exposed to, but a property a cell can actively modulate and change. However, in order to claim with certainty that this is or is not the case here, more detailed research is needed. For one, which role the cytoskeleton plays should be studied both optically by high-resolution microscopy methods as well as mechanistically by i.e., depolymerizing different cytoskeletal structures and quantifying the change in mechanics between non-hypoxic and hypoxic cells. Further, it may be worth looking into other, less mechanically highlighted subcellular structures, such as the nucleus, which has been found to change in shape and stiffness via an actin-modulated active process during cellular invasion [184–186]. Subsequently, changes in nuclear shape and mechanics may indirectly provide a clue to which processes are involved in cell softening upon hypoxia exposure. Especially, given as cell mechanics via AFM force spectroscopy in this work, as well as commonly in literature, usually measure directly above the nuclear region. In the case of tamoxifen-resistant cells, the stabilization of HIF-1α has additional implications via its direct link to estrogen-receptor expression. Thus, hypoxia not only exacerbates the resistance to tamoxifen in ER(+) breast cancer and potentially plays into factors that increase invasiveness It also promotes developing tamoxifen-resistance in not-yet-resistant cells residing in the hypoxic tumor core. In a less straightforward fashion, the self-renewal and stemness marker Sox2 can take on a plentitude of roles in different cancers. Thus, it influences – and is influenced by – several targets which do modulate cell mechanics and motility. Some of these are also heavily implicated in hypoxia-modulated signaling. While open questions regarding the exact mechanisms and pathways involved remain, nevertheless experiments conducted for this work show that Sox2-overexpressing MCF-7 cells show a sensitivity in their mechanics under hypoxic culture conditions.

Finally, while all cell lines regardless of their initial stiffness and viscoelastic character exhibit mechanical alterations upon hypoxia exposure, whether these changes arise because of the same processes in each of the cell lines or whether the molecular response causing the change is

different and somewhat unique to each cell line remains to be elucidated. After all, the tamoxifen-resistant MCF-7 variant especially and to some extent the Sox2-overexpressing one, show seemingly increased tolerance to hypoxia exposure. It is clear, however, that hypoxic culture conditions influence the mechanics of breast cancer cells regardless of subtype by causing them to acquire a significantly softer phenotype.

6. References

(1) Coleman, M. P.; Quaresma, M.; Berrino, F.; Lutz, J. M.; De Angelis, R.; Capocaccia, R.; Baili, P.; Rachet, B.; Gatta, G.; Hakulinen, T.; Micheli, A.; Sant, M.; Weir, H. K.; Elwood, J. M.; Tsukuma, H.; Koifman, S.; e Silva, G. A.; Francisci, S.; Santaquilani, M.; Verdecchia, A.; Storm, H. H.; Young, J. L. Cancer Survival in Five Continents: A Worldwide Population-Based Study (CONCORD). *Lancet Oncol.* **2008**, *9* (8), 730–756. https://doi.org/10.1016/S1470-2045(08)70179-7.

(2) Phung, M. T.; Tin Tin, S.; Elwood, J. M. Prognostic Models for Breast Cancer: A Systematic Review. *BMC Cancer* **2019**, *19* (1), 230–248. https://doi.org/10.1186/s12885-019-5442-6.

(3) World Health Organisation. Latest Global Cancer Data: Cancer Burden Rises to 19.3 Million New Cases and 10.0 Million Cancer Deaths in 2020. *Int. Agency Res. Cancer* **2020**, No. december, 13–15.

(4) Sung, H.; Ferlay, J.; Siegel, R. L.; Laversanne, M.; Soerjomataram, I.; Jemal, A.; Bray, F. Global Cancer Statistics 2020: GLOBOCAN Estimates of Incidence and Mortality Worldwide for 36 Cancers in 185 Countries. *CA. Cancer J. Clin.* **2021**, *71* (3), 209–249. https://doi.org/10.3322/caac.21660.

(5) Buzdar, A. U. Breast Cancer in Men. *Oncology* **2003**, *17* (10), 1361–1364. https://doi.org/10.1177/1557988311416495.

(6) Jain, S.; Gradishar, W. J. *Male Breast Cancer*, Fifth Edit.; Elsevier Inc., 2018. https://doi.org/10.1016/B978-0-323-35955-9.00076-3.

(7) Chen, L.; Linden, H. M.; Anderson, B. O.; Li, C. I. Trends in 5-Year Survival Rates among Breast Cancer Patients by Hormone Receptor Status and Stage. *Breast Cancer Res. Treat.* **2014**, *147* (3), 609–616. https://doi.org/10.1007/s10549-014-3112-6.

(8) Hanahan, D.; Weinberg, R. A. The Hallmarks of Cancer. *Cell* **2000**, *100* (1), 57–70. https://doi.org/10.1016/s0092-8674(00)81683-9.

(9) Hanahan, D.; Weinberg, R. A. Hallmarks of Cancer: The next Generation. *Cell* **2011**, *144* (5), 646–674. https://doi.org/10.1016/j.cell.2011.02.013.

(10) Warburg, O. On Respiratory Impairment in Cancer Cells. *Science* **1956**, *124* (3215), 269–270.

(11) Heiden, M. G. Vander; Cantley, L. C.; Thompson, C. B. TUnderstanding the Warburg Effect: The Metabolic Requirements of Cell Proliferation. *Encycl. Neurosci.* **2008**, *324* (5930), 3828–3828. https://doi.org/10.1007/978-3-540-29678-2_5605.

(12) Nakazawa, M. S.; Brian, K.; Simon, M. C. Oxygen Availability and Metabolic Adaptations. *Nat Rev Cancer.* **2016**, *16* (10), 663–673. https://doi.org/10.1038/nrc.2016.84.

(13) Semenza, G. L. Defining the Role of Hypoxia-Inducible Factor 1 in Cancer Biology and Therapeutics. *Oncogene* **2010**, *29* (5), 625–634. https://doi.org/10.1038/onc.2009.441.

(14) Loeb, L. A.; Bielas, J. H.; Beckman, R. A. Cancers Exhibit a Mutator Phenotype: Clinical Implications. *Cancer Res.* **2008**, *68* (10), 3551–3557. https://doi.org/10.1158/0008-5472.CAN-07-5835.

(15) Loeb, L. A. A Mutator Phenotype in Cancer. *Cancer Res.* **2001**, *61* (8), 3230–3239.

(16) Baugh, E. H.; Ke, H.; Levine, A. J.; Bonneau, R. A.; Chan, C. S. Why Are There Hotspot Mutations in the TP53 Gene in Human Cancers? *Cell Death Differ.* **2018**, *25* (1), 154–160. https://doi.org/10.1038/cdd.2017.180.

(17) Rivlin, N.; Brosh, R.; Oren, M.; Rotter, V. Mutations in the P53 Tumor Suppressor Gene: Important Milestones at the Various Steps of Tumorigenesis. *Genes and Cancer* **2011**, *2* (4), 466–474. https://doi.org/10.1177/1947601911408889.

(18) Prior, I. A.; Lewis, P. D.; Mattos, C. A Comprehensive Survey of Ras Mutations in Cancer. *Cancer Res.* **2012**, *72* (10), 2457–2467. https://doi.org/10.1158/0008-5472.CAN-11-2612.

(19) Antoniou, A.; Pharoah, P. D. P.; Narod, S.; Risch, H. A.; Eyfjord, J. E.; Hopper, J. L.; Loman, N.; Olsson, H.; Johannsson, O.; Borg, Å.; Pasini, B.; Radice, P.; Manoukian, S.; Eccles, D. M.; Tang, N.; Olah, E.; Anton-Culver, H.; Warner, E.; Lubinski, J.; Gronwald, J.; Gorski, B.; Tulinius, H.; Thorlacius, S.; Eerola, H.; Nevanlinna, H.; Syrjäkoski, K.; Kallioniemi, O. P.; Thompson, D.; Evans, C.; Peto, J.; Lalloo, F.; Evans, D. G.; Easton, D. F. Average Risks of Breast and Ovarian Cancer Associated

with BRCA1 or BRCA2 Mutations Detected in Case Series Unselected for Family History: A Combined Analysis of 22 Studies. *Am. J. Hum. Genet.* **2003**, *72* (5), 1117–1130. https://doi.org/10.1086/375033.

(20) Chen, S.; Parmigiani, G. Meta-Analysis of BRAC1 and BRAC2 Penetrance. *J. Clin. Oncol.* **2007**, *25* (11), 1329–1333.

(21) Kotsopoulos, J. BRCA Mutations and Breast Cancer Prevention. *Cancers (Basel).* **2018**, *10* (12), 524–539. https://doi.org/10.3390/cancers10120524.

(22) Kuchenbaecker, K. B.; Hopper, J. L.; Barnes, D. R.; Phillips, K. A.; Mooij, T. M.; Roos-Blom, M. J.; Jervis, S.; Van Leeuwen, F. E.; Milne, R. L.; Andrieu, N.; Goldgar, D. E.; Terry, M. B.; Rookus, M. A.; Easton, D. F.; Antoniou, A. C. Risks of Breast, Ovarian, and Contralateral Breast Cancer for BRCA1 and BRCA2 Mutation Carriers. *JAMA - J. Am. Med. Assoc.* **2017**, *317* (23), 2402–2416. https://doi.org/10.1001/jama.2017.7112.

(23) *SEER Cancer Statistics Review 1975-2013, U.S. National Cancer Institute*; 2016. http://seer.cancer.gov/csr/1975%7B_%7D2013/results%7B_%7Dmerged/sect%7B_%7D24%7B_%7Dstomach.pdf.

(24) De Boer, J. G. A New Mutator Phenotype in Breast Cancer? *Proc. Natl. Acad. Sci. U. S. A.* **2002**, *99* (6), 3368–3369. https://doi.org/10.1073/pnas.082095799.

(25) Yan, L.; Rosen, N.; Arteaga, C. Targeted Cancer Therapies. *Chin. J. Cancer* **2011**, *30* (1), 1–4. https://doi.org/10.5732/cjc.010.10553.

(26) Verma, A.; Mathur, R.; Farooque, A.; Kaul, V.; Gupta, S.; Dwarakanath, B. S. T-Regulatory Cells in Tumor Progression and Therapy. *Cancer Manag. Res.* **2019**, *11*, 10731–10747. https://doi.org/10.2147/CMAR.S228887.

(27) Pan, Y.; Yu, Y.; Wang, X.; Zhang, T. Tumor-Associated Macrophages in Tumor Immunity. *Front. Immunol.* **2020**, *11* (583084). https://doi.org/10.3389/fimmu.2020.583084.

(28) Soule, H. D.; Vazquez, J.; Long, A.; Albert, S.; Brennan, M. A Human Cell Line from a Pleural Effusion Derived from a Breast Carcinoma1,2. *J. Natl. Cancer Inst.* **1973**, *51* (5), 1409–1416. https://doi.org/10.1093/jnci/51.5.1409.

(29) Lippman, M. E.; Bolan, G.; Huff, K. Human Breast Cancer Responsive to Androgen in Long Term Tissue Culture. *Nat. Publ. Gr.* **1975**, *258* (5533), 339–341. https://doi.org/10.1038/258339a0.

(30) Lippman, M.; Bolan, G.; Huff, K. The Effects of Estrogens and Antiestrogens on Hormone Responsive Human Breast Cancer in Long-Term Tissue Culture. *Cancer Res.* **1976**, *36* (12), 4595–4601.

(31) Comşa, Ş.; Cîmpean, A. M.; Raica, M. The Story of MCF-7 Breast Cancer Cell Line: 40 Years of Experience in Research. *Anticancer Res.* **2015**, *35* (6), 3147–3154.

(32) Nugoli, M.; Chucana, P.; Vendrell, J.; Orsetti, B.; Ursule, L.; Nguyen, C.; Birnbaum, D.; Douzery, E. J. P.; Cohen, P.; Theillet, C. Genetic Variability in MCF-7 Sublines: Evidence of Rapid Genomic and RNA Expression Profile Modifications. *BMC Cancer* **2003**, *3* (13), 1–12. https://doi.org/10.1186/1471-2407-3-13.

(33) Chang, M. Tamoxifen Resistance in Breast Cancer. *Biomol. Ther.* **2012**, *20* (3), 256–267. https://doi.org/10.4062/biomolther.2012.20.3.256.

(34) Piva, M.; Domenici, G.; Iriondo, O.; Rábano, M.; Simões, B. M.; Comaills, V.; Barredo, I.; López-Ruiz, J. A.; Zabalza, I.; Kypta, R.; Vivanco, M. D. M. Sox2 Promotes Tamoxifen Resistance in Breast Cancer Cells. *EMBO Mol. Med.* **2014**, *6* (1), 66–79. https://doi.org/10.1002/emmm.201303411.

(35) Al Mamun, M.; Mannoor, K.; Cao, J.; Qadri, F.; Song, X. SOX2 in Cancer Stemness: Tumor Malignancy and Therapeutic Potentials. *J. Mol. Cell Biol.* **2020**, *12* (2), 85–98. https://doi.org/10.1093/JMCB/MJY080.

(36) Patel, S.; Alam, A.; Pant, R.; Chattopadhyay, S. Wnt Signaling and Its Significance Within the Tumor Microenvironment: Novel Therapeutic Insights. *Front. Immunol.* **2019**, *10* (2872). https://doi.org/10.3389/fimmu.2019.02872.

(37) Hiscox, S.; Jiang, W. G.; Obermeier, K.; Taylor, K.; Morgan, L.; Burmi, R.; Barrow, D.; Nicholson, R. I. Tamoxifen Resistance in MCF7 Cells Promotes EMT-like Behaviour and Involves Modulation of β-Catenin Phosphorylation. *Int. J. Cancer* **2006**, *118* (2), 290–301. https://doi.org/10.1002/ijc.21355.

(38) Petrova, V.; Annicchiarico-Petruzzelli, M.; Melino, G.; Amelio, I. The Hypoxic Tumour Microenvironment. *Oncogenesis* **2018**, *7* (1), 10.

https://doi.org/10.1038/s41389-017-0011-9.

(39) Marie-Egyptienne, D. T.; Lohse, I.; Peter, R. Cancer Stem Cells, the Epithelial to Mesenchymal Transition (EMT) and Radioresistance: Potential Role of Hypoxia. *Cancer Lett.* **2013**, *341* (1), 63–72. https://doi.org/10.1016/j.canlet.2012.11.019.

(40) Lee, P.; Chandel, N. S.; Simon, M. C. Cellular Adaptation to Hypoxia through Hypoxia Inducible Factors and Beyond. *Nat. Rev. Mol. Cell Biol.* **2020**, *21* (5), 268–283. https://doi.org/10.1038/s41580-020-0227-y.

(41) Tam, S. Y.; Wu, V. W. C.; Law, H. K. W. Hypoxia-Induced Epithelial-Mesenchymal Transition in Cancers: HIF-1α and Beyond. *Front. Oncol.* **2020**, *10*, 486–587. https://doi.org/10.3389/fonc.2020.00486.

(42) Carreau, A.; Hafny-Rahbi, B. El; Matejuk, A.; Grillon, C.; Kieda, C. Why Is the Partial Oxygen Pressure of Human Tissues a Crucial Parameter? Small Molecules and Hypoxia. *J. Cell. Mol. Med.* **2011**, *15* (6), 1239–1253. https://doi.org/10.1111/j.1582-4934.2011.01258.x.

(43) McKeown, S. R. Defining Normoxia, Physoxia and Hypoxia in Tumours - Implications for Treatment Response. *Br. J. Radiol.* **2014**, *87* (1035), 20130676. https://doi.org/10.1259/bjr.20130676.

(44) Muz, B.; de la Puente, P.; Azab, F.; Azab, A. K. The Role of Hypoxia in Cancer Progression, Angiogenesis, Metastasis, and Resistance to Therapy. *Hypoxia* **2015**, *3*, 83–93. https://doi.org/10.2147/hp.s93413.

(45) Barrak, N. H.; Khajah, M. A.; Luqmani, Y. A. Hypoxic Environment May Enhance Migration/Penetration of Endocrine Resistant MCF7- Derived Breast Cancer Cells through Monolayers of Other Non-Invasive Cancer Cells in Vitro. *Sci. Rep.* **2020**, *10* (1), 1127–1141. https://doi.org/10.1038/s41598-020-58055-x.

(46) Chen, L.; Endler, A.; Shibasaki, F. Hypoxia and Angiogenesis: Regulation of Hypoxia-Inducible Factors via Novel Binding Factors. *Exp. Mol. Med.* **2009**, *41* (12), 849–857. https://doi.org/10.3858/emm.2009.41.12.103.

(47) Mathieu, J.; Zhang, Z.; Zhou, W.; Wang, A. J.; Heddleston, J. M.; Pinna, C. M. A.; Hubaud, A.; Stadler, B.; Choi, M.; Bar, M.; Tewari, M.; Liu, A.; Vessella, R.; Rostomily, R.; Born, D. HIF Induces Human Embryonic Stem Cell Markers in Cancer

Cells. **2011**, *71* (13), 4640–4653. https://doi.org/10.1158/0008-5472.CAN-10-3320.

(48) Lv, X.; Li, J.; Zhang, C.; Hu, T.; Li, S.; Wen, M.; Zuo, J. The Role of Hypoxia-Inducible Factors in Tumor Angiogenesis and Cell Metabolism. *Genes Dis.* **2017**, *4* (1), 19–24. https://doi.org/10.1016/j.gendis.2016.11.003.

(49) Iriondo, O.; Rábano, M.; Domenici, G.; Carlevaris, O.; López-Ruiz, J. A.; Zabalza, I.; Berra, E.; Vivanco, M. D. M. Distinct Breast Cancer Stem/Progenitor Cell Populations Require Either HIF1α or Loss of PHD3 to Expand under Hypoxic Conditions. *Oncotarget* **2015**, *6* (31), 31721–31739. https://doi.org/10.18632/oncotarget.5564.

(50) Masson, N.; Ratcliffe, P. J. Hypoxia Signaling Pathways in Cancer Metabolism: The Importance of Co-Selecting Interconnected Physiological Pathways. *Cancer Metab.* **2014**, *2*, 3–20. https://doi.org/10.1186/2049-3002-2-3.

(51) Slemc, L.; Kunej, T. Transcription Factor HIF1A: Downstream Targets, Associated Pathways, Polymorphic Hypoxia Response Element (HRE) Sites, and Initiative for Standardization of Reporting in Scientific Literature. *Tumor Biol.* **2016**, *37* (11), 14851–14861. https://doi.org/10.1007/s13277-016-5331-4.

(52) Cheng, L.; Yu, H.; Yan, N.; Lai, K.; Xiang, M. Hypoxia-Inducible Factor-1α Target Genes Contribute to Retinal Neuroprotection. *Front. Cell. Neurosci.* **2017**, *11*, 20. https://doi.org/10.3389/fncel.2017.00020.

(53) Mori, H.; Yao, Y.; Learman, B. S.; Kurozumi, K.; Ishida, J.; Ramakrishnan, S. K.; Overmyer, K. A.; Xue, X.; Cawthorn, W. P.; Reid, M. A.; Taylor, M.; Ning, X.; Shah, Y. M.; MacDougald, O. A. Induction of WNT11 by Hypoxia and Hypoxia-Inducible Factor-1α Regulates Cell Proliferation, Migration and Invasion. *Sci. Rep.* **2016**, *6*, 21520. https://doi.org/10.1038/srep21520.

(54) Singh, A.; Wilson, J. W.; Scho, C. J.; Chen, R. Hypoxia-Inducible Factor (HIF) Prolyl Hydroxylase Inhibitors Induce Autophagy and Have a Protective Effect in an in-Vitro Ischaemia Model. *Sci. Rep.* **2020**, *10*, 1597. https://doi.org/10.1038/s41598-020-58482-w.

(55) Ayrapetov, M. K.; Xu, C.; Sun, Y.; Zhu, K.; Parmar, K.; D'Andrea, A. D.; Price, B. D. Activation of Hif1α by the Prolylhydroxylase Inhibitor Dimethyoxalyglycine Decreases Radiosensitivity. *PLoS One* **2011**, *6* (10), e26064.

https://doi.org/10.1371/journal.pone.0026064.

(56) Azab, A. K.; Hu, J.; Quang, P.; Azab, F.; Pitsillides, C.; Awwad, R.; Thompson, B.; Maiso, P.; Sun, J. D.; Hart, C. P.; Roccaro, A. M.; Sacco, A.; Ngo, H. T.; Lin, C. P.; Kung, A. L.; Carrasco, R. D.; Vanderkerken, K.; Ghobrial, I. M. Hypoxia Promotes Dissemination of Multiple Myeloma through Acquisition of Epithelial to Mesenchymal Transition-like Features. **2012**, *119* (24), 5782–5794. https://doi.org/10.1182/blood-2011-09-380410.There.

(57) Liekens, S.; De Clercq, E.; Neyts, J. Angiogenesis: Regulators and Clinical Applications. *Biochem. Pharmacol.* **2001**, *61* (3), 253–270. https://doi.org/10.1016/S0006-2952(00)00529-3.

(58) Sonveaux, P.; Végran, F.; Schroeder, T.; Wergin, M. C.; Verrax, J.; Rabbani, Z. N.; De Saedeleer, C. J.; Kennedy, K. M.; Diepart, C.; Jordan, B. F.; Kelley, M. J.; Gallez, B.; Wahl, M. L.; Feron, O.; Dewhirst, M. W. Targeting Lactate-Fueled Respiration Selectively Kills Hypoxic Tumor Cells in Mice. *J. Clin. Invest.* **2008**, *118* (12), 3930–3942. https://doi.org/10.1172/JCI36843.

(59) De la Cruz-López, K. G.; Castro-Muñoz, L. J.; Reyes-Hernández, D. O.; García-Carrancá, A.; Manzo-Merino, J. Lactate in the Regulation of Tumor Microenvironment and Therapeutic Approaches. *Front. Oncol.* **2019**, *9*, 1143. https://doi.org/10.3389/fonc.2019.01143.

(60) Li, Y.; Zhao, L.; Li, X. F. Hypoxia and the Tumor Microenvironment. *Technol. Cancer Res. Treat.* **2021**, *20*, 15330338211036304. https://doi.org/10.1177/15330338211036304.

(61) Rana, N. K.; Singh, P.; Koch, B. CoCl2 Simulated Hypoxia Induce Cell Proliferation and Alter the Expression Pattern of Hypoxia Associated Genes Involved in Angiogenesis and Apoptosis. *Biol. Res.* **2019**, *52* (1), 12. https://doi.org/10.1186/s40659-019-0221-z.

(62) Saxena, K.; Kumar, M.; Balamurugan, K. Translational Oncology Hypoxia , Partial EMT and Collective Migration : Emerging Culprits in Metastasis. *Transl. Oncol.* **2020**, *13* (11), 100845. https://doi.org/10.1016/j.tranon.2020.100845.

(63) Rodriguez, F. J.; Lewis-Tuffin, L. J.; Anastasiadis, P. Z. E-Cadherin's Dark Side:

Possible Role in Tumor Progression Fausto. *Biochim Biophys Acta* **2012**, *1* (1826), 23–31. https://doi.org/10.1016/j.bbcan.2012.03.002.E-cadherin.

(64) Hoffmann, C.; Mao, X.; Brown-clay, J.; Moreau, F.; Absi, A. Al; Wurzer, H.; Sousa, B.; Schmitt, F.; Berchem, G.; Janji, B.; Thomas, C. Hypoxia Promotes Breast Cancer Cell Invasion through HIF-1 α - Mediated up-Regulation of the Invadopodial Actin Bundling Protein. *Sci. Rep.* **2018**, *8* (1), 10191. https://doi.org/10.1038/s41598-018-28637-x.

(65) Zhang, Y.; Yan, J.; Wang, L.; Dai, H.; Li, N.; Hu, W.; Cai, H. HIF-1 a Promotes Breast Cancer Cell MCF-7 Proliferation. **2017**, *32* (8), 297–301. https://doi.org/10.1089/cbr.2017.2270.

(66) Zhang, M.; Gao, C. E.; Chen, W.; Tang, Y.; Nie, J. Y.; Shen, L.; Ma, X.; Chen, D. E. D. Opposite Response to Hypoxia by Breast Cancer Cells between Cell Proliferation and Cell Migration: A Clue from MicroRNA Expression Profile. *Oncol. Lett.* **2018**, *15* (3), 2771–2780. https://doi.org/10.3892/ol.2017.7636.

(67) Campinho, P.; Vilfan, A.; Vermot, J.; Anne, E.; Jones, V. Blood Flow Forces in Shaping the Vascular System : A Focus on Endothelial Cell Behavior. *Front. Physiol.* **2020**, *11*, 552. https://doi.org/10.3389/fphys.2020.00552.

(68) Cunningham, K. S.; Gotlieb, A. I. The Role of Shear Stress in the Pathogenesis of Atherosclerosis. *Lab Invest* **2005**, *85* (1), 9–23. https://doi.org/10.1038/labinvest.3700215.

(69) Lu, D.; Kassab, G. S. Role of Shear Stress and Stretch in Vascular Mechanobiology. *J. R. Soc. Interface* **2011**, *8* (63), 1379–1385.

(70) Barnes, J. M.; Przybyla, L.; Weaver, V. M. Tissue Mechanics Regulate Brain Development, Homeostasis and Disease. *J. Cell Sci.* **2017**, *130* (1), 71–82. https://doi.org/10.1242/jcs.191742.

(71) Cox, T. R.; Erler, J. T. Remodeling and Homeostasis of the Extracellular Matrix: Implications for Fibrotic Diseases and Cancer. *DMM Dis. Model. Mech.* **2011**, *4* (2), 165–178. https://doi.org/10.1242/dmm.004077.

(72) Roux, W. Gesammelte Abhandlungen Über Entwicklungsmechanik Der Organismen. *Nat. Publ. Gr.* **1896**.

(73) Eyckmans, J.; Boudou, T.; Yu, X.; Chen, C. S. A Hitchhiker's Guide to Mechanobiology. *Dev. Cell* **2011**, *21* (1), 35–47. https://doi.org/10.1016/j.devcel.2011.06.015.

(74) Jansson, J. O.; Palsdottir, V.; Hägg, D. A.; Schéle, E.; Dickson, S. L.; Anesten, F.; Bake, T.; Montelius, M.; Bellman, J.; Johansson, M. E.; Cone, R. D.; Drucker, D. J.; Wu, J.; Aleksic, B.; Törnqvist, A. E.; Sjögren, K.; Gustafsson, J. Å.; Windahl, S. H.; Ohlsson, C. Body Weight Homeostat That Regulates Fat Mass Independently of Leptin in Rats and Mice. *Proc. Natl. Acad. Sci. U. S. A.* **2017**, *115* (2), 427–432. https://doi.org/10.1073/pnas.1715687114.

(75) Ohlsson, C.; Hägg, D. A.; Hammarhjelm, F.; Dalmau Gasull, A.; Bellman, J.; Windahl, S. H.; Palsdottir, V.; Jansson, J. O. The Gravitostat Regulates Fat Mass in Obese Male Mice While Leptin Regulates Fat Mass in Lean Male Mice. *Endocrinology* **2018**, *159* (7), 2676–2682. https://doi.org/10.1210/en.2018-00307.

(76) David, T.; Yves, B. The Gravitostat Theory: Body Fat Is Lost but Is Fat-Free Mass Preserved? *EClinicalMedicine* **2020**, *27*, 100531. https://doi.org/10.1016/j.eclinm.2020.100531.

(77) Humphries, D. L.; Grogan, J. A.; Gaffney, E. A. Mechanical Cell – Cell Communication in Fibrous Networks : The Importance of Network Geometry. *Bull. Math. Biol.* **2017**, *79* (3), 498–524. https://doi.org/10.1007/s11538-016-0242-5.

(78) Schwager, S. C.; Taufalele, P. V; Reinhart-King, C. A. Cell – Cell Mechanical Communication in Cancer. *Cell. Mol. Bioeng.* **2019**, *12* (1), 1–14. https://doi.org/10.1007/s12195-018-00564-x.

(79) Viji Babu, P. K.; Rianna, C.; Mirastschijski, U.; Radmacher, M. Nano-Mechanical Mapping of Interdependent Cell and ECM Mechanics by AFM Force Spectroscopy. *Sci. Rep.* **2019**, *9*, 12317. https://doi.org/10.1038/s41598-019-48566-7.

(80) Kim, J.; Feng, J.; Jones, C. A. R.; Mao, X.; Sander, L. M.; Levine, H.; Sun, B. Stress-Induced Plasticity of Dynamic Collagen Networks. *Nat. Commun.* **2017**, *8*, 842. https://doi.org/10.1038/s41467-017-01011-7.

(81) Alberts, B., Johnson, A., Lewis, J., Raff, M., Roberts, K., Walter, P. *Molecular Biology of the Cell.*; 2002.

(82) Cooper, G. *Structure and Organization of Actin Filaments*, 2nd ed.; 2000.

(83) Brouhard, G. J.; Rice, L. M. Microtubule Dynamics : An Interplay of Biochemistry and Mechanics. *Nat. Rev. Mol. Cell Biol.* **2018**, *19* (7), 451–463. https://doi.org/10.1038/s41580-018-0009-y.

(84) Akhmanova, A.; Steinmetz, M. O. Control of Microtubule Organization and Dynamics: Two Ends in the Limelight. *Nat. Publ. Gr.* **2015**, *16*, 711–726. https://doi.org/10.1038/nrm4084.

(85) Fletcher, D. A.; Mullins, R. D. Cell Mechanics and the Cytoskeleton. *Nature* **2010**, *463* (7280), 485–492. https://doi.org/10.1038/nature08908.

(86) Civelekoglu-Scholey, G.; Scholey, J. M. Mitotic Force Generators and Chromosome Segregation. *Cell. Mol. Life Sci.* **2010**, *67* (13), 2231–2250. https://doi.org/10.1007/s00018-010-0326-6.

(87) Stricker, J.; Falzone, T.; Gardel, M. Mechanics of the F-Actin Cytoskeleton. *J Biomech* **2011**, *43* (1), 9. https://doi.org/10.1016/j.jbiomech.2009.09.003.Mechanics.

(88) Svitkina, T. The Actin Cytoskeleton and Actin-Based Motility. *Cold Spring Harb Perspect Biol* **2018**, *10* (1), a018267.

(89) Ohashi, K.; Fujiwara, S.; Mizuno, K. Roles of the Cytoskeleton, Cell Adhesion and Rho Signalling in Mechanosensing and Mechanotransduction. *J. Biochem.* **2017**, *161* (3), 245–254. https://doi.org/10.1093/jb/mvw082.

(90) Hubrich, H.; Mey, I. P.; Brückner, B. R.; Muehlenbrock, P.; Grabenhorst, L.; Oswald, T.; Steinem, C.; Janshoff, A. Viscoelasticity of Native and Artificial Actin Cortices Assessed by Nanoindentation Experiments. *Nano Lett* **2020**, *20* (9), 6329–6335. https://doi.org/10.1021/acs.nanolett.0c01769.

(91) Li, G.; Huang, S.; Yang, S.; Wang, J.; Cao, J.; Czajkowsky, D. M.; Shao, Z.; Zhu, X. AbLIM1 Constructs Non-Erythroid Cortical Actin Networks to Prevent Mechanical Tension-Induced Blebbing. *Cell Discov.* **2018**, *4*, 42. https://doi.org/10.1038/s41421-018-0040-3.

(92) Clausen, M. P.; Colin-York, H.; Schneider, F.; Eggeling, C.; Fritzsche, M. Dissecting the Actin Cortex Density and Membrane-Cortex Distance in Living Cells by Super-

Resolution Microscopy. *J. Phys. D. Appl. Phys.* **2017**, *50* (6), 064002. https://doi.org/10.1088/1361-6463/aa52a1.

(93) Clark, A. G.; Dierkes, K.; Paluch, E. K. Monitoring Actin Cortex Thickness in Live Cells. *Biophys. J.* **2013**, *105* (3), 570–580. https://doi.org/10.1016/j.bpj.2013.05.057.

(94) Khalilgharibi, N.; Fouchard, J.; Asadipour, N.; Barrientos, R.; Duda, M.; Bonfanti, A.; Yonis, A.; Harris, A.; Mosaffa, P.; Fujita, Y.; Kabla, A.; Mao, Y.; Baum, B.; Muñoz, J. J.; Miodownik, M.; Charras, G. Stress Relaxation in Epithelial Monolayers Is Controlled by the Actomyosin Cortex. *Nat. Phys.* **2019**, *15* (8), 839–847. https://doi.org/10.1038/s41567-019-0516-6.

(95) Salbreux, G.; Charras, G.; Paluch, E. Actin Cortex Mechanics and Cellular Morphogenesis. *Trends Cell Biol.* **2012**, *22* (10), 536–545. https://doi.org/10.1016/j.tcb.2012.07.001.

(96) Gunning, P. W.; Ghoshdastider, U.; Whitaker, S.; Popp, D.; Robinson, R. C. The Evolution of Compositionally and Functionally Distinct Actin Filaments. *J. Cell Sci.* **2015**, *128* (11), 2009–2019. https://doi.org/10.1242/jcs.165563.

(97) Pesen, D.; Hoh, J. H. Micromechanical Architecture of the Endothelial Cell Cortex. *Biophys. J.* **2005**, *88* (1), 670–679. https://doi.org/10.1529/biophysj.104.049965.

(98) Sadegh, S.; Higgins, J. L.; Mannion, P. C.; Tamkun, M. M.; Krapf, D. Plasma Membrane Is Compartmentalized by a Self-Similar Cortical Actin Meshwork. *Phys. Rev. X* **2017**, *7* (1), 011031. https://doi.org/10.1103/PhysRevX.7.011031.

(99) Chugh, P.; Clark, A. G.; Smith, M. B.; Cassani, D. A. D.; Dierkes, K.; Ragab, A.; Roux, P. P.; Charras, G.; Salbreux, G.; Paluch, E. K. Actin Cortex Architecture Regulates Cell Surface Tension. *Nat. Cell Biol.* **2017**, *19* (6), 689–697. https://doi.org/10.1038/ncb3525.

(100) Taubenberger, A. V.; Baum, B.; Matthews, H. K. The Mechanics of Mitotic Cell Rounding. *Front. Cell Dev. Biol.* **2020**, *8*, 687. https://doi.org/10.3389/fcell.2020.00687.

(101) An, B.; Quang, T.; Peters, R.; Cassani, D. A. D.; Chugh, P.; Clark, A. G.; Agnew, M.; Charras, G.; Paluch, E. K. Extent of Myosin Penetration within the Actin Cortex Regulates Cell Surface Mechanics. *Nat. Commun.* **2021**, *12*, 6511.

https://doi.org/10.1038/s41467-021-26611-2.

(102) Nambiar, R.; McConnell, R. E.; Tyska, M. J. Control of Cell Membrane Tension by Myosin-I. *Proc. Natl. Acad. Sci. U. S. A.* **2009**, *106* (29), 11972–11977. https://doi.org/10.1073/pnas.0901641106.

(103) Clark, A. G.; Wartlick, O.; Salbreux, G.; Paluch, E. K. Stresses at the Cell Surface during Animal Cell Morphogenesis. *Curr. Biol.* **2014**, *24* (10), R484–R494. https://doi.org/10.1016/j.cub.2014.03.059.

(104) Fehon, R. G.; McClatchey, A. I.; Bretscher, A. Organizing the Cell Cortex: The Role of ERM Proteins. *Nat. Rev. Mol. Cell Biol.* **2010**, *11* (4), 276–287. https://doi.org/10.1038/nrm2866.

(105) Kusumi, A.; Suzuki, K. G. N.; Kasai, R. S.; Ritchie, K.; Fujiwara, T. K. Hierarchical Mesoscale Domain Organization of the Plasma Membrane. *Trends Biochem. Sci.* **2011**, *36* (11), 604–615. https://doi.org/10.1016/j.tibs.2011.08.001.

(106) Sprenkeler, E. G. G.; Webbers, S. D. S.; Kuijpers, T. W. When Actin Is Not Actin' like It Should: A New Category of Distinct Primary Immunodeficiency Disorders. *J. Innate Immun.* **2021**, *13* (1), 3–25. https://doi.org/10.1159/000509717.

(107) Aidinis, V.; Carninci, P.; Armaka, M.; Witke, W.; Harokopos, V.; Pavelka, N.; Koczan, D.; Argyropoulos, C.; Thwin, M. M.; Möller, S.; Kazunori, W.; Gopalakrishnakone, P.; Ricciardi-Castagnoli, P.; Thiesen, H. J.; Hayashizaki, Y.; Kollias, G. Cytoskeletal Rearrangements in Synovial Fibroblasts as a Novel Pathophysiological Determinant of Modeled Rheumatoid Arthritis. *PLoS Genet.* **2005**, *1* (4), 0455–0466. https://doi.org/10.1371/journal.pgen.0010048.

(108) White, S. R.; Williams, P.; Wojcik, K. R.; Sun, S.; Hiemstra, P. S.; Rabe, K. F.; Dorscheid, D. R. Initiation of Apoptosis by Actin Cytoskeletal Derangement in Human Airway Epithelial Cells. *Am. J. Respir. Cell Mol. Biol.* **2001**, *24* (3), 282–294. https://doi.org/10.1165/ajrcmb.24.3.3995.

(109) O'Neill, G. M. The Coordination between Actin Filaments and Adhesion in Mesenchymal Migration. *Cell Adhes. Migr.* **2009**, *3* (4), 1–4. https://doi.org/10.4161/cam.3.4.9468.

(110) Seetharaman, S.; Etienne-manneville, S. Cytoskeletal Crosstalk in Cell Migration.

Trends Cell Biol. **2021**, *30* (9), 720–735. https://doi.org/https://doi.org/10.1016/j.tcb.2020.06.004.

(111) Aseervatham, J. Cytoskeletal Remodeling in Cancer. *Biology (Basel).* **2020**, *9* (11), 385. https://doi.org/10.3390/biology9110385.

(112) Lehmann, S.; Boekhorst, V.; Odenthal, J.; Grenman, R.; Rudin, M.; Friedl, P.; Bianchi, R.; Van Helvert, S. Hypoxia Induces a HIF-1-Dependent Transition from Collective-to-Amoeboid Dissemination in Epithelial Report Hypoxia Induces a HIF-1-Dependent Transition from Collective-to-Amoeboid Dissemination in Epithelial Cancer Cells. *Curr. Biol.* **2017**, *27* (3), 392–400. https://doi.org/10.1016/j.cub.2016.11.057.

(113) VanderVorst, K.; Dreyer, C. A.; Konopelski, S. E.; Lee, H.; Ho, H.-Y. H.; Carraway III, K. L. Wnt/PCP Signaling Contribution to Carcinoma Collective Cell Migration and Metastasis. *Cancer Res* **2019**, *79* (8), 1719–1730. https://doi.org/10.1158/0008-5472.CAN-18-2757.

(114) Katira, P.; Bonnecaze, R. T.; Zaman, M. H. Modeling the Mechanics of Cancer: Effect of Changes in Cellular and Extra-Cellular Mechanical Properties. *Front. Oncol.* **2013**, *3*, 145. https://doi.org/10.3389/fonc.2013.00145.

(115) Kim, B. G.; Sung, J. S.; Jang, Y.; Cha, Y. J.; Kang, S.; Han, H. H.; Lee, J. H.; Cho, N. H. Compression-Induced Expression of Glycolysis Genes in CAFs Correlates with EMT and Angiogenesis Gene Expression in Breast Cancer. *Commun. Biol.* **2019**, *2*, 313. https://doi.org/10.1038/s42003-019-0553-9.

(116) Kalli, M.; Stylianopoulos, T. Defining the Role of Solid Stress and Matrix Stiffness in Cancer Cell Proliferation and Metastasis. *Front. Oncol.* **2018**, *8*, 55. https://doi.org/10.3389/fonc.2018.00055.

(117) Li, X.; Wang, J. Mechanical Tumor Microenvironment and Transduction : Cytoskeleton Mediates Cancer Cell Invasion and Metastasis. *Int. J. Biol. Sci.* **2020**, *16* (12), 2014–2028. https://doi.org/10.7150/ijbs.44943.

(118) Kumar, S.; Weaver, V. M. Mechanics, Malignancy, and Metastasis: The Force Journey of a Tumor Cell. *Cancer Metastasis Rev.* **2009**, *28* (1–2), 113–127. https://doi.org/10.1007/s10555-008-9173-4.

(119) Plodinec, M.; Loparic, M.; Monnier, C. A.; Obermann, E. C.; Zanetti-Dallenbach, R.;

Oertle, P.; Hyotyla, J. T.; Aebi, U.; Bentires-Alj, M.; Lim, R. Y. H.; Schoenenberger, C. A. The Nanomechanical Signature of Breast Cancer. *Nat. Nanotechnol.* **2012**, *7* (11), 757–765. https://doi.org/10.1038/nnano.2012.167.

(120) Rianna, C.; Radmacher, M.; Kumar, S. Direct Evidence That Tumor Cells Soften When Navigating Confined Spaces. *Mol. Biol. Cell* **2020**, *31* (16), 1726–1734. https://doi.org/10.1091/mbc.E19-10-0588.

(121) Li, Q. S.; Lee, G. Y. H.; Ong, C. N.; Lim, C. T. AFM Indentation Study of Breast Cancer Cells. *Biochem. Biophys. Res. Commun.* **2008**, *374* (4), 609–613. https://doi.org/10.1016/j.bbrc.2008.07.078.

(122) Lv, J.; Liu, Y. Y.; Cheng, F.; Li, J.; Zhou, Y.; Zhang, T.; Zhou, N.; Li, C.; Wang, Z.; Ma, L.; Liu, M.; Zhu, Q.; Liu, X.; Tang, K.; Ma, J.; Zhang, H. H.; Xie, J.; Fang, Y.; Zhang, H. H.; Wang, N.; Liu, Y. Y.; Huang, B. Cell Softness Regulates Tumorigenicity and Stemness of Cancer Cells. *EMBO J.* **2021**, *40* (2), e106123. https://doi.org/10.15252/embj.2020106123.

(123) Staunton, J. R.; Doss, B. L.; Lindsay, S.; Ros, R. Correlating Confocal Microscopy and Atomic Force Indentation Reveals Metastatic Cancer Cells Stiffen during Invasion into Collagen I Matrices. *Sci. Rep.* **2016**, *6*, 19686. https://doi.org/10.1038/srep19686.

(124) Johnson, T. D.; Dequach, J. A.; Gaetani, R.; Ungerleider, J.; Elhag, D.; Nigam, V.; Behfar, A.; Christman, K. L. Human versus Porcine Tissue Sourcing for an Injectable Myocardial Matrix Hydrogel. *Biomater. Sci.* **2014**, *2* (5), 735–744. https://doi.org/10.1039/c3bm60283d.

(125) Wu, P.-H.; Aroush, D. R.-B.; Asnacios, A.; Chen, W.-C.; Dokukin, M. E.; Doss, B. L.; Durand, P.; Ekpenyong, A.; Guck, J.; Guz, N. V; Janmey, P. A.; Lee, J. S.; Moore, N. M.; Ott, A.; Poh, Y.-C.; Ros, R.; Sander, M.; Sokolov, I.; Staunton, J. R.; Wang, N.; Whyte, G.; Wirtz, D. Comparative Study of Cell Mechanics Methods. *Nat. Methods* **2018**, *15* (7), 491–498. https://doi.org/10.1038/s41592-018-0015-1.Comparative.

(126) Mierke, C. T. The Role of the Optical Stretcher Is Crucial in the Investigation of Cell Mechanics Regulating Cell Adhesion and Motility. *Front. Cell Dev. Biol.* **2019**, *7*, 184. https://doi.org/10.3389/fcell.2019.00184.

(127) Sander, M.; Flesch, J.; Ott, A. Using Cell Monolayer Rheology to Probe Average

Single Cell Mechanical Properties. *Biorheology* **2015**, *52* (4), 269–278. https://doi.org/10.3233/BIR-15070.

(128) Puig-De-Morales, M.; Grabulosa, M.; Alcaraz, J.; Mullol, J.; Maksym, G. N.; Fredberg, J. J.; Navajas, D. Measurement of Cell Microrheology by Magnetic Twisting Cytometry with Frequency Domain Demodulation. *J. Appl. Physiol.* **2001**, *91* (3), 1152–1159. https://doi.org/10.1152/jappl.2001.91.3.1152.

(129) Wirtz, D. Particle-Tracking Microrheology of Living Cells: Principles and Applications. *Annu. Rev. Biophys.* **2009**, *38* (1), 301–326. https://doi.org/10.1146/annurev.biophys.050708.133724.

(130) Boulter, E.; Tissot, F. S.; Dilly, J.; Pisano, S.; Féral, C. C. Cyclic Uniaxial Mechanical Stretching of Cells Using a LEGO® Parts-Based Mechanical Stretcher System. *J. Cell Sci.* **2020**, *133* (1), jcs234666. https://doi.org/10.1242/jcs.234666.

(131) Desprat, N.; Richert, A.; Simeon, J.; Asnacios, A. Creep Function of a Single Living Cell. *Biophys. J.* **2005**, *88* (3), 2224–2233. https://doi.org/10.1529/biophysj.104.050278.

(132) Desprat, N.; Guiroy, A.; Asnacios, A. Microplates-Based Rheometer for a Single Living Cell. *Rev. Sci. Instrum.* **2006**, *77* (5), 055111. https://doi.org/10.1063/1.2202921.

(133) Hao, Y.; Cheng, S.; Tanaka, Y.; Hosokawa, Y.; Yalikun, Y. Mechanical Properties of Single Cells : Measurement Methods and Applications. *Biotechnol. Adv.* **2020**, *45*, 107648. https://doi.org/10.1016/j.biotechadv.2020.107648.

(134) Zemła, J.; Danilkiewicz, J.; Orzechowska, B.; Pabijan, J.; Seweryn, S.; Lekka, M. Atomic Force Microscopy as a Tool for Assessing the Cellular Elasticity and Adhesiveness to Identify Cancer Cells and Tissues. *Semin. Cell Dev. Biol.* **2018**, *73*, 115–124. https://doi.org/10.1016/j.semcdb.2017.06.029.

(135) Gavara, N. A Beginner's Guide to Atomic Force Microscopy Probing for Cell Mechanics. *Microsc. Res. Tech.* **2017**, *80* (1), 75–84. https://doi.org/10.1002/jemt.22776.

(136) Kuznetsova, T. G.; Starodubtseva, M. N.; Yegorenkov, N. I.; Chizhik, S. A.; Zhdanov, R. I. Atomic Force Microscopy Probing of Cell Elasticity. *Micron* **2007**, *38* (8), 824–

833. https://doi.org/10.1016/j.micron.2007.06.011.

(137) Butt, H. J.; Cappella, B.; Kappl, M. Force Measurements with the Atomic Force Microscope: Technique, Interpretation and Applications. *Surf. Sci. Rep.* **2005**, *59* (1–6), 1–152. https://doi.org/10.1016/j.surfrep.2005.08.003.

(138) Benitez, R.; Toca-Herrera, J. L. Looking at Cell Mechanics with Atomic Force Microscopy: Experiment and Theory. *Microsc. Res. Tech.* **2014**, *77* (11), 947–958. https://doi.org/10.1002/jemt.22419.

(139) Alonso, J. L.; Goldmann, W. H. Feeling the Forces: Atomic Force Microscopy in Cell Biology. *Life Sci.* **2003**, *72* (23), 2553–2560. https://doi.org/10.1016/S0024-3205(03)00165-6.

(140) Roca-Cusachs, P.; Conte, V.; Trepat, X. Quantifying Forces in Cell Biology. *Nat. Cell Biol.* **2017**, *19* (7), 742–751. https://doi.org/10.1038/ncb3564.

(141) Moreno-Flores, S.; Benitez, R.; Vivanco, M. D. M.; Toca-Herrera, J. L. Stress Relaxation and Creep on Living Cells with the Atomic Force Microscope: A Means to Calculate Elastic Moduli and Viscosities of Cell Components. *Nanotechnology* **2010**, *21* (44), 445101. https://doi.org/10.1088/0957-4484/21/44/445101.

(142) Weber, A.; Toca-Herrera, J. L.; Zbiral, B.; Iturri, J.; Benitez, R. Measuring (Biological) Materials Mechanics with Atomic Force Microscopy. 2. Influence of the Loading Rate and Applied Force (Colloidal Particles). *Microsc. Res. Tech.* **2020**, *84* (5), 1078–1088. https://doi.org/10.1002/jemt.23643.

(143) Butt, H.-J.; Jaschke, M. Calculation of Thermal Noise in Atomic Force Microscopy. *Nanotechnology* **1995**, *6*, 1–7.

(144) Zbiral, B.; Weber, A.; Iturri, J.; Vivanco, M. D. M.; Toca-Herrera, J. L. Estrogen Modulates Epithelial Breast Cancer Cell Mechanics and Cell-to-Cell Contacts. *Materials (Basel).* **2021**, *14*, 2897.

(145) Benítez, R.; Bolós, V. J.; Toca-Herrera, J. L. AfmToolkit: An R Package for Automated AFM Force-Distance Curves Analysis. *R J.* **2017**, *9* (2), 291–308. https://doi.org/10.32614/rj-2017-045.

(146) Benítez, R.; Moreno-Flores, S.; Bolós, V. J.; Toca-Herrera, J. L. A New Automatic

Contact Point Detection Algorithm for AFM Force Curves. *Microsc. Res. Tech.* **2013**, *76* (8), 870–876. https://doi.org/10.1002/jemt.22241.

(147) Dimitriadis, E. K.; Horkay, F.; Maresca, J.; Kachar, B.; Chadwick, R. S. Determination of Elastic Moduli of Thin Layers of Soft Material Using the Atomic Force Microscope. *Biophys. J.* **2002**, *82* (5), 2798–2810. https://doi.org/10.1016/S0006-3495(02)75620-8.

(148) Wagh, A. A.; Roan, E.; Chapman, K. E.; Desai, L. P.; Rendon, D. A.; Eckstein, E. C.; Waters, C. M. Localized Elasticity Measured in Epithelial Cells Migrating at a Wound Edge Using Atomic Force Microscopy. *Am. J. Physiol. - Lung Cell. Mol. Physiol.* **2008**, *295* (1), 54–60. https://doi.org/10.1152/ajplung.00475.2007.

(149) Gerardo, H.; Lima, A.; Carvalho, J.; Ramos, J. R. D.; Couceiro, S.; Travasso, R. D. M.; Pires das Neves, R.; Grãos, M. Soft Culture Substrates Favor Stem-like Cellular Phenotype and Facilitate Reprogramming of Human Mesenchymal Stem/Stromal Cells (HMSCs) through Mechanotransduction. *Sci. Rep.* **2019**, *9*, 9086. https://doi.org/10.1038/s41598-019-45352-3.

(150) Navarrete, R. O.; Lee, E. M.; Smith, K.; Hyzy, S. L.; Doroudi, M.; Williams, J. K.; Gall, K.; Boyan, B. D.; Schwartz, Z. Substrate Stiffness Controls Osteoblastic and Chondrocytic Differentiation of Mesenchymal Stem Cells without Exogenous Stimuli. *PLoS One* **2017**, *12* (1), e0170312. https://doi.org/10.1371/journal.pone.0170312.

(151) Gil-Redondo, J. C.; Weber, A.; Zbiral, B.; Vivanco, M.; Toca-Herrera, J. L. Substrate Stiffness Modulates the Viscoelastic Properties of MCF-7 Cells. *J. Mech. Behav. Biomed. Mater.* **2021**, *125*, 104979. https://doi.org/10.1016/j.jmbbm.2021.104979.

(152) Najafi, M.; Farhood, B.; Mortezaee, K. Extracellular Matrix (ECM) Stiffness and Degradation as Cancer Drivers. *J. Cell. Biochem.* **2019**, *120* (3), 2782–2790. https://doi.org/10.1002/jcb.27681.

(153) Zhu, Y.; Liu, Y.; Zhang, C.; Chu, J.; Wu, Y.; Li, Y.; Liu, J.; Li, Q.; Li, S.; Shi, Q.; Jin, L.; Zhao, J.; Yin, D.; Efroni, S.; Su, F.; Yao, H.; Song, E.; Liu, Q. Tamoxifen-Resistant Breast Cancer Cells Are Resistant to DNA-Damaging Chemotherapy Because of Upregulated BARD1 and BRCA1. *Nat. Commun.* **2018**, *9* (1), 1595. https://doi.org/10.1038/s41467-018-03951-0.

(154) Zhou, C.; Zhong, Q.; Rhodes, L. V; Townley, I.; Bratton, M. R.; Zhang, Q.; Martin, E.

C.; Elliott, S.; Collins-burow, B. M.; Burow, M. E.; Wang, G. Proteomic Analysis of Acquired Tamoxifen Resistance in MCF-7 Cells Reveals Expression Signatures Associated with Enhanced Migration. *Breast Cancer Res.* **2012**, *14* (2), R45.

(155) Pullikuth, A. K.; Catling, A. D. Scaffold Mediated Regulation of MAPK Signaling and Cytoskeletal Dynamics: A Perspective. **2007**, *19* (8), 1621–1632.

(156) Bian, H.; Li, F.; Wang, W.; Zhao, Q.; Gao, S.; Ma, J. MAPK/P38 Regulation of Cytoskeleton Rearrangement Accelerates Induction of Macrophage Activation by TLR4, but Not TLR3. *Int. J. Mol. Med.* **2017**, *40*, 1495–1503. https://doi.org/10.3892/ijmm.2017.3143.

(157) Liu, L.; Zhang, L.; Zhao, S.; Zhao, X.; Min, P.; Ma, Y. Non-Canonical Notch Signaling Regulates Actin Remodeling in Cell Migration by Activating PI3K/AKT/Cdc42 Pathway. *Front. Pharmacol.* **2019**, *10*, 370. https://doi.org/10.3389/fphar.2019.00370.

(158) Croft, D. R.; Sahai, E.; Mavria, G.; Li, S.; Tsai, J.; Lee, W. M. F.; Marshall, C. J.; Olson, M. F. Conditional ROCK Activation In Vivo Induces Tumor Cell Dissemination and Angiogenesis. *Cancer Res.* **2004**, *64*, 8994–9001.

(159) Kerdivel, G.; Boudot, A.; Habauzit, D.; Percevault, F.; Demay, F.; Pakdel, F.; Flouriot, G.; Kerdivel, G.; Boudot, A.; Habauzit, D.; Percevault, F.; Demay, F. Activation of the MKL1/Actin Signaling Pathway Induces Hormonal Escape in Estrogen-Responsive Breast Cancer Cell Lines. *Mol. Cell. Endocrinol.* **2014**, *390* (1–2), 34–44. https://doi.org/10.1016.

(160) Flouriot, G.; Huet, G.; Demay, F.; Pakdel, F.; Boujrad, N.; Michel, D. The Actin/MKL1 Signalling Pathway Influences Cell Growth and Gene Expression through Large-Scale Chromatin Reorganization and Histone Post-Translational Modifications. *J. Biochem.* **2014**, *268*, 257–268. https://doi.org/10.1042/BJ20131240.

(161) Smolyakov, G.; Thiebot, B.; Campillo, C.; Labdi, S.; Severac, C.; Pelta, J.; Dague, É. Elasticity, Adhesion, and Tether Extrusion on Breast Cancer Cells Provide a Signature of Their Invasive Potential. *ACS Appl. Mater. Interfaces* **2016**, *8* (41), 27426–27431. https://doi.org/10.1021/acsami.6b07698.

(162) Sun, M.; Graham, J. S.; Hegedüs, B.; Marga, F.; Zhang, Y.; Forgacs, G.; Grandbois, M. Multiple Membrane Tethers Probed by Atomic Force Microscopy. *Biophys. J.* **2005**, *89*

(6), 4320–4329. https://doi.org/10.1529/biophysj.104.058180.

(163) Liverani, C.; Vita, A. De; Minardi, S.; Kang, Y.; Mercatali, L.; Bongiovanni, A.; Manna, F. La; Ibrahim, T.; Tasciotti, E. A Biomimetic 3D Model of Hypoxia- Driven Cancer Progression. *Sci. Rep.* **2019**, *9*, 12263. https://doi.org/10.1038/s41598-019-48701-4.

(164) Gilkes, D. M.; Xiang, L.; Joo, S.; Chaturvedi, P.; Hubbi, M. E.; Wirtz, D. Hypoxia-Inducible Factors Mediate Coordinated RhoA- ROCK1 Expression and Signaling in Breast Cancer Cells. *PNAS* **2013**, 384–393. https://doi.org/10.1073/pnas.1321510111.

(165) Evans, S. M.; Koch, C. J.; Laughlin, K. M.; Jenkins, W. T.; Van Winkle, T.; Wilson, D. F. Tamoxifen Induces Hypoxia in MCF-7 Xenografts. *Cancer Res.* **1997**, *57* (22), 5155–5161.

(166) Jögi, A.; Ehinger, A.; Hartman, L.; Alkner, S. Expression of HIF-1α Is Related to a Poor Prognosis and Tamoxifen Resistance in Contralateral Breast Cancer. *PLoS One* **2019**, *14* (12), e0226150. https://doi.org/10.1371/journal.pone.0226150.

(167) Li, Y.; Chen, X.; Zhou, Z. W.; Li, Q.; Westover, K. D.; Wang, M.; Liu, J.; Zhang, S.; Zhang, J.; Xu, B.; Wei, X. Dynamic Surveillance of Tamoxifen-Resistance in ER-Positive Breast Cancer by CAIX-Targeted Ultrasound Imaging. *Cancer Med.* **2020**, *9* (7), 2414–2426. https://doi.org/10.1002/cam4.2878.

(168) Yang, J.; Al-Tahan, A.; Jones, D. T.; Buffa, F. M.; Bridges, E.; Interiano, R. B.; Qu, C.; Vogt, N.; Li, J. L.; Baban, D.; Ragoussis, J.; Nicholson, R.; Davidoff, A. M.; Harris, A. L. Estrogen Receptor-α Directly Regulates the Hypoxia-Inducible Factor 1 Pathway Associated with Antiestrogen Response in Breast Cancer. *Proc. Natl. Acad. Sci. U. S. A.* **2015**, *112* (49), 15172–15177. https://doi.org/10.1073/pnas.1422015112.

(169) Peiró, C. H. F.; Encina, J. A.; Perez, M. M.; Aquino, G. S. A.; Veiga, G. L.; Fonseca, F.; Alves, B. C. A. The Role of Hypoxia-Induced Factor 1-Alpha in Breast Cancer. *J. Cancer Metastasis Treat.* **2019**, *5*, 49. https://doi.org/10.20517/2394-4722.2018.109.

(170) Gilreath, C.; Boerma, M.; Qin, Z.; Hudson, M. K.; Wang, S. The Hypoxic Microenvironment of Breast Cancer Cells Promotes Resistance in Radiation Therapy. *Front. Oncol.* **2021**, *10*, 629422. https://doi.org/10.3389/fonc.2020.629422.

(171) Oesterreich, S.; Deng, W.; Jiang, S.; Cui, X.; Ivanova, M.; Schiff, R.; Kang, K.;

Hadsell, D. L.; Lee, A. V. Advances in Brief Estrogen-Mediated Down-Regulation of E-Cadherin in Breast Cancer Cells 1. **2003**, No. 713, 5203–5208.

(172) Zhang, X.; Nugroho, R. W. N.; Farooq, M.; Lou, Y.; Yliperttula, M.; Valle-Delgado, J. J.; Monika, O. AFM Force Spectroscopy Reveals the Role of Integrins and Their Activation in Cell − Biomaterial Interactions. *ACS Appl Bio Mater* **2020**, *3*, 1406–1417. https://doi.org/10.1021/acsabm.9b01073.

(173) Helenius, J.; Heisenberg, C.; Gaub, H. E.; Muller, D. J. Single-Cell Force Spectroscopy. *J. Cell Sci.* **2008**, *121*, 1785–1791. https://doi.org/10.1242/jcs.030999.

(174) Panorchan, P.; George, J. P.; Wirtz, D. Probing Intercellular Interactions between Vascular Endothelial Cadherin Pairs at Single-Molecule Resolution and in Living Cells. *J. Mol. Biol.* **2006**, *358*, 665–674. https://doi.org/10.1016/j.jmb.2006.02.021.

(175) Engin, S.; Deichmann, C.; Oelkers, M. Covalent and Density-Controlled Surface Immobilization of E-Cadherin for Adhesion Force Spectroscopy. *PLoS One* **2014**, *9* (3), e93123. https://doi.org/10.1371/journal.pone.0093123.

(176) Wuebben, E. L.; Rizzino, A. The Dark Side of SOX2: Cancer - A Comprehensive Overview. *Oncotarget* **2017**, *8* (27), 44917–44943. https://doi.org/10.18632/oncotarget.16570.

(177) Seo, E. J.; Kim, D. K.; Jang, I. H.; Choi, E. J.; Shin, S. H.; Lee, S. I.; Kwon, S. M.; Kim, K. H.; Suh, D. S.; Kim, J. H. Hypoxia-NOTCH1-SOX2 Signaling Is Important for Maintaining Cancer Stem Cells in Ovarian Cancer. *Oncotarget* **2016**, *7* (34), 55624–55638. https://doi.org/10.18632/oncotarget.10954.

(178) Chen, G.; Liu, B.; Yin, S.; Li, S.; Guo, Y.; Wang, M.; Wang, K.; Wan, X. Hypoxia Induces an Endometrial Cancer Stem-like Cell Phenotype via HIF-Dependent Demethylation of SOX2 MRNA. *Oncogenesis* **2020**, *9* (9), 81. https://doi.org/10.1038/s41389-020-00265-z.

(179) Wang, Y.; Bibi, M.; Min, P.; Deng, W.; Zhang, Y.; Du, J. SOX2 Promotes Hypoxia-Induced Breast Cancer Cell Migration by Inducing NEDD9 Expression and Subsequent Activation of Rac1/HIF-1α Signaling. *Cell. Mol. Biol. Lett.* **2019**, *24*, 55. https://doi.org/10.1186/s11658-019-0180-y.

(180) Luo, W.; Li, S.; Peng, B.; Ye, Y.; Deng, X.; Yao, K. Embryonic Stem Cells Markers

SOX2, OCT4 and Nanog Expression and Their Correlations with Epithelial-Mesenchymal Transition in Nasopharyngeal Carcinoma. *PLoS One* **2013**, *8* (2), e56324. https://doi.org/10.1371/journal.pone.0056324.

(181) Zhang, C.; Samanta, D.; Lu, H.; Bullen, J. W.; Zhang, H.; Chen, I.; He, X.; Semenza, G. L. Hypoxia Induces the Breast Cancer Stem Cell Phenotype by HIF-Dependent and ALKBH5-Mediated M6A-Demethylation of NANOG MRNA. *Proc. Natl. Acad. Sci. U. S. A.* **2016**, *113* (14), E2047–E2056. https://doi.org/10.1073/pnas.1602883113.

(182) Dittmer, A.; Dittmer, J. Carcinoma-Associated Fibroblasts Promote Growth of Sox2-Expressing Breast Cancer Cells. *Cancers (Basel).* **2020**, *12* (11), 3435. https://doi.org/10.3390/cancers12113435.

(183) Domenici, G.; Aurrekoetxea-Rodríguez, I.; Simões, B. M.; Rábano, M.; Lee, S. Y.; Millán, J. S.; Comaills, V.; Oliemuller, E.; López-Ruiz, J. A.; Zabalza, I.; Howard, B. A.; Kypta, R. M.; Vivanco, M. d. M. A Sox2–Sox9 Signalling Axis Maintains Human Breast Luminal Progenitor and Breast Cancer Stem Cells. *Oncogene* **2019**, *38* (17), 3151–3169. https://doi.org/10.1038/s41388-018-0656-7.

(184) Deville, S. S.; Cordes, N. The Extracellular, Cellular, and Nuclear Stiffness, a Trinity in the Cancer Resistome—A Review. *Front. Oncol.* **2019**, *9*, 1376. https://doi.org/10.3389/fonc.2019.01376.

(185) Chiotaki, R.; Polioudaki, H.; Theodoropoulos, P. A. Differential Nuclear Shape Dynamics of Invasive Andnon-Invasive Breast Cancer Cells Are Associated with Actin Cytoskeleton Organization and Stability. *Biochem. Cell Biol.* **2014**, *92* (4), 287–295. https://doi.org/10.1139/bcb-2013-0120.

(186) Fischer, T.; Hayn, A.; Mierke, C. T. Effect of Nuclear Stiffness on Cell Mechanics and Migration of Human Breast Cancer Cells. *Front. Cell Dev. Biol.* **2020**, *8*, 393. https://doi.org/10.3389/fcell.2020.00393.

7. List of Tables

8. List of Figures

9. Acknowledgements

I would like to thank José for giving me the opportunity to pursue this project and for all the time and effort you spent in supervising and guiding me. I have learned many things and gained many new skills thanks to your teaching. I especially acknowledge how much liberty and autonomy I've been given in pursuing this project and the others I've gotten to contribute to. Especially at the master studies level this is not a given, but all the more I appreciate it greatly. I believe this to be somewhat unique to this group. I would also like to thank you for giving me something to do and work for during this pandemic, which may or may not have saved my mental sanity. I acknowledge Andi for his supervision and for ultimately teaching me some valuable life lessons pertaining to integrity and character.

I would like to thank Amsatou especially for her expertise and skill regarding all things cell culture and wet lab work, as well as for being a great conversation partner, a clever mind and always lending an ear when needed. More than that, thank you Amsatou for being a friend to me. I would like to thank Jacqueline for her helpfulness, kindness, and support and Hannah for being a great office mate. I would like to thank Uli and Ludi especially for all of the fantastic banter and coffee chats we had; I maintain my opinion that out time together at DBNS was way too short, however, I enjoyed every day we worked together and wish you both the very best. The world needs more people like you two. I would like to thank the rest of the DBNS crowd (Tayebeh, Max, Giacomo, Veronika, Mikhail, Peter, Juan-Carlos, and others) for being welcoming, kind, supportive and most of all for being great fun.

I want to say a heartful thank you to my family and friends (from BOKU and outside), especially to my parents, my brother, Marlene, Sabine, you are the best and I cannot put into words how much I appreciate all of the support and care you continue to give. I would like to thank the molecule caffeine for keeping the science machine alive. I am being dead serious.

10. Appendix

During my time at DBNS I got the chance to author and co-author several original scientific papers, attend conferences presenting my own data as posters and write a book chapter on methodology. However, my personal favorite "extracurricular" activity was hand drawing and

getting awarded a cover image for a journal our publication was featured in. The published version of the cover image is appended on page 113.

List of Publications (Original Papers and Conference Posters):

Zbiral B, Weber A, Iturri J, Vivanco MdM, Toca-Herrera JL**. Estrogen Modulates Epithelial Breast Cancer Cell Mechanics and Cell-to-Cell Contacts. Materials (Basel). 2021 May 28;14(11):2897. doi: 10.3390/ma14112897. PMID: 34071397; PMCID: PMC8198807.**

Weber A, **Zbiral B**, Iturri J, Benitez R, Toca-Herrera JL. **Measuring (biological) materials mechanics with atomic force microscopy. 2. Influence of the loading rate and applied force (colloidal particles).** Microsc Res Tech. 2021 May;84(5):1078-1088. doi: 10.1002/jemt.23643. Epub 2020 Nov 12. PMID: 33179834.

Zbiral B, Weber A, Toca-Herrera JL. **Measuring Mechanical Properties of Breast Cancer Cells with Atomic Force Microscopy.** Methods Mol Biol. 2022;2471:323-343. doi: 10.1007/978-1-0716-2193-6_19. **PMID: 35175607.**

Schmidt K, Hageneder S, Lechner B, **Zbiral B**, Fossati S, Ahmadi Y, Minunni M, Toca-Herrera JL, Reimhult E, Barisic I, Dostalek J. **Rolling Circle Amplification Tailored for Plasmonic Biosensors: From Ensemble to Single-Molecule Detection.** ACS Appl Mater Interfaces. 2022 Dec 14;14(49):55017-55027. doi: 10.1021/acsami.2c14500. Epub 2022 Nov 29. PMID: 36446038; PMCID: PMC9756284.

Gil-Redondo JC, Weber A, **Zbiral B**, Vivanco MdM, Toca-Herrera JL. **Substrate stiffness modulates the viscoelastic properties of MCF-7 cells.** J Mech Behav Biomed Mater. 2022 Jan;125:104979. doi: 10.1016/j.jmbbm.2021.104979. Epub 2021 Nov 18. PMID: 34826769.

Gil-Redondo JC, Weber A, Zbiral B, Toca-Herrera JL (2022): AFM meets biology: investigating the mechanical properties of biological materials.
[8th International IBERIAN BIOPHYSICS CONGRESS, Bilbao, Spain, 20.06.2022 - 21.06.2022]

Zbiral B, Weber A, Vivanco MdM, Toca-Herrera JL (2022): **Changes in nuclear morphology correlate with invasiveness in breast cancer cells.** [Poster]
[27th Congress of the European Society of Biomechanics, Porto, Portugal, 26.06.2022 - 29.06.2022]

Zbiral B, Weber A, Vivanco MdM, Toca-Herrera JL. **Influence of hypoxia on MCF-7 breast cancer cell mechanics**. EUR BIOPHYS J BIOPHY. 2021; 50(SUPPL 1): 137-137.

Weber A, Zbiral, B, Iturri J, Vivanco MdM, Toca-Herrera JL (2020): Influence of tamoxifen resistance on the mechanical properties of breast cancer epithelial cells. [11th Annual Symposium Physics of Cancer , Leipzig, Germany, 22.09.2020 - 24.09.2020]

Zbiral B, Weber A, Vivanco MdM, Toca-Herrera JL (2021): The more aggressive the softer – comparing breast cancer cell mechanics. [Poster]
Cell Physics, SEP 29-OKT 1, 2021, Saarbrücken, GERMANY

Zbiral B, Weber A, Vivanco MdM, Toca-Herrera JL (2021): Hypoxic conditions alter breast cancer cell mechanics and rheology. [Poster]
12th Annual Symposium Physics of Cancer, AUG 30 - SEP 1, 2021, Leipzig, Germany

Zbiral B, Weber A, Vivanco MdM, Toca-Herrera JL (2021): Tamoxifen Resistance Leads to Softening of Breast Cancer Cells. [Poster]
26th Congress of the ESB (ESBiomech2021), JUL 11-14, 2021, Milan, ITALY

Weber A, Zbiral B, Benitez R, Vivanco MdM, Toca-Herrera JL (2021): Power Law Rheology to Describe Cell Mechanics.
26th Congress of the ESB (ESBiomech2020), JUL 11-14, 2021, Milan, Italy

VOLUME 84, ISSUE 5, May 2021

Editor-in-Chief
ALBERTO DIASPRO

MICROSCOPY RESEARCH & TECHNIQUE

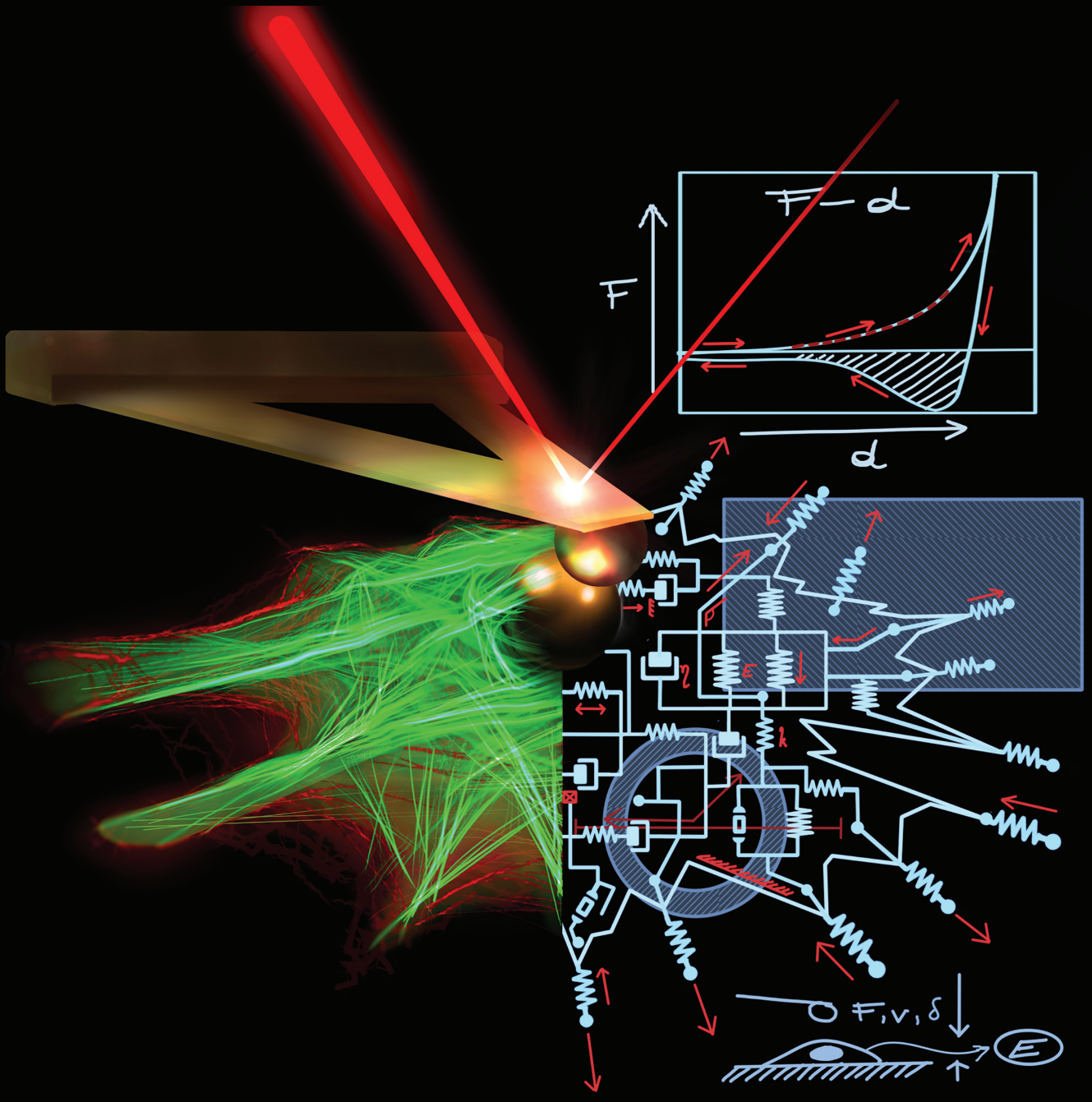

wileyonlinelibrary.com/journal/mrt

WILEY